الجمهورية الجزائرية الديموقراطية الشعبية
وزارة التعليم العالي و البحث العلمي
People's Democratic Republic of Algeria
Ministry of Higher Education and Scientific Research

University of Batna

Faculty of Engineering
Department of Electrical Engineering

THESIS

Presented by

Achour BETKA

Ingénieur d'Etat en Electrotechnique, Centre Universitaire de Biskra
Magistère en Electrotechnique, Université de Biskra.

Thesis submitted for the award of the degree of

Docteur d'Etat Es-Science

Speciality : Electrical Enginnering

PERSPECTIVES FOR THE SAKE OF PHOTOVOLTAIC PUMPING DEVELOPMENT IN THE SOUTH

Examiner's Jury :

Mohamed Said NAIT SAID	Prof.	U. Batna	President
Ammar MOUSSI	Prof.	U. Biskra	Supervisor
Salah Eddine ZOUZOU	Prof.	U. Biskra	Examiner
Boubakeur AZOUI	M.C.	U. Batna	Examiner
Mayouf BELHAMEL	Docteur.	CDER. Alger	Examiner
Abderrahmane HAMIDAT	Docteur	CDER, Alger	Examiner

ACKNOWLEDGEMENTS

I wish to express my sincere gratitude to Prof. Ammar Moussi for his excellent supervision, interest and encouragement throughout this work.

The author wish to thank the staff of the department of electrical engineering of the University of Nottingham for the facilities provided and valuable suggestions in improving this work.

I would like to extend my thanks to the Examiner's Jury composed of :

- Prof. M.S. Nait Said , University of Batna.
- Prof. S. E. Zouzou, University of Biskra.
- Dr. B. Azoui, University of Batna.
- Dr. M. Belhamel, CDER , Alger.
- Dr. A. Hamidat, CDER , Alger.

My thanks also go to all colleagues from Oum El- Bouaghi University who gave me great help and advice.

DECLARATION

The author declares that this contribution has not been submitted in support of an application for another degree or qualification of this or any university.

…….
Achour BETKA

ABSTRACT

The utilisation of photovoltaic conversion of solar energy to power water pumps is today an emerging technology, characterised by gradually declining costs and increasing acquitance with the technology. Since the first installations in the end of the seventies, solar water pumping systems for providing domestic, livestock and irrigation water supplies in remote areas have gained enormously in acceptance, reliability and performance and nowadays belong most significant applications of photovoltaic energy. This can be mainly attributed to the fact that it is not economically viable to connect such remote locations to national electric grids. It is now estimated that over 12000 PV pump units made up of different configurations have been supplied worldwide.

The present work suggests how an optimal operation of a direct photovoltaic pumping system based on an induction motor can be achieved. The optimisation problem consists in maximising the daily pumped water quantity via the minimisation of a non-linear criterion for any operating point. This has led to an optimum ' v-f ' relationship useful in controlling the motor. The voltage source inverter feeding the motor was controlled via one of the following three PWM strategies called : the 'sinusoidal PWM strategy'; the *'Harmonic Elimination Technic'* or the '*Harmonic Minimisation Technic'*. The chosen optimisation criterion fixes the maximisation of the motor efficiency or the power factor, since these two objective functions provides similar results. The extracted electric power is controlled by the inverter frequency instead of MPPT, which leads to a less expensive and non complex implementation. Thus the advantages described in are acquired mean while overriding their inconvenient.

The obtained simulation results show that an increase of all the system performances such as the daily pumped quantity, the motor power factor and the pump efficiency are reached by the proposed approach when either the 'sinusoidal PWM strategy' or the '*Harmonic Minimisation Technic'* is used.

To illustrate the economic performance brought by the proposed approach, the irrigated area by this solar pumping system is calculated under sahara climate conditions for two crops. The pumped volume collected in the ten typical years and the irrigated area show well promising results.

TABLE OF CONTENTS

PREFACE 1
Chapter 1 : PHOTOVOLTAIC TECHNOLOGY AND APPLICATIONS 5
1.1 Introduction 5
1.2 Grid Connected PV systems 7
1.2.1 *Grid-connected PV systems without battery storage* 7
1.2.2 *Grid-connected PV systems with battery storage* 8
1.3 PV-Powered solar domestic hot water systems 10
1.4 Photovoltaic water pumping systems 11
1.5 Background of photovoltaic pumping systems 14
1.6 Conclusion 16
Chapter 2 : MODELLING OF THE PHOTOVOLTAIC PUMPING SYSTEM 18
2.1 Introduction 18
2.2 The photovoltaic effect 19
2.3 The photovoltaic generator model 20
2.3.1 *The one exponential model* 20
2.3.2 *The two exponential model* 21
2.3.3 *The conversion efficiency* 24
2.3.4 *The form factor* 25
2.4 The voltage source inverter model 25
2.4.1 *Converter requirements* 25
2.4.2 *Sinusoidal PWM strategy* 25
2.4.3 *Selective harmonic elimination PWM strategy (SHE PWM)* 26
2.4.4 *The pondered harmonic minimisation strategy* 27
2.5 The unsaturated cage induction motor model 28
- Inherent advantages 28
- Inherent disadvantages 28
- Typical applications 28
- Equivalent circuit 29
2.6 The centrifugal pump model 30
2.6.1 *Influence of the blade thickness S* 32
2.6.2 *Influence of the blades finite number Z* 32
2.6.3 *Pump efficiency* 33
2.7 Pipeline model 33
2.8 Insolation model 34
2.9 Conclusion 35
Chapter 3 : DESCRIPTION OF THE MOTOR OPERATING APPROACHES 36
3.1 Introduction 36
3.2 Constant air-gap flux operation 36
3.3 Constant motor efficiency operation 38
3.3.1 *Control law Elaboration* 39
3.3.2 *Control law Determination* 39
3.3.3 *Maximum power point tracking algorithm* 40
3.4 The proposed approach 41
3.4.1 *Problematic* 41
3.4.2 *Induction motor efficiency optimisation* 42
3.4.2.1 Optimisation criterion 42
A- Use of the Sinusoidal PWM strategy 42
B-Use of the Harmonic Elimination PWM Strategy 43

C- Use of the the Pondered Harmonic Minimisation method 43
3.4.3 *Motor power factor optimisatio*n 43
3.5 Optimisation method 44
3.5.1 *Sequential quadratic programming (SQP*) 44
3.5.2 *QP subproblem* 45
3.5.3 *SQP implementation* 45
3.6 Conclusion 46
Chapter 4 : SIMULATION PERFORMANCE RESULTS 47
4.1 Introduction 47
4.2 Simulation Results 47
4.2.1 *Induction motor efficiency optimisation* 47
A : Sinusoidal PWM strategy 47
B : Selective harmonic elimination and Pondered Minimisation PWM 53
4.2.2 *Induction motor power factor optimisation* 58
4.3 Influence of head changing 60
4.3.1 *The sinusoidal PWM technic* 60
4.3.2 *The harmonic minimisation technic* 62
4.4 Influence of temperature variation 62
4.5 The economic aspect 65
4.6 Influence of the motor saturation 67
4.7 Conclusion 71
CONCLUSION 72
RECOMMENDATION 73
REFERENCES 75

NOMENCLATURE

V	output generator voltage (V).
I	generator current (A).
I_{sc}	generator short-circuit current (A).
V_{th}	thermic voltage (V).
I_o	reverse saturation current (A)
R_s	series generator resistance (Ω).
I_{op}	optimum generator current (A).
V_{op}	optimum generator voltage (V).
V_{oc}	open circuit voltage (V).
P_M	maximum (optimum) generator power (W).
E	insolation (W/m²).
t_{sr}	sunrise time (h).
t_{ss}	sunset time (h).
V_m	rms motor voltage (V).
r_1	stator resistance per phase (Ω).
r_2	equivalent rotor resistance per phase (Ω).
r_m	core loss resistance (Ω).
x_1	stator leakage reactance (Ω).
x_2	equivalent rotor leakage reactance (Ω).
x_m	magnetizing reactance (Ω).
x_{11}	stator cyclic reactance (Ω).
x_{22}	rotor cyclic reactance (Ω).
ω_s	angular frequency of the supply (rd/s).
ω_{sl}	slip speed (rd/s)
ω	motor speed (rd/s).
f	motor frequency (Hz).
p	pair pole number.
H	total head (m).
H_{th}	theoretical total head (m)
$H_{th\,\infty}$	theoretical total head for an infinit number of blades (m).
H_g	geodetic head (m).

Q flow rate (m^3/h).

ρ water volumic mass (kg/m^3).

d_1 entry impeller diameter (cm).

d_2 ejection impeller diameter (cm).

β_2 output fluid angle (degs).

PREFACE

According to the World Health Organization (WHO), arround one half of the population in developing countries do not have access to safe drinking water. Unsafe water accounts for 80% of all sickness in those countries. Efforts to overcome this problem have made water pumping programs a priority of many developing countries and donor groups. In many regions this goal can be achieved by the utilisation of ground water resources. In remote areas far away from national electric grids, there are diverse possibilities to make use of this resource: hand pumps, diesel pumps or solar pumps. In comparison to diesel pumps, solar pumps are today economically advantageous below an hydraulic equivalent (head x flow-rate) of 2000 m^4. The costs are naturally dependent on local prices. The typical heads lie between 1 m – 100 m.

The utilization of photovoltaic conversion of solar energy to power water pumps is today an emerging technology, characterized by gradually declining costs and increasing acquitance with the technology. Since the first installations in the end of the seventies, solar water pumping systems for providing domestic, livestock and irrigation water supplies in remote areas have gained enormously in acceptance, reliability and performance and nowadays belong most significant applications of photovoltaic energy. This can be mainly attributed to the fact that it is not economically viable to connect such remote locations to national electric grids. It is now estimated that over 12000 PV pump units made up of different configurations have been supplied worldwide.

The main barrier to widespread use of PVP-systems continues to be their high initial cost. The cost of water from these systems is directly related to the cost , efficiency, and reliability of the individual system components and the level of solar irradiation. The cost of photovoltaic modules accounts for between 30 % and 60 % of the total investment cost depending on the design of the system.
While improvements in the cost effective photovoltaic module manufacturing techniques are continuously researched, there still remains a clear need for development towards both improved reliability and efficiency values of solar pumping subsystems in order to extract the maximum power capability of the solar generator at all times. Thus, matching of system components, has been of interest to many workers over the last ten years .

Solar energy represents a significant potential in Algeria. Indeed, the country receives more than 3000 h of sunshine per year with a high level of radiation. The yearly average of daily solar irradiance from 5 to 7 kWh/m²/day as far as tilted surfaces at optimum angles are considered. Photovoltaic applications in situ were initiated in 1985. Also, technical and economical for research, in close collaboration with the universities, for the last twenty years.

The dissemination of PV systems is due to national programs which have been undertaken and funded by the government. The first program which was initiated in 1985 is called ‘the solar energy great south program’. This program covered a five-year period (1985-1989). Its purpose was to install stand alone PV plants for different applications. This program was achieved by the Renewable Energy Development Center (CDER). The fulfillment of this program has allowed the following:

- The electrification of small isolated villages in the sahara desert. The total power expected to be installed was 94 kWp but, only 67 kWp were effectively installed.
- Photovoltaic systems for water pumping, with a total power of 85 kWp, were installed.
- A power of 30 kWp was used fot lighting in rural houses.

- Telecommunication repeaters were also supplied by PV modules in remote sites. The total power involved is 80 kWp.

The second program which started in 1995 is the ‘ south rural electrification program’. It is part of the national electrification program which covered the period of 1995-1998 and mobilized 24 billion Algerian dinars. The aim of this program was to supply 216,000 rural houses gathered in 4000 centers. Also this program aimed to supply more than 300 agricultural sites located near the considered centers. Furthermore, it was expected to introduce significantly, solar energy in the national energetic consumption model. The achievement of this program was assigned to the National Company of Electricity and Gaz (SONELGAZ). This program has initiated pilot projects in the sites of Tahifet (latitude 22° 53’ north, longitude 6° east and altitude 1400 m) and Imehrou (latitude 26° north, longitude 8° 50’ east and altitude 600 m). In these sites, two PV installations of 720 Wp were built and put into operation in 1992 with the aim of testing and disseminating PV programs.

In 1999, the renewable energy national program for research was adopted. The PV energy forms a significant part of this program. The main topics are summarised as follows:

- Cristalline silicon solar cells and technologies.
- PV systems and components.
- PV applications.

In the scope of this program, many scientific projects have to be submitted for agreement to the National Commission for Scientific Research (CNRS). The accepted projects will be funded by the National Agency for the Development of University Research (ANDRU).

Few projects dealing with the topics mentioned above were undertaken in collaboration with foreign partners. One of the few projects carried out under an international co-operation program is the intersudmed project. Its main objective is to perform technical and economical studies dealing with the electricity production from renewable energy sources in the southern Mediterranean countries. This work is partially financed through the JOULE and INCO programs of the European Commission Directorate. Sonelgaz is the partner representing Algeria. In the case of this country, the location of Djanet (latitude 24° 33’ north, longitude 9° 28’ east and altitude 1054 m) was selected for pre-feasibility study related to the installation of medium size PV plants (~ 600 kWp) to support local diesel powered grid with production costs.

A number of types and sizes of PVP-systems are available commercially, in various stages of product development, that meet the range of existing pumping needs. The significant design variations of these systems are centered mainly on:

- The choice of the solar cell material.
- The type of the electric motor.
- The type of the pump.
- The method of source/load matching.

Most commercially available systems use silicon solar cells, of either mono or polycrystalline type. Other types of solar cells, which may be less expensive, are under development. There have been significant advances in the development of techniques which use thin films of

semiconductor materials such amorphous silicon. Other high efficient techniques using thin film cells are being extensively researched, as for example Copper-Indium-Dieselenide (CIS). PVP technology will certainly benefit from these developments in the future.

The first generation of solar pumping systems, particularly those for low and medium head applications, incorporated basically permanent magnet DC-motors. However, in the course of the last 15 years the asynchronous motor driven by a variable frequency converter has become the standard motor for solar pumping applications mainly due its simplicity, robustness and small price compared to a DC-motor.

Single-stage centrifugal pumps are frequently used for heads of less than 10 meters. For higher heads, either multi-stage centrifugal or positive displacement (piston or progressive cavity) types are more efficient. If the pump is above ground or floating, it is usually closed coupled to the motor; if submerged, the pump may either be coupled to a submersible motor or driven by a vertical shaft. Positive displacement pumps are ordinarily submerged except in cases where the lift is small but the total head is high.

SCOPE OF THE WORK

The field experiences discussed above have shown that the PVP-technology has reached considerable maturity, the systems have been well accepted by the users, the level of reliability has improved, and that they are economically viable today, under certain conditions. However, quantitative results concerning system performance are few and far from satisfactory. These facts point out that although PVP-systems have proven themselves as one of the most favorable solutions for the supply of drinking water in dry or remotes areas of sunny regions.

The research done in the present work deals with the optimisation of the daily pumped water quantity of a PVP-system based on an induction motor since in several small scale systems, currently installed by the 'Renewable Energy Development Center' (CDER) in the south-East of Algeria, which are addressed especially to irrigation, we have interest to store the maximum pumped water quantity in the day before starting irrigation with pressure. The effectiveness of the proposed algorithm is described by simulation and the obtained results are compared with those of similar work pieces presented in literature.

In the present work, the operational behaviour of the different PVP-system concepts are investigated in great detail on the basis of computer simulation. For each system, mathematical models are developed and used in simulation calculations.

Chapter 1 describes a general overview of the photovoltaic technology applications, such as grid-connected and PVP- systems, their predicted advantages and drawbacks. The chapter also contains as an illustration of how a PVP works and the problems involved with it.

In chapter 2, the physical background of the individual components that form a PVP-system will be described, and the detailed mathematical models developed for each of the components will be presented.

Chapter 3 deals with an explicit presentation of the optimisation algorithm suggested in this work. It contains especially the problematic, the elaboration of the inverter control law and the main steps allowing the simulation of the proposed optimisation algorithm over a standard clear day. To carry on a comparative study, the chapter starts with a detailed description of a

first system called ‘the constant air-gap flux operation’. Following, similarly a second system called ‘the constant motor operation’ is presented.

In chapter 4, the simulation results are fairly presented in a comparative manner, and where the motor is controlled by one of the control laws described in the previous chapter. These results include the main performances provided by a photovoltaic pumping system such as the pump flow-rate, the daily water amount and the subsystem efficiencies. As a complementary part to this study, the economic aspect of its perspectives is unfolded at the end. It comprises the irrigated area calculated under sahara climate conditions for two crops, namely potato and tomato.

Chapter 1
PHOTOVOLTAIC TECHNOLOGY AND APPLICATIONS

1.1 INTRODUCTION:

As conventional energy sources are dwindling fast with a consequent rise in cost, considerable attention is being paid to other alternative sources. Solar energy which is free and abundant in most parts of the world has proven to be an economical source of energy in many applications. The energy the earth receives from the sun is so enormous and so lasting that the total energy consumed annually by the entire world is supplied in as short a time as a half hour. On a clear day the sun's radiation on the earth can be 3000 watts per square meter depending on the location. The sun is a clean and renewable energy source, which produces neither green-houseeffect gas nor noxious waste through its utilization.

The photovoltaic process is completely solid state and self contained. There are no moving parts and no materials are consumed or emitted. Consider the advantages that photovoltaic systems have over competing power options:[1]

They are non-polluting with no detectable emissions or odors.
They can be stand-alone systems that reliably operate unattended for long periods.
They require no connection to an existing power source or fuel supply.
They may be combined with other power sources to increase system reliability.
They can withstand severe weather conditions including snow and ice.
They consume no fossil fuels - their fuel is abundant and free.
They can be installed and upgraded as modular building blocks - as power demand increases, more photovoltaic modules may be added.

Photovoltaic (PV) is a technology in which radiant energy from the sun is converted to direct current (DC) electricity. Although the scientific basis of the photovoltaic effect has been known for nearly 150 years, the modern photovoltaic cell was not developed until 1954.

Many pumping systems are at remote sites where the power demand is relatively small (< 1000 watts). Photovoltaic systems are often the most economical option for this type of application.
Unfortunately solar cells are still far to produce a significant fraction of the world's energy needs because of the initial investment cost. However, per watt of peak power price is considerably decreasing since the seventis as shown in **figure 1.2** [1]. This leads to a wide application of photovoltaic systems in several promising areas. Nevertheless, the field of application is still open to mankind creativity.

Lowering the cost of photovoltaic electricity from solar cells is essential for the technology to further extend its use, especially among utilities. Several promising areas of photovoltaic technology applications are recently in work.

Algeria is a large area country (2382000 km²) with variety in sites leading to a diversity in climate. Solar energy represents a significant potential in Algeria. Indeed, the country receives more than 3000 h of sunshine per year with a high level of radiation.
The yearly average of daily solar irradiance from 5 to 7 kWh/m²/day (**figure 1.1**) as far as tilted surfaces at optimum angles are considered. Algeria can be devided into 8 climatic zones which have approximately a homogenous insolation.

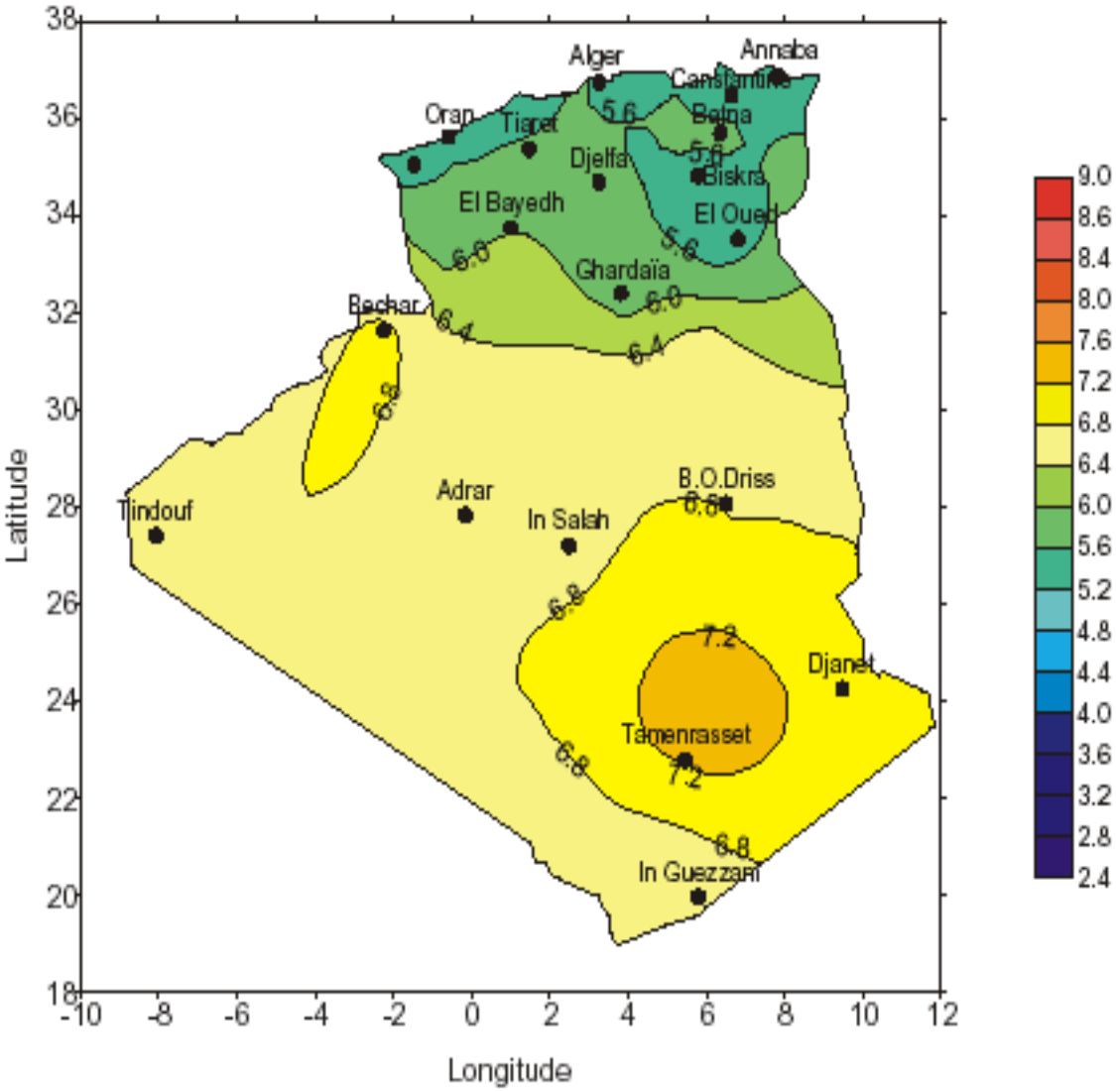

FIG 1.1 Algeria Solar Irradiation [59].

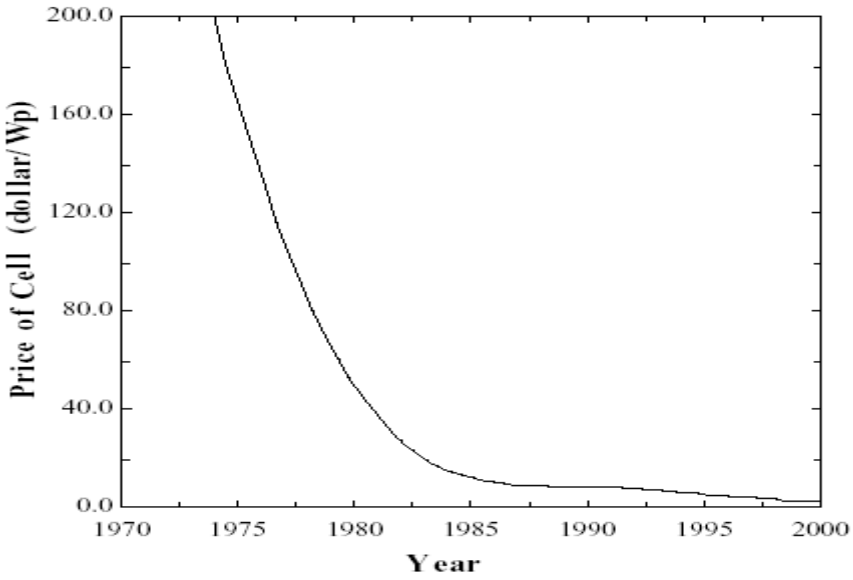

FIG 1.2 Trend of Solar Cell Manufacturing Cost [1].

1.2 GRID CONNECTED PV SYSTEMS :

In recent years, increased advancements in equipment, technologies and reductions in price have resulted in numerous applications and increasing markets for grid-connected PV systems on residential and commercial buildings (**figure 1.3**).

Generally, two types of Grid-connected Photovoltaic Systems are considered [2]:

- Grid-Connected PV systems without Battery storage.
- Grid-Connected PV systems with Battery storage.

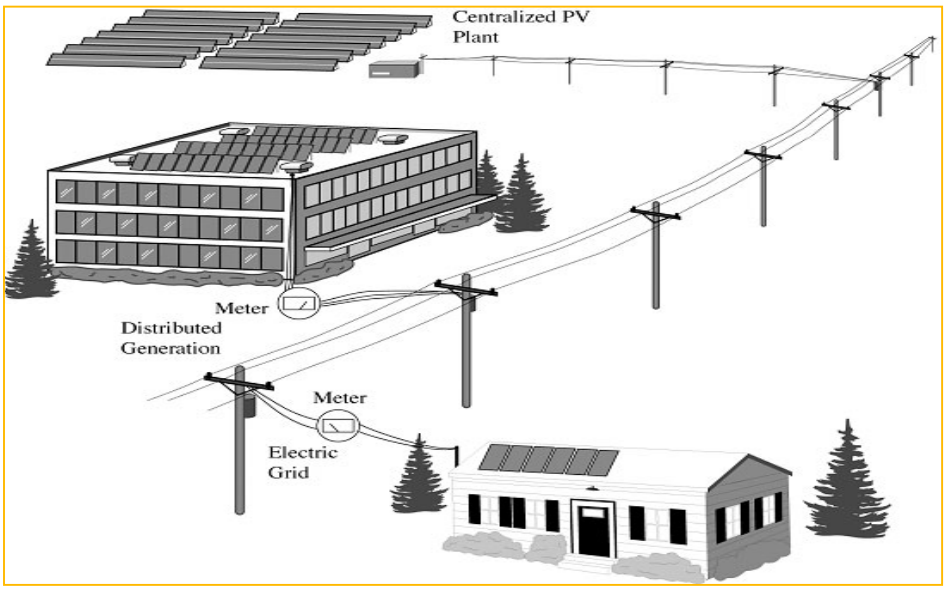

FIG 1.3 Overview of the Grid-Connected PV systems [2].

1.2.1 Grid-Connected PV systems without Battery storage :

PV systems without batteries are simple and reliable, requiring little maintenance. Photovoltaic modules themselves very rarely fail or malfunction, although inverters do require occasional repair or replacement.

Grid-connected or *utility-interactive* PV systems are designed to operate in parallel and interconnected with the electric utility grid as shown in **figure 1.4**. The primary component in grid-connected PV systems is the *inverter,* or *power-conditioning unit* (PCU). The PCU converts the DC power produced by the PV array into AC power consistent with the voltage and power quality requirements of the utility grid. A bi-directional interface is made between the PV system AC output circuits and the electric utility network, typically at an on-site distribution panel or service entrance. This allows the AC power produced by the PV system to either supply on-site electrical loads, or to back feed the grid when the PV system output is greater than the on-site load demand. At night and during other periods when the electrical loads are greater than the PV system output, the balance of power required by the loads is received from the electric utility. When the utility grid is down, these systems automatically shut down and disconnect from the grid. This safety feature is required in all grid-connected PV systems, and ensures that the PV system will not continue to operate and feed back onto the utility grid when the grid is down for service or repair [2].

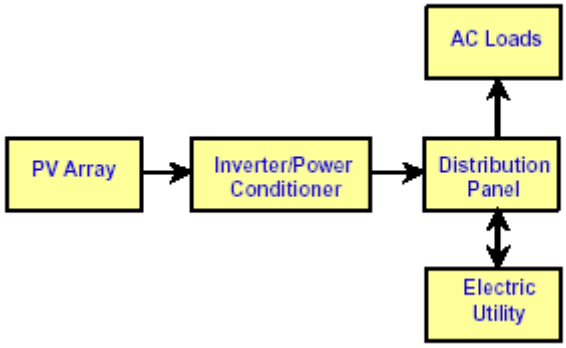

FIG 1.4 Synoptic of Grid-Connected systems without batteries [2].

A typical interconnection of a grid-connected PV power plant including two dc-ac inverters and transformers is shown in **figure 1.5**. The capacitor in parallel with the PV array operates to limit the change of the PV voltage, Vpv, supplied to the dc-ac inverters. The inverters comprise of two 6-switch 3-phase bridge converters. Switching signals for the inverters are generated by a neural network controller for MPPT of the PV array. The objective of the transformer setup is to reduce harmonics involved in the inverter output ac voltage [3].

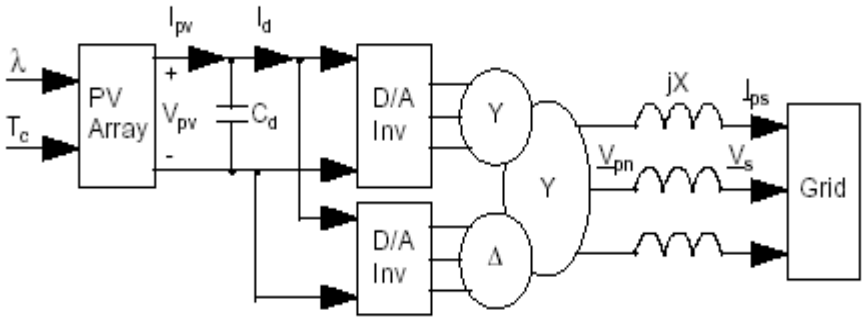

FIG 1.5 Diagram of the grid-connected PV system [3].

1.2.2 Grid-Connected PV systems with Battery storage:

This type of system is extremely popular for homeowners and small businesses where backup power is required for critical loads such as refrigeration, lighting and other necessities

(**figure 1.6**). Under normal circumstances, the system operates in a grid-connected mode, supplementing the on-site loads or sending excess power back onto the grid while keeping the battery fully charged. In the event the grid becomes de-energized, control circuitry in the inverter opens the connection with the utility through a *bus transfer mechanism*, and operates the inverter from the battery to supply power to the dedicated critical loads only. In this configuration, the critical loads must be supplied from a dedicated sub panel [2].

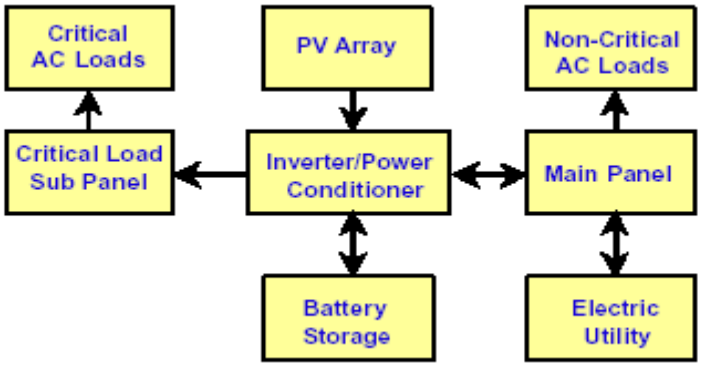

FIG 1.6 Synoptic of Grid-Connected systems with battery storage included [2].

From an operational point of view, a photovoltaic array experiences large variations of its output power under intermittent weather conditions. Those phenomena may cause operational problems at a central control center in a power utility, such as excessive frequency deviations, spinning reserve increase, etc. **Figure 1.7** illustrates two samples of PV power variations for one day [3].

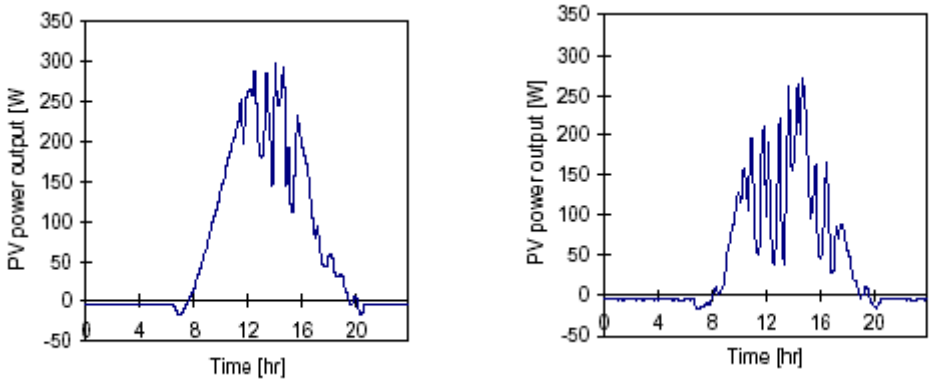

FIG 1.7 Samples of PV power output variations [3].

One method to overcome the above problem is to integrate the PV power plant with other power sources such as diesel backup, fuel cell backup or battery backup. The diesel backup for PV power is able to make a continuous 24-hour power supply be possible. However, it has a couple of severe drawbacks. Its electricity efficiency decreases significantly at a low level of power output, and the diesel power generation is environmentally detrimental as well. Both the battery backup and the fuel cell backup are the most likely technologies to provide backup power for the PV power system in the near future.

A fuel cell power is a very attractive option being used with an intermittent power generation source like the PV power because the fuel cell power system contains lots of great features such as high efficiency, fast load-response, modular production and fuel flexibility. Its feasibility in coordination with a photovoltaic power system has been successfully

demonstrated for both grid-connected and stand-alone applications [3]. Due to the fast ramping capability of the fuel cell power system, a PV-fuel cell hybrid system may be able to solve the PV's inherent problem of intermittent power generation. Unlike a storage battery, which also contains attractive attributes such as fast response rate, modular construction and flexibility for site selection, the fuel cell power can produce electricity continuously to support the PV power. Therefore, the quality of overall power generated from the PV-fuel cell hybrid power plant may be improved. The combination of the photovoltaic and fuel cell power plants is now a viable technology to commercial applications.

Figure 1.8 illustrates a simplified diagram of a grid-connected PV-fuel cell hybrid power plant [3].

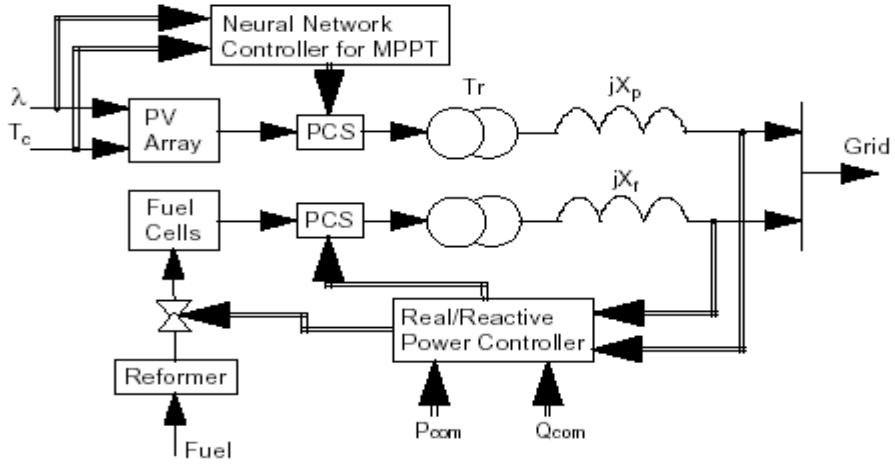

FIG 1.8 Diagram of the grid-connected PV-fuel system [3].

1.3 THE PV–POWERED SOLAR DOMESTIC HOT WATER SYSTEMS:

An alternative means of deriving water heating from the sun was patented by Fanney and Dougherty in 1994. The basic photovoltaic-powered solar domestic hot water (PV-SDHW) system consists of a photovoltaic (PV) array connected to several resistive heating elements within a water storage tank. The PV array produces electrical power during periods of solar insolation and this power is immediately dissipated in the resistive elements.

Several configurations of the PV-SDHW system have been proposed. The original design consists of two water storage tanks as depicted in **figure 1.9**.

A preheat tank heats water drawn from the water mains by thermal energy derived from six resistive elements connected to the PV array. Three of the resistive elements are located in the upper heating element port and three in the lower port.

The auxiliary tank draws water from the preheat tank and performs any additional heating required via two AC resistive elements connected to the utility grid. Other configurations of one –tank are currently suggested which allows the reduction of the overall system cost [4].

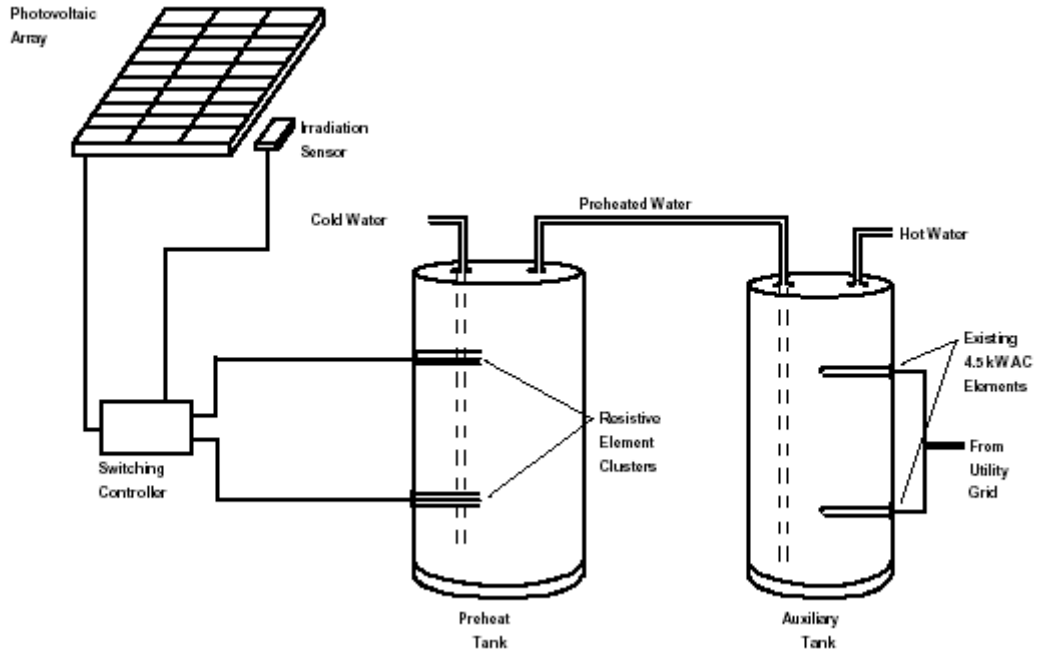

FIG 1.9 Two-tank PV-SDHW system configuration [4].

The PV-SDHW concept has several potential advantages over its solar thermal rivals :

- The PV-SDHW system eliminates the plumbing required in a thermal SDHW system. These pipes can be a significant source of heat losses.
- The new system requires no heat exchanger. These heat exchangers reduce the efficiency of thermal SDHW systems.
- The installation of a PV-SDHW system is simpler than for a thermal system.

The PV-SDHW system also possess a couple of key disadvantages relative to the traditional thermal system :

- For systems sized to meet the same load, the PV array of a PV-SDHW system may cost two to three times the total cost of purchasing and installing a thermal SDHW system.
- The necessary surface area of the PV array for a PV-SDHW system may be three to five times greater than that of the collectors of a thermal SDHW system of comparable performance. This larger area results primarily from the lower solar energy conversion efficiency of PV arrays in comparison to thermal collectors.

1.4 THE PHOTOVOLTAIC WATER PUMPING SYSTEMS :

According to the World Health Organisation (WHO), around one half of the population in developing countries do not have access to safe drinking water. Efforts to overcome this problem have made water pumping programs a priority of many developing countries. In remote areas far away from national electric grids, the use of solar pumps is today economically advantageous where the typical heads lie between 1m-100m [5].

The utilisation of photovoltaic conversion to power water pumps is today an emerging technology, characterised by gradually declining costs. It is now estimated that over 12000 pump units made up of different configurations have been supplied worldwide.

The main barrier to a widespread use of PVP- systems continues to be their high initial cost. The cost of the photovoltaic parts accounts for 60% of the total investment cost.

Figure 1.10 gives the contribution of various components to the overall cost of PVP-systems [5].

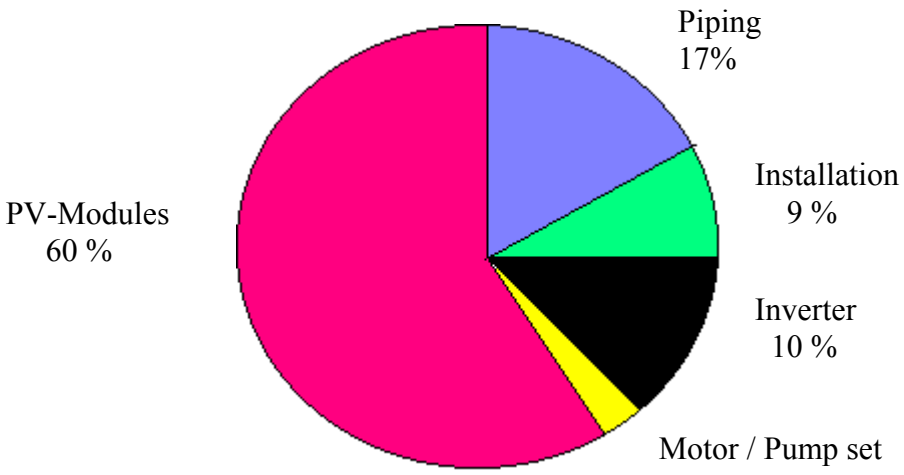

FIG 1.10 Contribution of various components to investment cost of PVP systems [10].

A number of types and sizes of PVP-systems are available commercially, in various stages of product development, that meet the range of existing pumping needs. The significant design variations of these systems are centered mainly on :

- The choise of the solar cell material.
- The type of electric motor.
- The type of pump and the method of source/load matching.

Single-stage centrifugal pumps are frequently used for heads of less than 10 meters. For higher heads, either multi-stage centrifugal or positive displacement (piston or progressive cavity) types are more efficient. If the pump is above ground, it is straight coupled to the motor. If submerged, the pump may either be coupled to a submersible motor or driven by a vertical shaft.

PV-pumping efficiency has considerably improved. System efficiencies from 1-3 % in 1981 have been raised up to 3.5-5% in 1990. Novel system technics are available with efficiencies of more than 5% [5].

The usual elements of a PV water pumping system are:

- Photovoltaic array – to provide electricity supply for the motor-pump. This supply could be direct current (DC), usually at 110 volts, or alternating current (AC) which is produced by inverting the DC power to AC power.
- Motor-Pump set.
- Battery storage if used – to provide electricity storage and allow pumping in cloudy conditions or at night.
- Storage tank – normally elevated, making water available at night or when it is cloudy.
- Maximum power point tracker (MPPT) which forces the PV array to generate its maximum power.

The volume of pumped water is dependent on five major factors:

- The radiation level which is a measure of the sun's available energy.
- The photovoltaic array area.
- The conversion efficiency of the photovoltaic array.
- The ambient temperature.
- The pump-motor –hydraulic system characteristics.

Three different system configurations are currently in use :

- The first is the directly coupled system where a PV array is directly coupled to a DC motor and a pump.
- The second system is the battery buffered PV pumping system where a battery is connected across the array to feed the DC motor driving a pump.
- The third system uses maximum power point tracker (MPPT) or array tracking to improve the efficiency of system.

The typical range of sizes for photovoltaic-powered pumps is a few hundred watts to a few kilowatts.

Direct coupled systems, where the PV array is directly coupled to a DC motor-pump system, is shown in **figure 1.11**. Such a system is simple and reliable, but the system does not operate continuously at its optimum point due to the continuous variation of solar radiation .

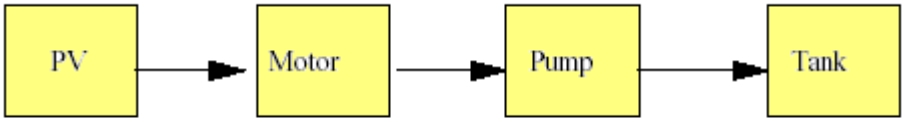

FIG 1.11 Direct coupled PV pumping system

Battery buffered systems with a storage battery is shown in **figure 1.12**. In this system, a battery is connected across the PV array and the DC motor is operating at almost constant voltage, and as a result, the DC motor is operated close to its optimum operating point.
This system has two advantages over the directly coupled one:

- water may be pumped day and night, thus the water discharge is larger.
- the DC motor is operating at its optimum operating point, and consequently, the system efficiency is enhanced.

A major disadvantage of such a system is the extra system cost and unreliability due to the battery.

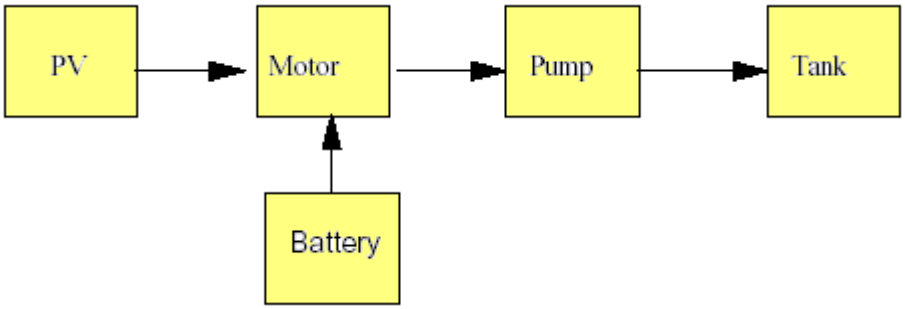

FIG 1.12 PV pumping system with a battery storage

The photovoltaic modules are often mounted on a tracking device that maximize energy production by tracking the sun from east to west each day as shown in **figure 1.13**. The tracker uses little or no power and may increase water production as much as 20 to 40 percent during summer months [1].

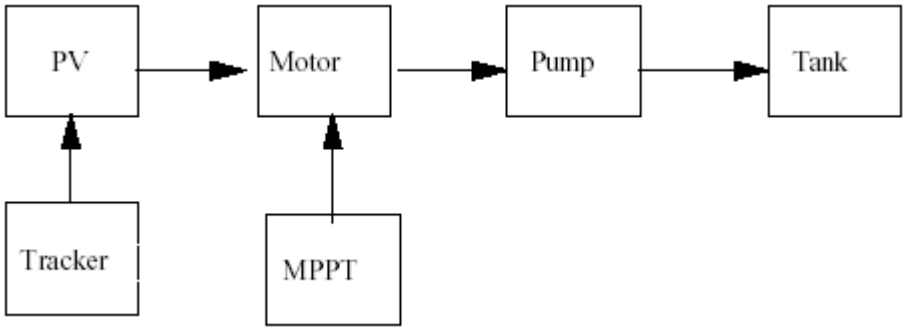

FIG 1.13 PV pumping scheme with sun tracking

1.5 BACKGROUND OF PHOPTOVOLTAIC PUMPING SYSTEMS :

The PV power sources are, by nature, non-linear. They are subject to large variation under environmental factors, mainly the insolation and cell temperature. In order to speed up the amortisation of the system cost, it is essential to opearate the PV generator at its maximum power point on a continuous basis. Therefore power-conditioning units are used for this purpose. This unit depends on the type of load being feed by the PV array. For a pumping system, the load is generally a DC or AC motor.

The first generation of solar pumping systems, particularly those for low and medium head applications, incorporated basically permanent magnet DC motors. However in the course of the last 10 years the asynchronous motor driven by a variable frequency converter has become the standard for solar pumping applications because of its simplicity, robustness and low price compared to DC motor. Electronically-commuted brushless DC motors have in the last 5 years or so gained much popularity because they require less maintenance than standard DC motors.

Many researchers have investigated and proposed different methods for designing and optimising the PVPS to improve system efficiency and reduce investments. Such systems operate in open-loop speed control because precision and transient performance are not required. In addition, the system operates at steady state for long periods.

Several experimental results and theoritical analyses of PVPS have been published. The simplest way to achieve a pumping system is to perform a direct coupling of the motor-pump to the PV generator. In [6] Hsiao describes such impementation. However, even the size is initially optimised, it is shown that the efficiency varies broadly on insolation. It is seen that, depending on the load I-V characteristic, a directly connected motor-PV system with a given load characteristic can be naturally optimised at the intersection point of the load characteristic and maximum power locus. This occurs for one value of insolation. As the insolation varies, the system becomes sub-optimal. In order to track the maximum power various techniques are used; these are called Maximum Power Point Trackers or MPPT technics. These technics are devided in two sets [7]: fixed voltage and true MPPT. For the first technic, there are two ways to implement it. The reference voltage can be a constant predetermined value derived from observing the generator characteristic and choosing a single value thereafter. This value is chosen around 62-80 % of the open circuit V_{oc} [8]. In the second technique, a predetermined optimal reference current is chosen around 70-90 % of the

short- circuit current I_{sc}. A pilot module is then used to track the new reference current when the insolation varies [9].

As the power drawn from a PV generator depends on insolation, temperature and array voltage, it is necessary to match the load and PV array. Several ways have been tried out in order to seek the maximum power point [10-11]. The ideal way is to calculate the output power and compare it with the ideal one . The system is then pushed towards the operating point. This method is tedious, complex and time consuming. The accuracy is affected for low insolation levels because the integration becomes more difficult. One possibility is to exploit perturbation technics, in which the operating point is moved towards the maximum power by perturbing the system periodically by increasing or decreasing the array voltage [11-12-13]. If a given perturbation leads to an increase (decrease) in array power, the subsequent perturbation is made in the same (opposite) direction. Hence the MPPT hunts continuously the peak power operating condition. Since the PV power sources are generally connected to various load types such as energy storage [14], fuel cells [3], therefore designing systematically an MPPT controller is not an easy task. Thus modern control approaches, such as Fuzzy Logic, Neural Network have been suggested for fullfiling the function of tracking the maximum power point of a PV system [10-12-15-16-17--18]. In [10], the search is based on fuzzy heuristic rules which claims not to need parameter information. Thus no transducers were used in this application. Tsai-Fu Wu [12] has proposed a fuzzy logic controlled lightning system with battery backup powered by a solar cell generator. A fuzzy logic controller was suggested to control the battery charge/discharge and maximum power point tracking using a a perturb and observe algorithm. These are collected by the fuzzy rule algorithm and used to control the system to meet the desired performances after the defuzzification process. Artificial neural networks ANN have been reported by other authors. An ANN based real-time maximum power tracking controller for a PV grid-connected system was reported in [15-17]. In order to estimate the optimal power, the open circuit V_{oc} and the short circuit current I_{sc} are measured through monitoring cells and mapped to the optimal inverter voltage which is fed to switching control of the inverter. However, a non-linear identification is necessary to get the optimal voltage from the measured V_{oc}. An ANN is therefore used for this estimation purpose. In another publication, the same authors used only the actual array voltage V_g and V_{oc} for maximum power tracking [16].

One can optimise either the gross mechanical output power [19-20] or the motor efficiency [21-22-23-24]. It is shown that motor efficiency optimisation diminishes the PV generator efficiency.

In [25] Appelbaum analysed starting and steady-state characteistics of a DC motor powered by PV cell generator. It was found that the starting time is larger when any type od DC machines is connected PV source. In addition, the system starts to rotate only at high insolation level for constant load characteristics. For aerodynamic load (centrifugal pumps), the system requires a relatively lower static torque and the system starts to rotate at lower insolation level. Appelbaum and Sarm [26] have examined the starting of a DC motor - pump powered by a PV array with/out MPPT. Alghuwainem [27] exposed the steady state operation of a separatly excited DC motor with Step Up converter working as an MPPT. Anis *et al* [28] reported that a load composed of a DC motor driving a constant volume pump represents a non-matched load for PV array. The matching of a DC motor to a PV generator to maximise gross mechanical energy has been reported by Saied [19] and Akbaba *et al* [20]. Weiner *et al* [29] have examined the global efficiency optimisation of a PVPS based on a DC motor. In [11], Atlas *et al* experimentally proposed an algorithm witch determines the MPP for a PV array for any temperature and solar irradiance level and where the pump is coupled to a PMDC motor. In [30], Veerachary *et al* proposed a Neural Network algorithm of an MPP tracking for PV supplied DC motors.

In [8] , Langridge *et al* studied the operation of a direct PVPS based on a brushless DC motor driving a helical rotor pump and where the array maximum power is made available by a proper control. The reference array voltage is based on a fraction of the open circuit voltage. Moussi *et al* [22] proposed an optimal operation of a PVPS using a BLDC motor driving a centrifugal pump. The purpose was the maximisation of the daily pumped water amount by a proper adjustment of the motor voltage. The dynamic performance of a permanent magnet BLDC motor powered by a PV array were investigated by Swamy *et al* [31].

Since the use of brushless permanent magnet motors is limited to low power PV systems due to their high cost, several PVPS based on an induction motor fed either by a voltage source inverter or a current source inverter have been proposed with scalar and vector control strategies. These works treated various optimisation approaches, such as improving the array use efficiency, or maximising the pump flow-rate. Bhat *et al* [32] analysed a vector control of an induction motor fed by a PV source via a current-controlled voltage source inverter (CC-VSI) . The motor was controlled so to improve the system efficiency. The array maximum power is continuously extracted via a boost-chopper. Yao *et al* [33] proposed to achieve a permanent optimal motor efficiency value for any insolation level with an appropiate frequency control of a VS inverter. In [21], Aziza *et al* investigated the case of a PV pumping system based on an induction motor for a maximum gross mechanical power operation through the control of a voltage source inverter feeding the motor. Olorunfemi [34] proposed the transient and steady state analysis of an induction motor fed from a PV source through a current-source inverter and where the extracted electric power is properly controlled by the chopping ratio of a buck-boost converter. For steady state, chopping ratio and slip frequency of the inverter were manipulated to achieve a maximum efficiency. The analysis of small signal perturbation showed that the system is lightly damped for operating voltages of the array that are less than that of the array voltage corresponding to array maximum output power and the system presents a non-minimum phase response. In [35], Nayar *et al* described two schemes of a solar water pumping system using an induction motor driving a submersible pump. In the first scheme, the pannel output voltage was converted into AC by a three phase PWM inverter. The output voltage is stepped up by a three phase transformer before connecting to the motor. In the second scheme, the panel voltage was boosted by a microprocessor controlled dc-dc converter.The dc output voltage from the booster was then converted into AC by the PWM inverter. The major control systems involved in the system is to achieve a constant V/f operation. The inverter acts as both a variable-frequency source to improve the output of the water pump and a peak-power tracker. Betka et Moussi [23] proposed the daily water amount maximisation of a PVPS using an induction motor fed by an optimal PWM inverter. This was achieved by a proper control of four swiching angles. In addition the electric power was controlled via the inverter frequency instead of the MPPT circuit. Other works treated the operation of the two – phase induction motor [36] or the single-phase in photovoltaic pumping applications.

1.6 CONCLUSION :

Essential information about PV arrays and their connection to several technology applications systems has been presented in this chapter. Renewable energy technologies must do more than be environmentally friendly to be successful; they must also be economically feasible. A failure to meet this second requirement is the reason that many renewable energy applications have not gained more widespread acceptance. The major drawback which limits these applications is the initial cost of the plant. Neverthless, several promising areas of photovoltaic technology applications such as water pumping in remote areas are recently in

work. An explicit study of a PVP system based on an induction motor driving a centrifugal pump will be the focus of next chapters.

Chapter 2
MODELLING OF THE PHOTOVOLTAIC PUMPING SYSTEM

2.1 INTRODUCTION :

The philosophy behind digital simulation of renewable energy systems is that experiments which normally should be done on real systems under high assembling costs can be done numerically in a short time on a computer, thus saving time and investments.

Digital simulation of these systems serve for the purpose of understanding the operational behaviour of the various components of the system and the interaction among them, since by simulating the system performance, one can trace all steps of energy conversion and identify the losses throughout the system in details. Because computer simulation allows a wide range of system parameters to be varied, and the operating characteristics of the system to be investigated. Finally, computer simulation permits the extrapolation of a system design to other localities, with different meteorological conditions, and make it possible to compare different systems. Basis for a computer simulation is a reflection of a real system which is based on theoretical analysis of the various physical processes occurring in a system. Mathematical equations describing quantitatively the system characteristics are formulated from this analysis and translated into computer to be used in the simulation process.

The schematic diagram of the photovoltaic pumping system analysed in this thesis is shown in **Figure 2.1**. It consists of a photovoltaic array, a PWM voltage source inverter and a three-phase squirrel cage induction motor driving a monocellular centrifugal pump. The specification of different components is illustrated in **Table 1.**

In the derivation of the system equations, some assumptions are made:

- ♦ The motor is supposed to be unsaturated.
- ♦ The power losses in the inverter and stray losses in the motor are also supposed negligible. Furthermore, dynamic equations are not taken into consideration since the system is assumed to run at steady state.

In this work, prior to global system simulation, each component of the proposed system should be studied and mathematical model deduced thereafter.

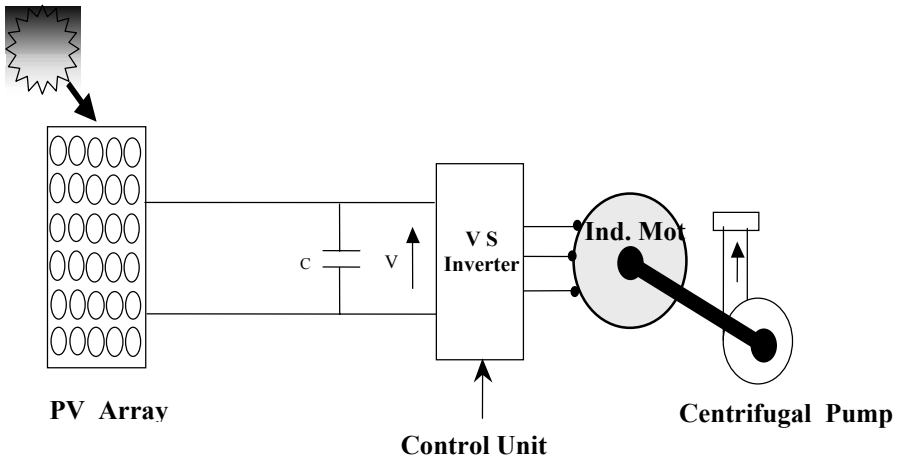

FIG 2.1 The proposed PV Scheme Structure

Table 1 PV pumping system specifications

Subsysem	Specification
Pump :	
Type	Centrifugal , Monocellular
Head	14 m
Flow rate	2.59 l/s
Speed	3000 rpm
Power	521 W
Pipe Network	Φ = 0.06 m H_g = 7.4 m
Motor :	
Type	three-phase induction motor
Voltage	380 V Δ
Current	2.5 A.
Power	1 kW.
Speed	2880 rpm.
Resistances	r_1=22.5 Ω r_2=7.87 Ω, r_m=1.127 K Ω.
Reactances	x_1=x_2= 15.7 Ω, x_m = 586 Ω
PV Array :	
Type	AEG-40 polycristalline silicon
Peak power rating	**614 Wp @ 280 v, 2.2 A.**

2.2 THE PHOTOVOLTAIC EFFECT :

A brief description of the physics behind photovoltaics is helpful in understanding the origin of the equivalent circuits used to model these devices. Photovoltaic cells are semiconductor devices; the vast majority of commercial PV cells are fabricated from silicon.
A PV cell may consist of a single crystal, a number of smaller crystals (polycrystalline), or it may lack crystal structure all together (amorphous). Other semi-conducting materials such as gallium, arsenide are employed in PVs for extraterrestrial or sun concentrator applications, but this description will concern a silicon PV cell.

A PV cell is essentially a large diode that produces a voltage when exposed to incident light. It may be considered to be a light-emitting diode "run backward;" the analogy is similar to a heat engine and a refrigerator. The semiconductor band-gap is the difference in energy between valence and conduction bands. It is a material-dependent property; in undoped silicon it has a value of 1.12 electron-volts or 1.79×10^{-19} joules. An incident photon with at least this much energy may interact with a valence electron in the p-type material, forcing it up into the conduction band, **Figure 2.2**. Any photon with a wavelength less than about 1100 nm has sufficient energy to initiate this reaction. This wavelength corresponds to radiation in the near infrared portion of the spectrum.
If the PV cell is connected to a load in a closed loop circuit, the new conduction band electron will be repelled by the excess negative charge in the p-type side of the PV cell. It travels through the circuit, producing a current through the load [37].

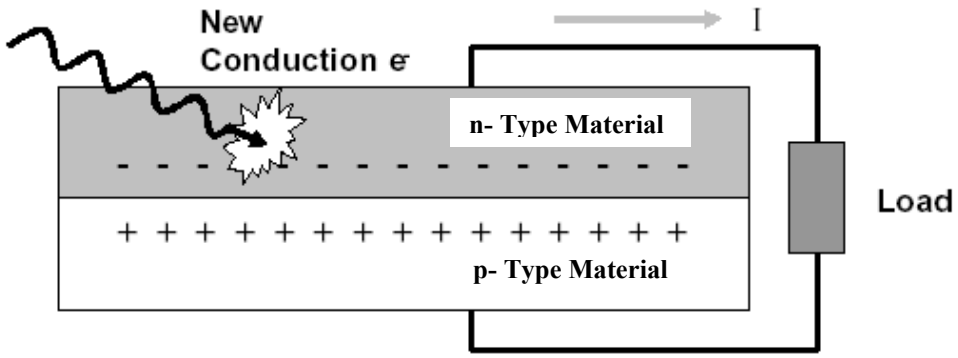

FIG 2.2 Photovoltaic effect-incident light moves an electron from the valence band to the conduction band [37].

2.3 THE PHOTOVOLTAIC GENERATOR MODEL :

Photovoltaic generators are neither constant voltage sources nor current sources but can be approximated as current generators with dependant voltage sources. The array considered in this study is a 16 series connected modules type AEG.40, each having a rated peak power of 38 w and containing 36 series/parallel cells. For the modelling of the PV generator, either the called 'One exponential Model' or the 'Two exponential Model' have been widely used in literature to describe the electrical characteristics of a solar cell.

2.3.1 The One Exponential Model :

The PV generator is a non-linear device and is usually described by its I-V characteristics and by the equivalent circuit, as shown in **figure 2.3**; this model called also ***'the Four-Parameter Model'*** which is widly used by different softwares such as TRNSYS [37], developped by Eckstein (1990), assumes that the PV generator may be modeled as an insolation–dependent current source in parallel with a diode. The current source I_L represents the light-generated current and is function of the cell-characteristics, cell temperature and insolation level. The diode which represents the p-n junction of the silicon cell provides a means for some current to be shunted across the load without actually reaching it. Physically, this is equivalent to a photoelectron falling back into a valence hole before leaving the semi-conductor material; if this occurs the electron can no longer contribute to useful current. In addition to the photo-current source and diode, a single resistor is added to the model to account for ohmic losses as current travels through the PV generator. The four-parameter model has been implemented into many programs, and it reliably predicts with success the performance of single crystal and polycrystalline PV arrays. The four parameter model assumes that the slope of the IV curve is flat at the short-circuit region ($\frac{dI}{dV} = 0$ at V= 0). Therefore the effect of the shunt resistance is negligible, since its value is generally very high[37].

However, this assumption is not generally valid for amorphous photovoltaics. The short-circuit IV slope is finite and negative, so the four-parameter model cannot reproduce I-V characteristics typical of amorphous silicon. A modification is necessary to broaden the model to include amorphous PV cells.

The "five-parameter model" introduces a shunt resistance in the PV equivalent circuit.
In the 'four parameter model' which is adopted in the present work , the I-V characteristic at a given insolation level can be expressed in an implicit equation as follow [24]:

$$I = I_{sc} - I_0 \cdot \left(\exp\left(\frac{V + R_S . I}{V_{th}} \right) - 1 \right) \tag{2.1}$$

Where I and V represent the current and the voltage at the load. The useful power generated by the PV is the product of these two quantities.
In equation (2.1), the reverse saturation current I_o and the thermal voltage V_{th} are written in terms of manufacturer generator data obtained at 1000 w/m² and 25°C [22]:

$$I_o = \left(I_{sc} - I_{op} \right) \exp\left(- \frac{V_{op} + R_s . I_{op}}{V_{th}} \right) \tag{2.2}$$

$$V_{th} = \frac{\left(V_{op} + R_s . I_{op} - V_{oc} \right)}{Ln\left(1 - \frac{I_{op}}{V_{op}} \right)} \tag{2.3}$$

The cell temperature T_c is calculated by a simplified linear relationship as a function of the incident global insolation E, and where the ambiant Temperature T_a determines the crossing point of the function on the vertical axis [8] :

$$T_c = T_a + \left(NOCT - 20 \right) \frac{E}{800} \tag{2.4}$$

NOCT denotes the Normal operation Cell Temperature, which indicates the junction temperature at 800 w/m² and 20°c; the wind velocity is assumed to be1m/s.

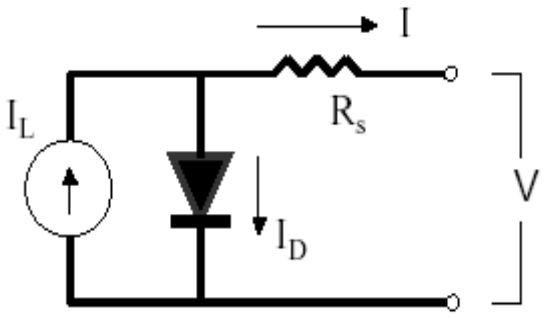

FIG 2.3 The four parameters equivalent circuit

2.3.2 The Two Exponential Model :

For the modelling of a PV generator, the so called 'Two Exponential Model' has been also used in several softwares such as the block oriented simulation system INSEL [5]. The relationship between the voltage V and the generator current is given by the following equation :

$$I = I_{sc} - I_{o1} \left[\exp\left(\frac{V + R_s . I}{\alpha . V_{th}} \right) - 1 \right] - I_{o2} \left[\exp\left(\frac{V + R_s . I}{\beta . V_{th}} \right) - 1 \right] \tag{2.5}$$

It is obvious that the main difference with the previous model is the presence of two exponential factors in the mathematical model.
The cell ideality factors are assumed to be $\alpha = 2$ and $\beta = 2$ according to [5].
In addition, The two reverse saturation currents I_{o1} and I_{o2} are expressed by the following quantities :

$$I_{O1} = \frac{1}{2} \frac{I_{sc}}{\left[\exp\left(\frac{e.V_{oc}}{k.T_c} \right) - 1 \right]} \tag{2.6}$$

$$I_{O2} = \frac{1}{2} \frac{I_{sc}}{\left[\exp\left(\frac{e.V_{oc}}{2.k.T_c} \right) - 1 \right]} \tag{2.7}$$

k denotes the Boltzmann constant ($k = 1.381.\ 10^{23}$ J/K) and e is the electron charge ($e = 1.602\ .10^{-19}$ C).

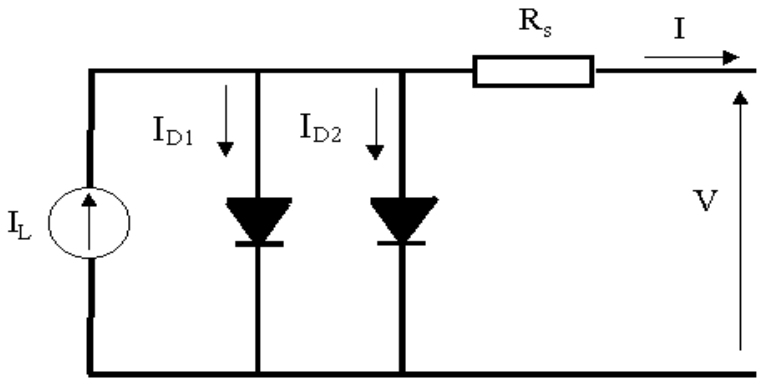

FIG 2.4 The two-diodes model equivalent circuit

Besides, the generator 'four model' parameters are related to those of a single module via the following expressions and where the index 'mod' denotes 'module':
$I_{sc} = N_p\ .\ I_{sc\ 'mod'}$
$I_{op} = N_p\ .\ I_{op\ 'mod'}$
$V_{oc} = N_s\ .\ V_{oc\ 'mod'}$
$V_{op} = N_s\ .\ V_{op\ 'mod'}$

$$R_s = \frac{N_s}{N_p} R_{s\ 'mod'}$$

N_s and N_p are respectively the number of modules in series and the number of strings in parallel.

The I-V curve is essentially affected by the variation of two inputs: the solar insolation and the array temperature. The adaptation of equation (2.1) for different levels of solar insolation and temperature can be handled by the following equations [24] :

$$\Delta T = T - T_r \tag{2.8}$$

$$\Delta I = \alpha \left(\frac{E}{E_r} \right) \Delta T + \left(\frac{E}{E_r} - 1 \right) I_{sc} \tag{2.9}$$

$$\Delta V = -\beta\, \Delta T - R_s\, \Delta I \tag{2.10}$$

$$I = I_r + \Delta I \tag{2.11}$$

Here the suffix 'r' refers to rated conditions given by $E_r = 1000$ W/m^2 and $T_r = 25^oC$.

The characteristics of any PV generator may be simulated through equations (2.1) to (2.11) under a variety of operating conditions (ambiant temperature, insolation, cloud cover, etc).

Figure 2.5 shows typical I-V characteristics for increasing insolation levels of the used PV array. One could see that short circuit current varies in proportion to the insolation level, while the open circuit voltage is approximately constant. Consequently the extracted electric power will increase accordingly. Each curve has a maximum power point P_M (dashed line), which is the optimal operating point for an efficient use of the solar array.

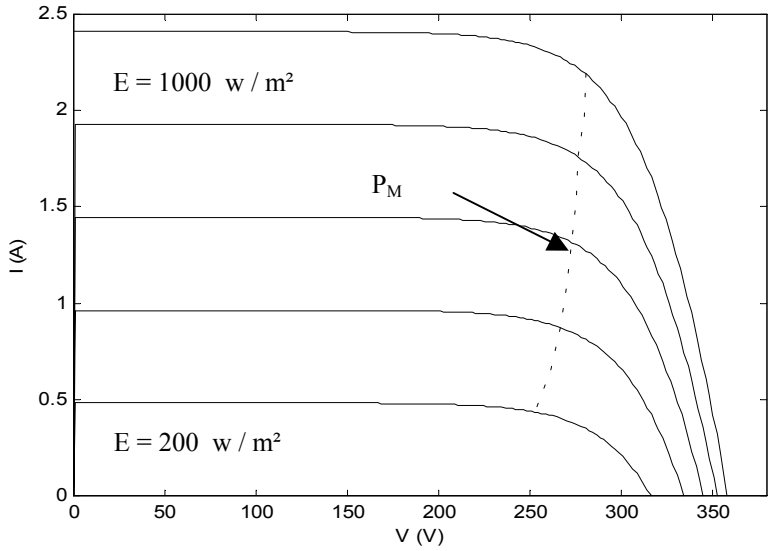

FIG 2. 5 I-V Characteristics for variable Insolation level ($T_c = 25°C$).

Since the operating temperature of a solar cell varies over a wide range, it is essential to understand the effect of temperature changes on both the open circuit voltage and short circuit current. The current increases slightly as the temperature increases; this is due to increased light absorption. However, as the temperature increases the open circuit voltage tends to decrease as shown in **Figure 2.6**. As a result of V_{oc} reduction, the output power decreases by 0.44 %/°C for the used array.

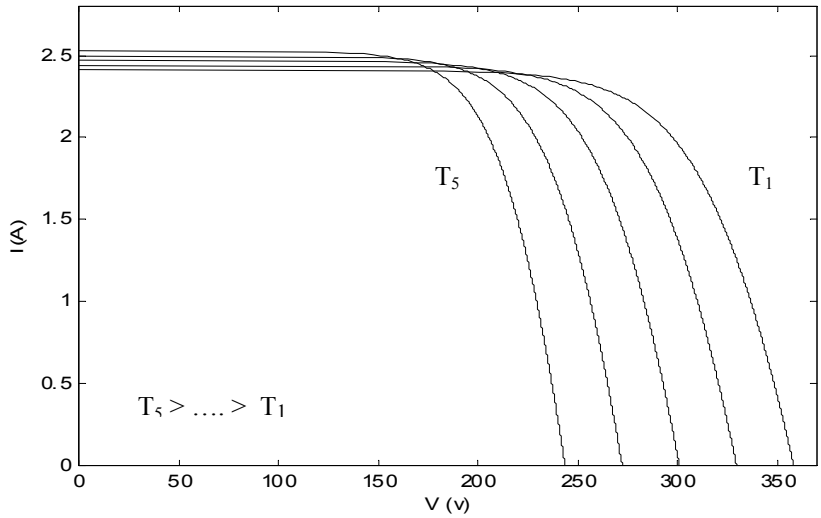

FIG 2.6 Typical I-V Characteristics for variable Temperature (E =1000 W/m²)

To avoid the destruction of PV-cells due to the 'hot-spot effect', manufacturers connect by-pass diodes over a group of cells, **figure 2.7**; with this arrangement a substring with a shaded cell will be short-circuited by the by-pass diode and the non-shaded substrings can work, but the energy from the by-passed substring is lost. It is important to underline that this is normally only a method for the protection of PV cells. If by-pass diodes are to be used to make the PV-module more shade-tolerant, they should be connected to significantly fewer PV cells [37].

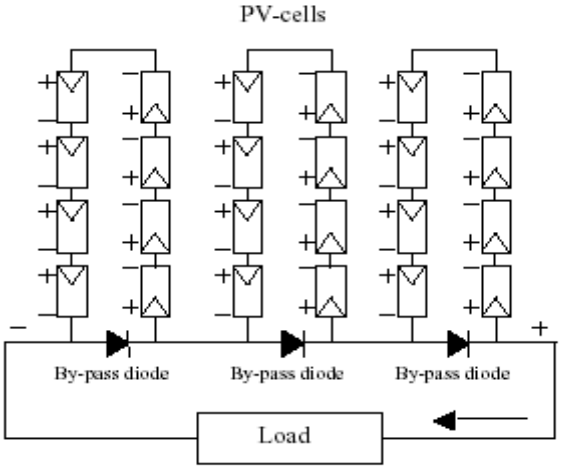

FIG 2.7 Protection by by-pass diodes [37]

2.3.3 The Conversion efficiency :

The conversion efficiency of a PV generator is defined as the ratio of the useful maximum electrical power output to the incident solar power [25] :

$$\eta_{con} = \frac{V_{op} . I_{op}}{E . A} \qquad (2.12)$$

A is the generator effective area in m^2.

Manufacturers may quote a "reference efficiency." This is simply the module efficiency at reference testing conditions, taken generally for an insolation of 1000 W/m^2 and a cell temperature of 25° C. The maximum power is given as the product of current and voltage at the maximum power point.

Figure 2.8 shows performance levels reached over the last 50 years development period, showing that the rate of progress varying quite significantly with material understanding [5].

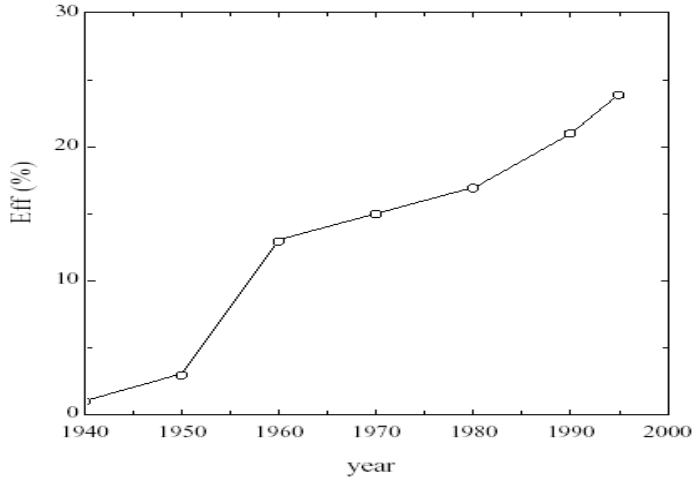

FIG 2.8 Evolution of Silicon solar cell efficiencies [5]

2.3.4 The Form Factor :

This is a module performance factor, identified by the ratio of the maximum extracted power to the product of the short-circuit current and the open-circuit voltage [23]:

$$FF = \frac{V_{op} \cdot I_{op}}{I_{sc} \cdot V_{oc}} \tag{2.13}$$

2.4 THE VOLTAGE SOURCE INVERTER MODEL :

The supply of an induction motor by the solar generator requires the use of an inverter which transforms the DC-voltage into a three phase AC-system with variable frequency and voltage. There are two basic types of forced-commutated inverter : The *current source inverter* and the *voltage source inverter* .

In photovoltaic pumping applications, it has been concluded that the latter inverter is considered the best choice [5]. Other types of inverters such as multi–level inverter with separated DC sources and Optimised harmonic-stepped waveform technic [38] which is well adapted in such applications can also be used.

2.4.1 Converter Requirements :

Basic requirements imposed to DC-AC converter are :

- Generate smooth Variable-Frequency Variable-Voltage (VVVF) power.
- Produce nearly sinusoidal current waveforms throughout the operating range to avoid undesirable torque oscillations
- Permit highly dynamic control both in motoring and braking operation.
- Provide as nearly as possible equivalent performance to the dual converter-fed dc drives as regards cost, service reliability, and harmonic effect on the system.

In the scope of the present work, three different technics are used to control the VS inverter feeding the induction motor.

2.4.2 Sinusoidal PWM Strategy :

A natural PWM switching technique is used to drive the full bridge inverter with an amplitude modulation index M and a frequency modulation index P. The capacitor across the inverter input terminals as shown in **figure 2.1**, serves to smooth the output voltage of the DC source and to reduce the source impedance. The three phase inverter consists of three legs, one for each phase. It is assumed that the switches and diodes are ideal devices. The control signals are generated by modulating three low frequency sinusoidal signals (called reference waveforms) with a common high frequency triangular carrier wave as shown in **figure 2.9**. The switching instants are determined by the crossover of the two waveforms.

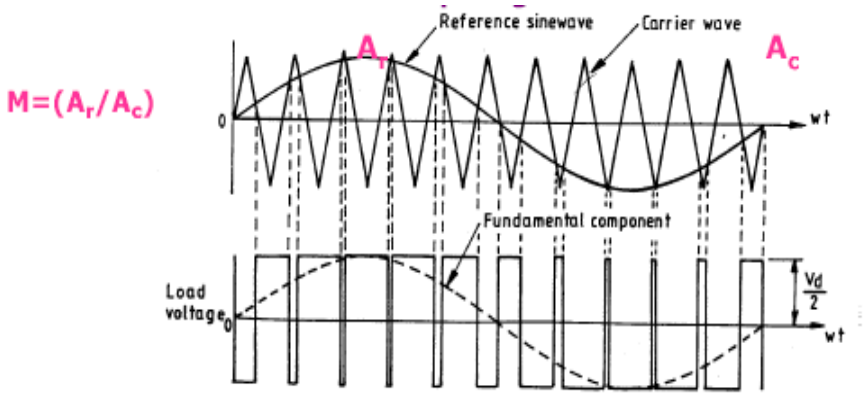

FIG 2.9 Sinusoidal PWM strategy principle

As shown in **figure 2.10,** for a balanced, three-phase, star connected, the r.m.s value of the fundamental component of the modulated line to neutral voltage V_m is proportional to M in the range of $0 \leq M \leq 1$, for all values of P > 9 [39]:

$$V_m = \frac{M \cdot V}{\sqrt{2}} \qquad (2.14)$$

An increase of the fundamental component is possible by making M>1; however V_m will be no longer proportional to M. In this condition of overmodulation, some intersections between the carrier wave and the modulating wave are lost [40]. In the extreme, when M reaches the value M = 3.24 the original forms of PWM waveform are lost and the phase voltages then revert to the quasi-square wave-shape.

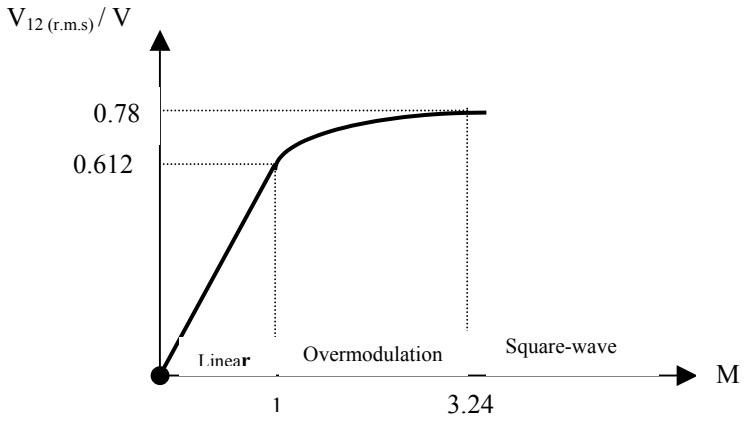

FIG 2.10 Voltage index-rms value relationship [39]

In the present study, the carrier frequency is fixed at 750 Hz and P is set at P = 15 for the nominal insolation level E = 1000 W/m². Consequently, the motor will be unaffected by the high order harmonics generated by the inverter for all insolation levels since these harmonics, which appear as side-bands centred around the switching frequency multiples (k.P.f) are naturally filtered by the motor itself.

2.4.3 Selective Harmonic Elimination PWM Strategy (SHE PWM) :

In this method called also ***Optimal PWM Control,*** the (m-1) unwanted lowest odd harmonics of a square wave need to be eliminated and the fundamental voltage component can be controlled.

To achieve this, the inverter switchings occur at chops defined as α_1, α_2, …., α_m in a quarter-cycle of the period as shown in **figure 2.11**. Fourrier analysis of the above waveform indicates that the rms value of the n^{th} harmonic is given by [39] :

$$V_m = \frac{2.\sqrt{2}}{n.\pi} V . \left[1 + 2. \sum_{i=1}^{m} (-1)^i . \cos\ (n.\alpha_i) \right] \tag{2.15}$$

Generally, in a three-phase system, the lowest non-triplen harmonic components are to be eliminated, whereas, all triplen-harmonics are naturally eliminated.
In the present case, the fundamental component is controlled throughout the continuous control of the switching angles α_i, which are adjusted properly to eliminate the lowest order harmonics 5, 7 and 11. Thereafter, the four angles are obtained by resolving the following equations [23]:

$$V_m = \frac{2.\sqrt{2}}{\pi} V \begin{bmatrix} 1 - 2.\cos(\alpha_1) + 2.\cos(\alpha_2) - \\ 2.\cos(\alpha_3) + 2.\cos(\alpha_4) \end{bmatrix} \tag{2.16}$$

$$\begin{bmatrix} 1 - 2.\cos(5.\alpha_1) + 2.\cos\ (5.\alpha_2) - \\ 2.\cos(5.\alpha_3) + 2.\cos(5.\alpha_4) \end{bmatrix} = 0 \tag{2.17}$$

$$\begin{bmatrix} 1 - 2.\cos(7.\alpha_1) + 2.\cos\ (7.\alpha_2) - \\ 2.\cos(7.\alpha_3) + 2.\cos(7.\alpha_4) \end{bmatrix} = 0 \tag{2.18}$$

$$\begin{bmatrix} 1 - 2.\cos(11.\alpha_1) + 2.\cos\ (11.\alpha_2) - \\ 2.\cos(11.\alpha_3) + 2.\cos(11.\alpha_4) \end{bmatrix} = 0 \tag{2.19}$$

$$0 \le \alpha_1 \le \alpha_2 \le \alpha_3 \le \alpha_4 \le \frac{\pi}{4} \tag{2.20}$$

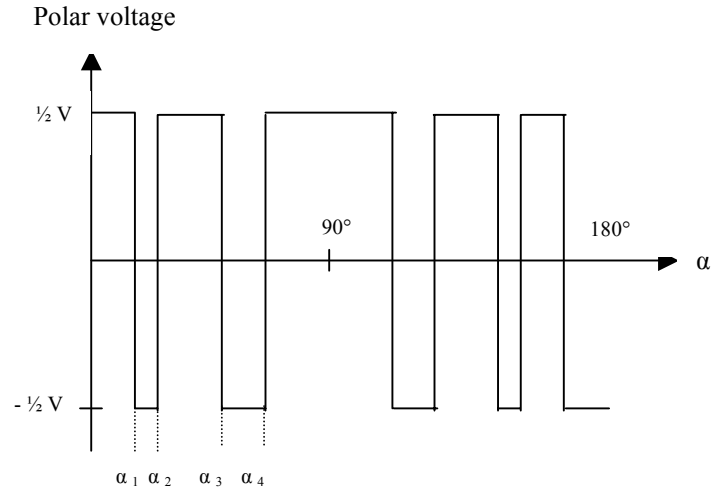

FIG 2.11 Polar voltage curve of a PWM inverter

The non-linear nature of the above equations calls the use of numerical resolution methods such as Newton-Raphson to get the required solution. For an eventual implementation, the switching angles could be stored in look-up tables and then sent to down-counters .

2.4.4 The Pondered Harmonic Minimization Strategy :

Instead of eliminating specific harmonics, one could use another alternative where performance indexes are considered. This approach is to define a performance index related to the undesirable effects of the harmonics and to select the switching angles so that the fundamental voltage is controlled and the performance index is minimised. This is called a

distortion minimisation PWM technic. In this method the total harmonic voltage distortion factor (THD) is minimised . The minimisation of this quantity and the control of the fundamental are achieved by an appropriate positioning of the four switching angles. The THD performance factor is defined as [39] :

$$THD = \left[\sum_{K \neq 1}^{n} \left(V_K / k \right)^2 \right]^{1/2} \tag{2.21}$$

Other mathematic forms of the THD factor could be also used.
In the present work, the number of the lowest odd harmonics to be minimised is chosen as k =41.

Taking into consideration equation (2.15), the THD factor showed in equation (2.21) becomes :

$$\min im \left[\sum_{K \neq 1}^{n} \left(\frac{\frac{2.\sqrt{2}}{n.\pi} V . \left[1 + 2. \sum_{i=1}^{m} (-1)^i . \cos\ (n.\alpha_i) \right]}{n} \right)^2 \right]^{1/2} \tag{2.22}$$

2.5 THE UNSATURATED CAGE INDUCTION MOTOR MODEL :

The operation principle of the asynchronous motor is well known and is extensively described in classical motor literature [39]. Based on the induction law the rotating magnetic field induces a voltage in the standstill rotor which causes a current to flow in the rotor windings. According to Lenz law, the current flowing through the winding conductors of the rotor produces a tangential force which produces a torque in the rotor axis and sets the rotor in movement. The asynchronous motor runs at a shaft speed ω that is less that the synchronous speed ω_s. We define thus the slip frequency :

$$\omega_{sl} = \omega_s - \omega \tag{2.23}$$

Inherent Advantages:

- Lower cost and size
- Less maintenance
- Single supply, absence of excitation control loop
- Simple and robust structure
- Quick response
- High overload capacity

Inherent Disadvantages:

- Low power factor
- Speed regulation with load

Typical Applications

- Steel Mills
- Paper /Textile Mills .
- Servos
- Cement Mills /Ore Grinders
- Electric Vehicles /Traction /Ship Propulsion
- Mine winders
- Pumping Systems.

Equivalent Circuit :

The steady state performance of an induction motor is modelled using the conventional equivalent circuit , **Figure 2.12**.

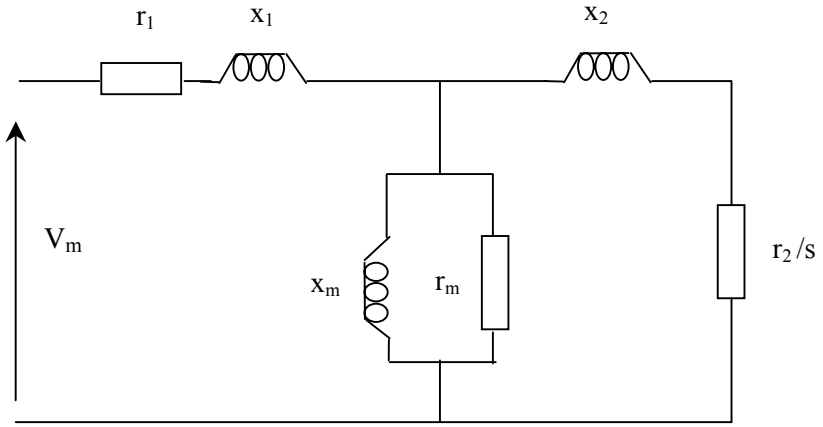

FIG 2.12 Induction motor equivalent circuit

The input electric power is given by :

$$P_{abs} = 3 . R_{eq} . \frac{V_m^2}{Z_{eq}^2} \tag{2.24}$$

Where Z_{eq} is the equivalent input impedance per phase :

$$Z_{eq} = R_{eq} + j X_{eq} \tag{2.25}$$

The mechanical equation in steady state is given by:

$$T_e = T_r + f_r . \omega \tag{2.26}$$

Here the electromagnetic torque T_e is expressed as follows [39]:

$$T_e = 3.p.(\frac{V_m}{\omega_s})^2 \frac{\omega_{sl} . \frac{x_m^2}{r_2}}{\left[r_1 - \frac{\omega_{sl}}{\omega_s . r_2} \left(x_{11} . x_{22} - x_m^2 \right) \right]^2 + \left[x_{11} + \frac{\omega_{sl} . r_1 . x_{22}}{\omega_s . r_2} \right]^2} \tag{2.27}$$

The centrifugal pump load torque T_r presents an aerodynamic shape and is assumed to be proportional to the square of the rotor speed [24] :

$$T_r = C \left(1 - \frac{\omega_{sl}}{\omega_s} \right)^2 . \omega_s^2 \tag{2.28}$$

C is a constant which depends on pump nominal data and f_r the friction coefficient.
Considering the fundamental harmonic component, the motor power factor is given by the following expression:

$$PF = \frac{R_{eq}}{Z_{eq}} \tag{2.29}$$

The breakdown torque occurs at a particular slip frequency known as the rotor breakdown frequency, given by the familiar form [39]:

$$\omega_{slb} = \frac{\omega_s . r_2}{\sqrt{\left(r_2^2 + (x_1 + x_2)^2\right)}} \tag{2.30}$$

The serious reduction of the breakdown torque occurs at low frequencies. To improve the low-frequency characteristics, the terminal voltage must be increased as it will be investigated in the next chapter.

When the induction motor is fed through an inverter instead of a sinusoidal supply, the motor behaviour can be analysed independently for the fundamental and for each harmonic term, and the overall response is then obtained by the summation of the responses to the individual components. For the k^{th} harmonic term, the following equivalent circuit can be used [40].

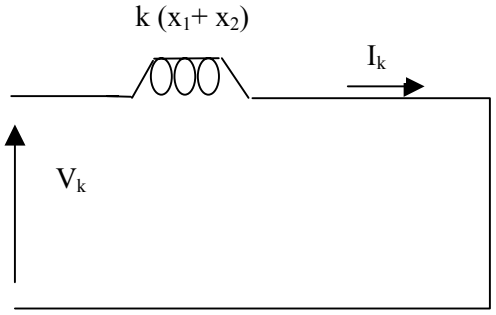

FIG 2.13 Harmonic equivalent circuit

If V_k denotes the k^{th} harmonic component of the supply, the corresponding stator current is given by :

$$I_k = \frac{V_k}{k.(x_1 + x_2)} \tag{2.31}$$

This formulae permits a rapid evaluation of the total r.m.s harmonic current, given by :

$$I_h = \sqrt{I_5^2 + I_7^2 + I_{11}^2 + I_{13}^2 + ... + I_k^2 + ...} \tag{2.32}$$

2.6 THE CENTRIFUGAL PUMP MODEL :

A pump is a machine for converting input kinetic power into fluid output power. The output power is represented by the delivery of the pump in terms of flow-rate and head. Depending on the application and the type of water source supply (deep well or surface water form), different pump principles are utilised in PV-pumping systems. For the selection of a solar pump, this later has to :

1- meet the required performances as :
   a- capacity
   b- head
   c- suction
2- provide satisfactory working, viz :
   a- be efficient
   b- be easy to maintain.

The most world-wide used pumps are :

- Centrifugal pumps, which are more suitable for small to medium head have their power output increased with speed accordingly.
- Positive displacement pumps, suitable for deep wells have a flow-rate which is normally independent of head. On the other hand, have a water output proportional to speed.

According to [79], the most drawback of the use of centrifugal pump is that a threshold speed (35-40 Hz) is required to convey water to the surface. The rotating displacement pumps present a viable solution, starting pumping at nearly zero speed.

There are various combinations of motors and pumps, which are suitable for use with solar power, such as [5]:

1- Submerged motor/pump with centrifugal multi-stage pump.
2- Submerged pump arrangement with pump below the water, driven by the shaft from a motor mounted above the water.
3- Surface mounted pumps with a self priming tank.

In the present study, a squirrel cage induction motor, mounted on the surface driving a submerged monocellular centrifugal pump is analysed, **figure 2.1**.
A centrifugal pump basically comprises an impeller (rotating part) and a volute (stationary part). The main parts of the centrifugal pump are shown in **figure 2.14**.
The energy transfer is achieved through flow deflection of the fluid in the impeller. The fluid entering the impeller centre is picked up by the blades. The rotation motion of the impeller transfers energy to the fluid as it flows outwards through the impeller.

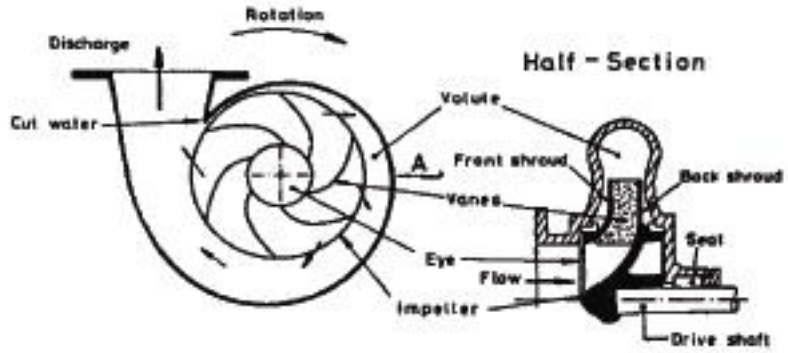

FIG 2.14 Sectional view of the basic construction of a centrifugal pump [5]

The operation of centrifugal pumps is generally described by their Head-Flow-rate characteristics. For an ideal pump with an infinite number of blades and where the blades channels are infinitely thin, the H-Q characteristic at a given rotational speed ω_0 can be obtained from the theoretical head H_{th}, when the friction losses and shock losses within the pump are subtracted.
The theoretical head is given by [41] :

$$H_{th\infty} = \frac{(\omega_0 . r_2)^2}{g} - \frac{\omega_0 . Q}{2.\pi.g.b_2 . \ _v . tg(\beta_2)} \tag{2.33}$$

where η_v represents the pump volumetric efficiency, given as the ratio between the flow-rate in the delivery canalisation Q and the that inside the impeller Q_t :

$$\eta_v = \frac{Q}{Q_t} \tag{2.34}$$

The influence of the finite number of blades Z is manifested via two corrections:

2.6.1 Influence of the blade thickness S:

The influence of the blade thickness S is introduced via a corrective coefficient φ_2 [41]:

$$\varphi_2 = \frac{1}{1 - \frac{S}{T_2 . \sin(\beta_2)}} \tag{2.35}$$

where T_2 is the step between two consecutive blades, given by:

$$T_2 = \frac{\pi . d_2}{Z} \tag{2.36}$$

2.6.2 Influence of the blades finite number Z:

The influence of the finite number of blades Z is manifested via a second correction factor, called '*PFLEIDER coefficient*'[41]:

$$\varepsilon_P = \frac{1}{1 + P_p} \tag{2.37}$$

where:

$$P_p = \frac{1.2}{Z} \frac{1 + \sin(\beta_2)}{1 - \left(\frac{d_1}{d_2}\right)^2} \tag{2.38}$$

Taking into consideration of the two above corrections, theoretical head expression becomes :

$$H_{th} = \frac{\varepsilon_p}{g} \left[(\omega_0 . r_2)^2 - \frac{\varphi_2 . \omega_0}{2 . \pi . r_2 . b_2 . tg(\beta_2)} Q \right] \tag{2.39}$$

In the case of a real pump, the friction losses (head losses) which are caused by turbulent flow occurring in the pump bearings, in the shaft seals and at the impeller shrouds are not negligible. These losses have the following form [41]:

$$\Delta H_{fr} = A_1 . Q^2 \tag{2.40}$$

Where A_1 is the load losses coefficient, identified at the nominal operating point (H_n , Q_n) by:

$$A_1 = \frac{H_{th\,n}(Q_n) - H(Q_n)}{Q_n^2} \tag{2.41}$$

The real total head-flow-rate dependence at a given speed ω_0 becomes then:

$$H = H_{th} - \Delta H_{fr} \tag{2.42}$$

Finally, the Flow-Head characteristics of a centrifugal pump, **figure 2.15**, driven at a rotor speed ω can be approximated by quadratic form using Pfleider-Peterman model [24]:

$$H = a_0 . \omega^2 + a_1 . \omega . Q + a_2 . Q^2 \tag{2.43}$$

where the motor speed ω is expressed as :

$$\omega = \left(1 - \frac{\omega_{sl}}{\omega_s}\right).\omega_s \tag{2.44}$$

a_0, a_1 a_2 are constants depending on the pump dimensions, and given by :

$$a_0 = \frac{\varepsilon_p}{g.\omega_0^2}\ r_2^2 \tag{2.45}$$

$$a_1 = \frac{\varphi_2}{2.\pi.r_2.tg(\beta_2).\omega_0^2} \tag{2.46}$$

$$a_2 = A_1 \tag{2.47}$$

For the pump considered in this study, the constants a_0, a_1 a_2 were found as:

$a_0 = 1.93.\ 10^{-4}$ $a_1 = 2.36$ $a_3 = 451538.94$

2.6.3 Pump efficiency:

The pump efficiency is defined as the ratio of hydraulic power imparted by the pump to the fluid to mechanical power at the pump shaft, and is given by [23] :

$$\eta_p = \frac{\rho\, g\, H\, Q}{C\left(1 - \frac{\omega_{sl}}{\omega_s}\right)^3 \omega_s^3} \tag{2.48}$$

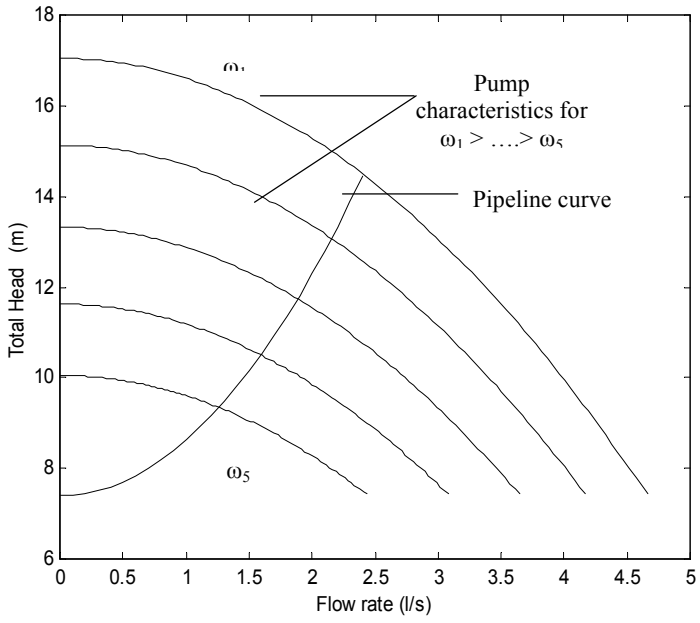

FIG 2.15 Pump Head-flow-rate characteristics

2.7 PIPELINE MODEL :

The proposed optimisation algorithm is carried out on a system installed at the research unit of Batna university as shown in **figure 2.16**. It comprises a suction and a delivery tank, that are separated by a single pipeline.

The volume of the two buffer tanks are respectively : 2.88 m^3 and 0.78 m^3, while the geodetic head of the plant is: $H_g = 7.4$ m.

The H-Q characteristic of the pipe network can be expressed by [22]:

$$H = H_g + \Delta H \tag{2.49}$$

Where ΔH are the sum of the linear losses due to friction inside the pipeline and singular losses caused by section changing. In the case of the present testing rig, these head losses are given by [41]:

$$\Delta H_1 = \lambda \frac{1}{d} \frac{C_1^2}{2.g} + \xi . \frac{C_1^2}{2.g} \tag{2.50}$$

Where C_1 is the average flow speed, expressed by :

$$C_1 = \frac{4.Q}{\pi . d^2} \tag{2.51}$$

Finally, the H-Q characteristic of the pipe network is given as a function of the geodetic head and flow-rate by [23]:

$$H = H_g + \psi . Q^2 \tag{2.52}$$

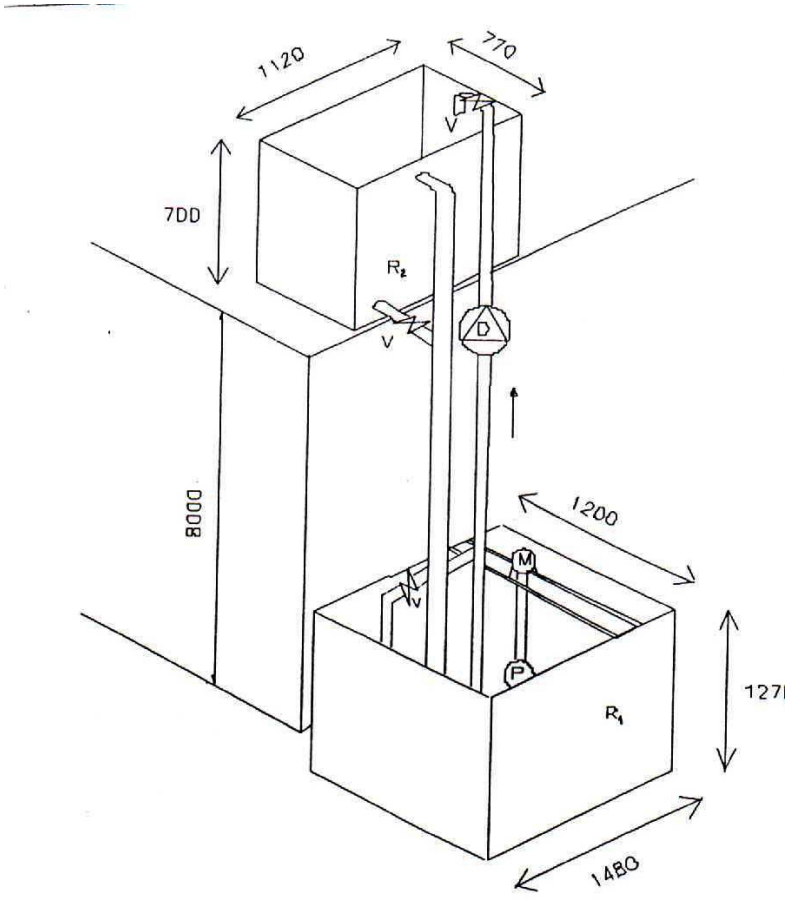

FIG 2.16 Overview of the PV pumping plant

2.7 INSOLATION MODEL:

As shown in **figure 2.16**, a simplified approach was elaborated according to [42], and which will serve as a first approximate quantification of the incidental insolation. This model quantifies the irradiation for a standard clear day:

$$E = E_M \sin(15.(t - t_{sr})).\frac{\pi}{180} \tag{2.53}$$

The sunrise time is chosen as : t_{sr} = 6 h.00'.

One can notice that in the case of a centrifugal pump, a threshold power (insolation) is required to convey water to the surface. This behaviour is important for the design of standard impeller pumps used in deep wells, since at larger depth an increasing amount of energy is not used due to this phenomenon.

We define so the solar radiation utilisability as the ratio of the total insolation levels that exceed the threshold value to the total available insolation over the day [5]:

$$\mu = \frac{\int_{t_l}^{t_{ss}-t_l} (E - E_{th})\,dt}{\int_{t_{sr}}^{t_{ss}} E\,dt} \tag{2.54}$$

t_l is the hourly time when the insolation crosses the threshold level.
t_{ss} is the sunset time chosen as : t_{ss} = 18 h.00'.

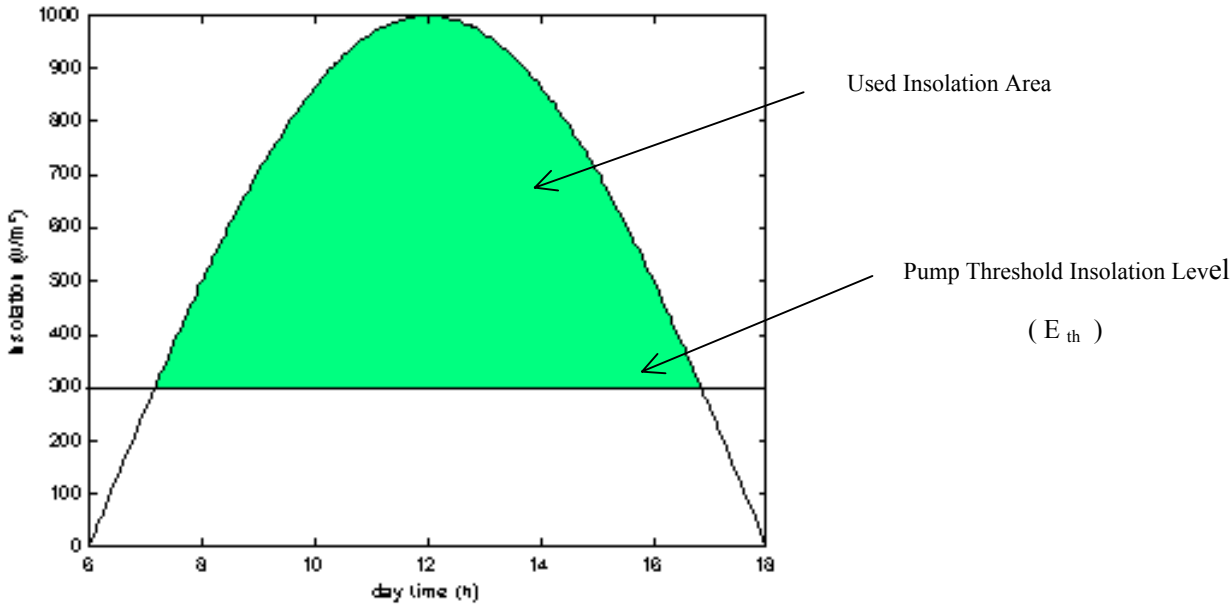

FIG 2.17 Daily insolation curve

2.8 CONCLUSION :

PV pumping system component models for use in the present work were identified and developed as necessary in this chapter. The fundamental components of the system like the PV array, the motor, the pump and the pipeline were modeled in a straightforward manner based on fundamental principles verified by previous researchers. These models will simulate the performance of a real system correctly as can be seen in chapter 4. In the derivation of the system equations, the motor was supposed unsaturated and the the inverter was also supposed ideal.

Chapter 3
DESCRIPTION OF THE MOTOR OPERATING APPROACHES

3.1 INTRODUCTION :

The performances of a photovoltaic pumping system based on an induction motor are degraded once the insolation varies far from the value called nominal, for which the system is sised. To surmount this handicap, an improvement of these performances is explicitly described in this chapter. The study fixes as a goal the maximisation of the daily pumped water quantity, which is the requirement of everyone. People are interested in storing the maximum water quantity in the day before starting irrigation at night with pressure. This is achieved by establishing an optimal 'v-f' relationship useful in controlling the induction motor, and where the VS inverter control is achieved through the three previously described PWM strategies. The effectiveness of the proposed algorithm is proved by simulation and the obtained results are compared with those of similar work pieces presented in literature called ***'constant air-gap flux system'*** provided by [5] and ***'constant motor efficiency system'*** given by [33].

The chapter starts with the detailed description of the first system called 'Constant air-gap flux operation', including the derivation of the required equations allowing simulation of the complete system over a standard clear day described in the second chapter. Afterword, similarly the second system called 'Constant motor operation' is presented. The chapter will be concluded by an explicit analysis of the proposed optimisation approach, criterion and method for the three inverter control strategies.

3.2 CONSTANT AIR-GAP FLUX OPERATION [5] :

The solar pumping system described in [5] is a small scale system where the photovaltaic array is directly coupled to the asynchronous motor driving the monocellular centrifugal pump via a sinusoidal PWM voltage source inverter, **figure 3.1.** This figure is mentioned in chapter 2 and entitled (figure 2.1). Motor voltage is controlled accordingly to frequency variation so that motor air-gap flux is kept constant.

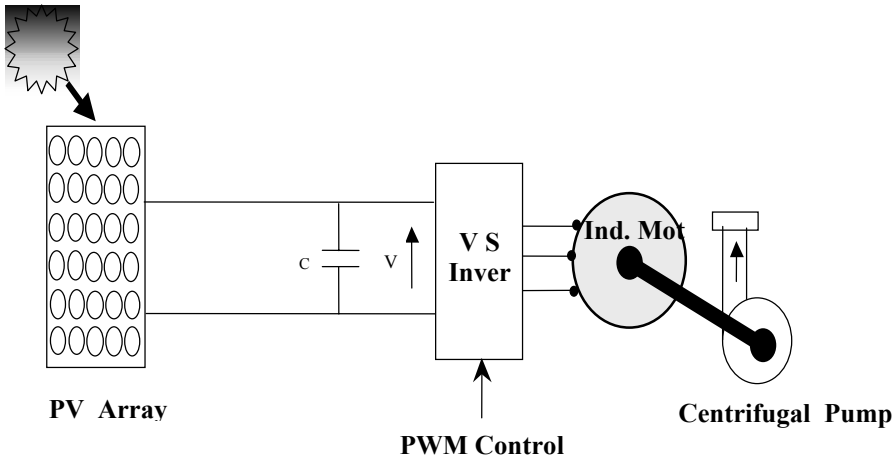

FIG 3.1 The PV scheme structure

Generally, in variable speed drives, motor air-gap flux is maintained constant at all frequencies so that the motor can deliver a constant torque. This will occur if the V_m/f ratio

is kept constant at its nominal value. To compensate the voltage drop due to stator resistance effect at low frequencies, a boost voltage V_{mo} is added to phase voltages. For aerodynamic loads, the stator voltage as function of frequency is given by [5] :

$$V_m = V_{mo} + k.f^n \qquad \text{for } 0 \le f \le f_N \tag{3.1}$$

If $f > f_N$, the motor operates at constant power mode :

$$V_m = V_{mN} \quad \text{for } f \ge f_N \tag{3.2}$$

In steady state operation, identification of equation (3.1) for the concerned load needs solving the mechanical equation for a stator frequency range (f = 0 to f = 50 Hz), and where the electromagnetic torque is expressed as a function of the slip frequency ω_{sl} [39]:

$$T_e = 3.p\left[\frac{E_1}{\omega_s}\right]^2\left[\frac{\omega_{sl}.r_2}{r_2^2 + (\omega_{sl} L_2)^2}\right] \tag{3.3}$$

The solution of the above mechanical equation is carried out using Newton-Raphson method which is well adapted to non-linear equations.

Under constant-flux conditions, air-gap emf, E_1, is varied linearly with stator frequency :

$$E_1 = \frac{V_N}{\omega_{sN}}.\omega_s \tag{3.4}$$

Stator voltage values depicted in **figure 3.2,** allowing constant air-gap operation, are derived thereafter from combination of motor equations given by motor equivalent circuit (see chapter 2).

Stator current I_1 is given by the phasor sum of I_m and the rotor current I_2 . Thus [39]:

$$I_1 = \left[\frac{E_1}{\omega_s}\right]\left[\frac{r_2 + j.\omega_{sl}.L_{22}}{-\omega_{sl}.L_2.L_m + j.r_2.L_m}\right] \tag{3.5}$$

Terminal voltage V_m is then obtained by phasor addition of the air-gap emf E_1 and stator voltage drop $(r_1 + j\, x_1)$. I_1:

$$V_m = E_1 + (r_1 + j.x_1).I_1 \tag{3.6}$$

Finally, for the concerned load, equation (3.1) expressed in **figure 3.2** is identified by the **least square** method for the constants :

$$V_{mo} = 6.3366 \text{ v} \qquad k = 3.2485 \qquad n = 1.0965$$

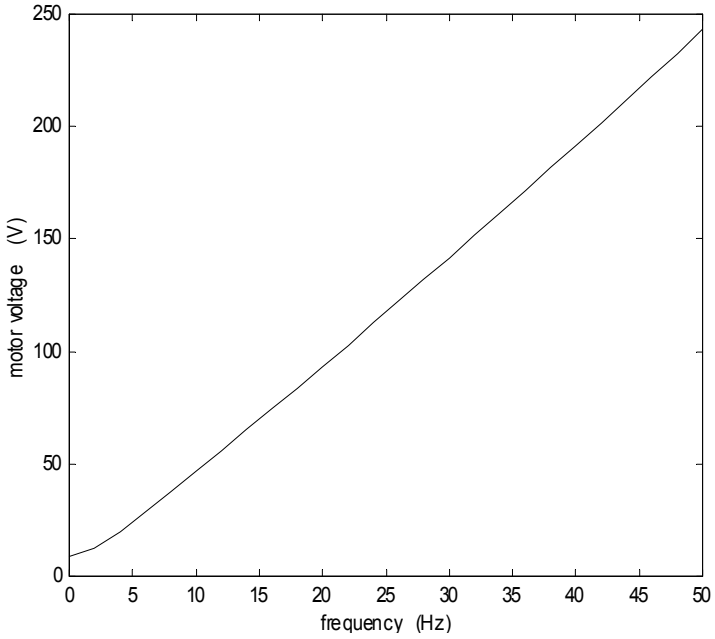

FIG 3.2 Voltage-frequency relationship for air-gap flux operation

In order to optimise the extracted electric energy, the PV array should always be operated close to its maximum output power. This will be obtained by setting up a linear relationship between the generator voltage and frequency [5]:

$$V = C_{10} + C_{11}.f \tag{3.7}$$

In the generator I-V plan and under equation. (3.7), the system may operate in three intervals:

a) $V < V_{op} \longrightarrow P_e < P_M$
b) $V = V_{op} \longrightarrow P_e = P_M$
c) $V > V_{op} \longrightarrow P_e < P_M$

It was shown in [34] that case (a) corresponds to an unstable motor operation since the motor speed presents a non-minimum phase response and highly oscillating evolutions of ω are noticed. Case (b) implies the use of MPPT [6]. In this study, the last case is adopted since a stable operation is ensured [5]. In order to avoid operation in case (a), constant C_{10} should be greater than V_{op} for low frequencies. However, C_{11} which gives the curve slope should not be too small so as the operating point would not be far from the optimum one for high insolation values.

For the present study, constants are chosen as follows:
C_{10} = 260 v (corresponding to V_{op} of insolation level E = 100 w/m²), and C_{11} = 0.3.
The equation (3.7) must verify the I-V array equation:

$$V_{th}.\ln\left(\frac{I_{sc} - I + I_o}{I_o}\right) - I.R_s = C_{10} + C_{11}.f \tag{3.8}$$

In addition, the power balance equation of the system leads to the following expression:

$$\left(V_{th}.\ln\left(\frac{I_{sc} - I + I_o}{I_o}\right) - I.R_s\right).I = 3.\frac{R_{eq}}{Z_{eq}^2}.V_m^2 \tag{3.9}$$

Simulation of the 'Constant Air-gap flux system' :

The interaction of system components is explained bellow. The system's technical data are those given in **Table1** of chapter 2. In addition, it is supposed the system does not consider any transient behaviour.
The model is fed with meteorological operating parameters, such as solar insolation given by equation (2.53), and for a reference temperature T_r = 25 °C. The geodetic head of the plant is set to H_g = 7.4 m.
The model of the complete PVP-system searches automatically, for each insolation level, a working point characterised by a triplen (ω_{sl} , f , I) solution of non-linear equations system
F (X) = 0 formed by the set of equation (2.24), (2.26), (3.8) and (3.9), taking into consideration equation (3.1), and (3.20).
The non-linear nature of F(X) calls for numerical methods to be used. The solution sequences are then performed by Newton-Raphson method.

the pump flow- rate is then obtained by equating pump H-Q characteristics and pipeline H-Q expression, given respectively by equation (2.43) and (2.52).

3.3 CONSTANT MOTOR EFFICIENCY OPERATION:[33]

Similarly to the previous system, the 'Constant Motor efficiency system' described in [33] is a small scale PVP-plant where the photovoltaic generator is coupled to an asynchronous motor via two static converters: the first is a buck-boost chopper working as an impedance adapter, while the second is a PWM voltage source inverter as shown in **figure 3.3**.

Yao said that by a proper adjustment of the inverter frequency, a constant optimum value of the motor efficiency is ensured, while the maximum power of the PV generator is made available to the load by a the chopper operating as a Maximum Power Point Tracker (MPPT). Even if an optimal motor efficiency is preserved, the preservation of the DC/DC power stage makes the implementation more expensive.

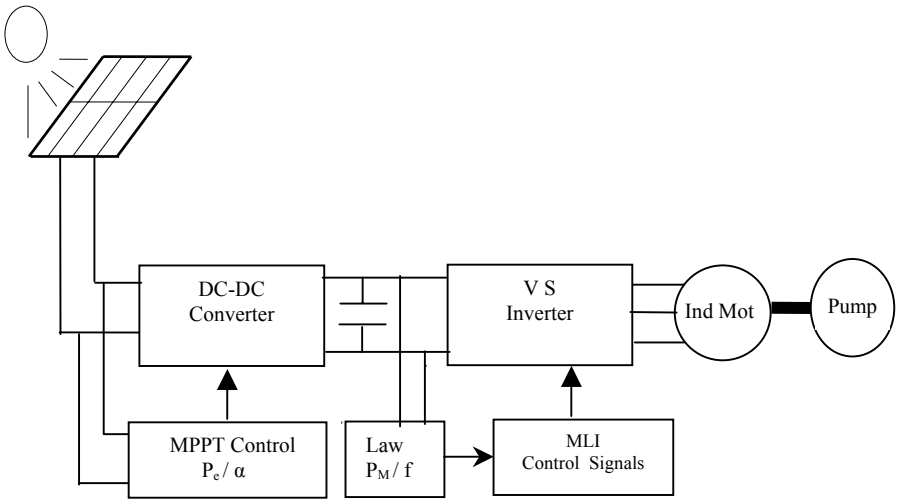

FIG 3.3 PV scheme structure described in [33]

3.3.1 Control Law Elaboration :

A new system with variable frequency control has been designed by Yao *et al*. The work reports on an investigation carried out to improve the motor efficiency leading to an improvement of the whole system. The motor efficiency and, therefore, the power delivered to the load are adjusted according to insolation conditions by controlling inverter frequency. This eliminates the mismatch between the maximum power that is available from the source and the power that is required by the load.[33].

Generally, the power required by a mechanical load depends on its speed and in a PV-powered system, the rated speed of the motor is designed for normal insolation level, under which the system works well. When a variation of insolation appears, motor efficiency drops and even unstable operation may occur. This is usually being revealed by oscillations in the motor speed, but Yao proposes a frequency-control algorithm to avoid these drawbacks. It is achieved by adjusting the control signal frequency of 'the modulating waveform' of the natural PWM strategy in a self-manner according to the power available from the PV array. Optimum motor efficiency can thus be reached for both a temporay variation and long term operation.

3.3.2 Control law Determination :

In the case of Parabolic torque load such as centrifugal pumps, the following relation between input power and mechanical output power for nominal insolation condition exist, and where static converters are assumed ideal :

$$P_{MN} . \eta_o = C_1 . (1 - s_o)^3 . f_N^3 \qquad (3.10)$$

η_o and s_o are respectively the optimum motor efficiency and optimum slip obtained under rated condition (E = 1000 W/m²) for which the system was sized. P_{MN} is the input power, equal to the maximum output power of the PV array at nominal insolation level, and f_N is the normal source frequency (f = 50 Hz). In the present work, the rated motor efficiency and slip are found as : $\eta_0 = 0.71$ and $s_0 = 0.02$.

When the insolation changes, equation (3.9) becomes :

$$P_M.\eta = C_1 (1 - s)^3 f^3 \quad (3.11)$$

Where P_M is the input power corresponding to the changed insolation level, and f is the new frequency to be found.
Since it is desirable that the system operates at its optimum efficiency η_o and motor slip s_o, Equation (3.11) is now :

$$P_M.\eta_o = C_1 (1 - s_o)^3 f^3 \quad (3.12)$$

From equation (3.10) and (3.12), the new control frequency of the inverter is found to be :[33]

$$f = \sqrt[3]{\frac{P_M}{P_{MN}}} f_N \quad (3.13)$$

The control strategy is [33]:

1- *Increase the control signal frequency of the inverter when the input power is larger than its nominal value, so as to keep the motor slip down.*
2- *Decrease the control signal frequency as an effort to maintain the slip at its optimum value when the input power is low.*

For an eventual implementation, f denotes the modulating waveform frequency of the sinusoidal PWM inverter; whereas the modulation index is always kept constant: M = 0.8.

The main steps to simulate the interaction of the system components are:

i. Introduce the rated data of the PVP system
ii. Introduce the insolation initial level.
iii. Calculate the maximum power P_M.
iv. Calculate the correspondant inverter frequency f given by equation (3.13).
v. Increase the insolation level.
vi. Go then to step iii.

3.3.3 Maximum Power Point Tracking Algorithm:

It is reasonable to assume that the DC–DC converter is loss free, that is, all power converted by the PV array can be transformed to the load.
The firing angle of the chopper α_m which corresponds to the maximum power point is found and tracked by the following algorithm [43]:

$$\Delta\alpha = h.\text{sign}\left(\frac{\Delta P}{\Delta\alpha}\right) \quad (3.14)$$

$$\alpha_{i+1} = \alpha_i + \Delta\alpha_{i+1} \quad (3.15)$$

Here, h is a positive constant.

The search starts with a large increment $\Delta\alpha$ until the first overshoot of the maximum power point (indicated by sign changing of $\frac{\Delta P}{\Delta\alpha}$) is obtained. Then the search process will continue in the inverse direction of variation with the reduced amplitude « $\Delta\alpha_2 = \frac{\Delta\alpha_1}{2}$ » until a new change of the sign of $\frac{\Delta P}{\Delta\alpha}$ appears,… etc.

This process is repeated until $\Delta\alpha_n$ is negligible, which provides an optimum firing angle α_m. The search process will start again when a variation of insolation or temperature is detected.

3.4 THE PROPOSED APPROACH:

The present PV pumping system is that described in figure 3.1, where the photovoltaic array is directly coupled to the induction motor without electric storage, and where the MPPT circuit present in the previous system is omitted, which leads to a less expensive implementation. The motor is fed by one of the three VS Inverter control strategies described in chapter 2, which are:

- The Sinusoidal PWM strategy.
- The Selective Harmonic Elimination PWM Strategy (SHE PWM).
- The Pondered Harmonic Minimisation Strategy.

3.4.1 Problematic :

Since water supply in remote areas of sunny regions is one of the most attractive applications of photovoltaic energy conversion, several small scale systems are currently installed by the 'Renewable Energy Development Center' (CDER) in the south-East of Algeria. These systems are oriented especially to irrigation, and where we have interest to store the maximum pumped water quantity in the day before starting irrigation with pressure.

The present work suggests how an optimal operation of a photovoltaic pumping system based on an induction motor driving a centrifugal pump can be realised. The optimisation problem consists in maximising the daily pumped water quantity via the minimisation of a non-linear criterion for any operating point. This has led to an optimal ' v-f ' relationship for controlling the motor.

In the centrifugal pump theory, it was concluded that the flow-rate is monotonically increasing with mechanical power at the pump shaft, as can be seen on the ENPMH manufacturer sheet shown in **figure 3.4**. Thus, the improvement of the flow-rate and then of the daily water pumped amount is obtained by the maximisation of the mechanical power for every operating point. This will be reached by the improvement of the motor efficiency as the insolation varies.

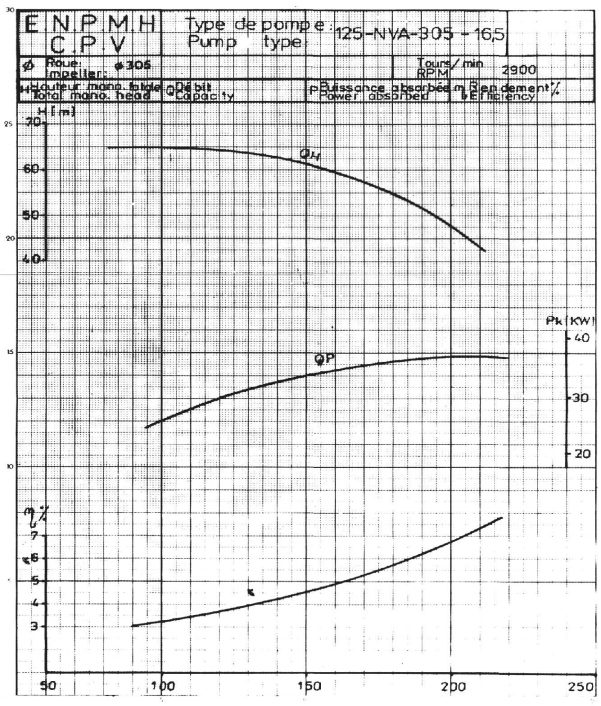

FIG 3.4 ENPMH manufacturer sheet

As shown in [44], the induction motor losses can be minimised by adjusting the following :
• minimization of the input absorbed power which is used as the controlled variable.
• minimization of the current (I) at the DC link of the inverter instead of the input power ($P_{in} = (3/2).V.\ I$). Since V is practically constant, P_{in} variations follow I variations.
• minimisation of the stator current I_s in the sense to improve the motor power factor.

The use of either the input power P_{in} or the dc current I as the controlled variables still suffer from low sensitivity especially for air-gap flux variations. More sensitive to the air-gap flux variations is the stator current, where we conclude that the minimum of I_s is more distinct than the minimum of P_{in}.

For these reasons the chosen optimisation criterion to be maximised is either the induction motor efficiency or the motor power factor.

3.4.2 Induction Motor Efficiency optimisation :

As demonstrated in induction motor theory, if the air-gap flux is kept constant for light loads (low torque values due to weak insolation levels in our case), an increase of iron losses is noticed, and consequently the motor efficiency falls as depicted in (chapter 4, **figure 4.1)**. As a result, a significant degradation of the plant performances is remarked (flow-rate, pump efficiency…etc).

In the present work, a correction of this efficiency by a variable air-gap flux operation is proposed. This will be achieved through the optimisation of a non-linear criterion representing either the motor efficiency or the power factor and by varying specified freedom degrees, which are :

- ***The inverter frequency* 'f'** and ***the modulation index* 'M'** in the Sinusoidal PWM strategy, where f indicates the frequency of the modulation waveform.
- ***The four switching angles*** 'α_1 - α_4 'and ***the inverter frequency* 'f'** when the Selective Harmonic Elimination PWM Strategy (SHE PWM) or the Pondered Harmonic Minimisation method are used.

3.4.2.1 Optimisation Criterion :

A - Use of the Sinusoidal PWM Strategy :

The maximisation of the motor efficiency is chosen as the optimisation criterion, which makes possible determining the momentary value of the vector :

$$X = [\omega_{sl}\ \ f\ \ I\ \ M\ ]^T \tag{3.16}$$

Maximising the criterion:

$$J = \max f(X) \tag{3.17}$$

where f (X) is the motor efficiency given by :

$$f(X) = \frac{C.(1 - \frac{\omega_{sl}}{2.pi.f})^3.(2.pi.f)^3}{(V_{th}.\ln(\frac{I_{sc} - I + I_o}{I_o}) - I.R_s).I} \tag{3.18}$$

subject to the equality constraints :

$$g(X) = 0 \tag{3.19}$$

In addition, the generator current I and the modulation index M are limited as follows :

$$0 \leq I \leq I_{sc} \tag{3.20}$$

$$0 \leq M \leq 1 \tag{3.21}$$

The equality constraints g (X) are formed by the set of equation (2.26), (3.8), (3.9) and considering equations (2.14), (3.20) and (3.21).

B- Use of the Selective Harmonic Elimination PWM Strategy (SHE PWM):

In this technique, the fundamental voltage component is to be controlled and the suppressed harmonics are 5^{th}, 7^{th} and 11^{th} ones. Flow-rate improvement is obtained by maximisation of mechanical power at the pump shaft. This will be reached by optimisation of a non-linear criterion representing the motor efficiency and varying the four switching angles and the inverter frequency. This permits the determination of the following vector :

$$X= [\omega_{sl} \;\; f \;\; I \;\; \alpha_1 \;\; \alpha_2 \;\; \alpha_3 \;\; \alpha_4]^T \tag{3.22}$$

which optimises the motor efficiency, given by equation (3.18), and subject to the equality constraints g(X) = 0, formed by the set of equations (2.17), (2.18), (2.19), (2.26), (3.8), (3.9) and considering equation (2.16). Besides, the array current and the switching angles are limited respectively by equations (3.20) and (2.20).

C- Use of the the Pondered Harmonic Minimisation method :

In the *'Harmonic Minimisation Method'* , the motor efficiency has to be maximised and the total harmonic distortion factor (THD) to be minimised. Hence, the optimising criterion J is given by :

$$J = - f (X) + K_1 . \left[\sum_{k=2}^{41} \left(V_k / k \right)^2 \right]^{1/2} \tag{3.23}$$

Subject to the equality constraints g (X) = 0 formed by the equations (2.26), (3.8),(3.9) and considering (2.16). In addition, the array current and the switching angles are always limited by equation (3.20) and (2.20).

Where f(X) denotes the motor efficiency given by equation (3.18), K_1 is a weight factor, and the number of harmonics to be minimised is chosen as k = 41.

3.4.3 Motor Power Factor Optimisation :

As illustrated in the 'Problematic section', the improvement of the induction motor efficiency and the pump flow-rate afterword can be easily obtained by the optimisation of the **Motor Power Factor,** which will be chosen as the optimisation criterion.

In this section, only the pondered Harmonic Minimisation strategy has to be considered since It gives the same results as the Sinusoidal PWM method and better than the SHPWM method. The inverter frequency and the four switching angles are the liberty degrees to be manipulated.

So, we have to determine the momentary value of the vector :

$$X= [\omega_{sl} \;\; f \;\; I \;\; \alpha_1 \;\; \alpha_2 \;\; \alpha_3 \;\; \alpha_4]^T \tag{3.24}$$

optimising the objective function :

$$J = -\frac{R_{eq}}{Z_{eq}} + K_1 . \left[\sum_{k=2}^{41} \left(V_k / k \right)^2 \right]^{1/2} \qquad (3.25)$$

subject to the equality constraints g(X) = 0 formed by equations (2.26), (3.8), (3.9) and considering (2.16).
In the optimising criterion J, a combination of maximising the motor power factor and minimising the THD factor is to be achieved.

After performing the optimisation process, the daily pumped water quantity is defined as :

$$D = \int_{t_{sr}}^{t_{ss}} Q \, dt \qquad (3.26)$$

Where the t_{sr} and t_{ss} indicate respectively the solar sunrise and sunset times, which are chosen in the present work for a clear standard day as :

t_{sr} = 6 h.00' and t_{ss} = 18 h.00'.

3.5 OPTIMISATION METHOD :

In constrained optimisation, the general aim is to transform the problem into an easier subproblem that can then be solved and used as the basis of an iterative process. A characteristic of a large class of early methods is the translation of the constrained problem to a basic unconstrained problem by using a penalty function for constraints, which are near or beyond the constraint boundary. In this way the constrained problem is solved using a sequence of parameterised unconstrained optimisations, which in the limit (of the sequence) converge to the constrained problem. These methods are now considered relatively inefficient and have been replaced by methods that have focused on the solution of the Kuhn-Tucker (KT) equations. The KT equations are necessary conditions for optimality for a constrained optimisation problem.

The nonlinear nature of the optimization criterion (exp: equation (3.18)) as well as of the constraints (equation (2.26), (3.8), (3.9)…etc) calls for application of nonlinear programming methods. This is carried out by the 'FMINCON' function of the 'MATLAB' software.

At each iteration, the constrained problem is transformed to an other unconstrained one with linearised constraints using the Lagrangian function [45] :

$$L(X, \lambda) = -f(X) + \sum_{i=1}^{m} \lambda_i . g_i(X) \qquad (3.27)$$

The solution is, then, carried out using the Quadratic Programming Algorithm, where g contains all the constraints, λ_i (i=1,…m) are Lagrange Multipliers and m is the number of the constraints. The Hessian Matrix updating is made by the formula of Broyden, Fletcher, Goldfarb and Shanno (BFGS) [46].

3.5.1 Sequential Quadratic Programming (SQP)

SQP methods represent state-of-the-art in non-linear programming methods. At each major iteration an approximation is made of the Hessian of the Lagrangian function using a quasi-Newton updating method. This is then used to generate a QP sub-problem whose solution is used to form a search direction for a line search procedure.

The principal idea is the formulation of a QP subproblem based on a quadratic approximation of the Lagrangian function given by equation (3.27).
The QP sub-problem is obtained by linearising the nonlinear constraints.

3.5.2 QP Subproblem [45] :

$$\begin{aligned} &\min imize \ \frac{1}{2} d^T . H_k . d + \nabla . f(X_k)^T . d \\ &\nabla g_i (X_k)^T . d + g_i (X_k) = 0 \quad i = 1, ... m_e \\ &\nabla g_i (X_k)^T . d + g_i (X_k) \le 0 \quad i = m_e + 1, ... m \end{aligned} \tag{3.28}$$

This sub-problem can be solved using any QP algorithm . The solution is used to form a new iterate $X_{k+1} = X_k + \alpha_k . d_k$.

The step length parameter α_k is determined by an appropriate line search procedure so that a sufficient decrease in a merit function is obtained while d^k is a real number . The matrix H_k is a positive definite approximation of the Hessian matrix of the Lagrangian function. H_k can be updated by any of the quasi-Newton methods, although the BFGS.

3.5.3 SQP Implementation:

The SQP implementation consists of three main stages:
- Updating of the Hessian matrix of the Lagrangian function.
- Quadratic programming problem solution
- Line search and merit function calculation

Updating the Hessian Matrix

At each major iteration a positive definite quasi-Newton approximation of the Hessian of the Lagrangian function, H,is calculated using the BFGS method:

$$\begin{cases} H_{k+1} = H_k + \dfrac{q_k . q_k^T}{q_k^T . s_k} - \dfrac{H_k^T H_k}{s_k^T . H_k . s_k} \\ s_k = X_{k+1} - X_k \\ q_k = \nabla f(X_{K+1}) + \sum_{i=1}^{n} \lambda_i . \nabla g_i (X_{k+1}) - \left(\nabla f(X_k) + \sum_{i=1}^{n} \lambda_i . \nabla g_i (X_k) \right) \end{cases} \tag{3.29}$$

The main steps followed to extract performances of the optimized PVP-system are described bellow. They expose in fact the interaction of the different components of the system and where the VS inverter is controlled by one of the three PWM technics discussed above.

i. Introduce the rated data of the PVP system
ii. Choose the optimization criterion by setting (1) for the motor efficiency and (2) for the power factor.
iii. Choose the inverter control technique by setting (1) for the Sinusoidal PWM Strategy, (2) for the SHE PWM technique and (3) for the Harmonic Minimization method.
iv. Introduce the insolation initial level.
v. Set up an initial vector X_0 .
vi. Call the FMINCON function to resolve the objective function.
vii. Increase the insolation level.
viii. Go then to step vi.

3.6 CONCLUSION :

In the scope of the present chapter, a detailed description of the optimisation criterion using three control strategies of the inverter is done. The study fixes as a goal the maximisation of the daily pumped water quantity by establishing an optimum 'v-f' relationship for controlling the induction motor. The effectiveness of the proposed algorithm will be described by simulation in the next chapter and the obtained results are compared with those of similar work pieces presented in literature called 'constant air-gap flux system' and 'constant motor efficiency system', fully described here.

Chapter 4
SIMULATION PERFORMANCE RESULTS

4.1 INTRODUCTION:

In the previous, the detailes of the proposed optimisation approach as well as the comparative pieces were presented. In the present one, the simulation results using these technics are analysed and discussed. An analysis of the operational behavior of the whole pumping system, taking into account the interactions of its components and how they influence each other will be carried out. Also, the effect of weather and plant conditions such as cell temperature and geodetic head on the system will be investigated. These two parameters can be viewed as input disturbances. The chapter starts with a presentation of system performances for a specific standard clear day, which was described in chapter 2.

Following, to assess the influence of the optimisation criterion on the PVP-system output predictions, simulation results using motor power factor as the objective function are presented.

Then, the influence of the geodetic head change, which simulates the watertable decrease and the cell temperature variation on the system performances will be also considered and discussed afterword.

The chapter will be concluded by a long-term performance analysis, which will be carried out for a period of ten typical years with chosen measured meteorological data.

4-2 SIMULATION RESULTS :

Time step simulation using the proposed approach for the three control technics of the inverter and those of the systems called 'constant efficiency system' and 'constant air-gap flux system' were performed. In this section, the results of these simulation calculations will be discussed in a comparative way; they were achieved in time steps of one minute, which corresponds to an increase of the insolation by 1w/m².

The simulation is carried out on a system comprising a suction and a delivery tank, that are separated by a single pipeline. The volume of the two buffer tanks are respectively : 2.88 m^3 and 0.78 m^3, while the geodetic head of the plant is: H_g = 7.4 m. **Figures** 4.1-4.21 display the daily course of the most important characteristics describing the system performance as a function of insolation, which is considered as the simulation input. Here, the reference temperature is T_r =25°C.

4-2-1 INDUCTION MOTOR EFFICIENCY OPTIMISATION :

A - Sinusoidal PWM Strategy :

In **Figure 4.1** the motor efficiency of the first control technic is displayed. It could be seen that an optimum efficiency η_m=73.6% can be maintained using the proposed optimisation criterion. The control law given by equation (3.17) mainly governs the reduction of losses which are frequency dependant (iron and friction losses).This represents an improvement with regard to the constant airgap flux system [5] in particular for the weak values of insolation (E<650 w/m²).The algorithm presented in [33] generates similar optimal results where a constant motor efficiency value η_m=0.71 is maintained. The electronic control of the inverter adjusts the frequency and the motor voltage so that to have an equilibrium between iron and copper losses.

The low efficiency values noticed in 'the constant air-gap flux system' at weak insolation levels present serious disadvantages :

- Wasted energy has to be paid for at the same cost as useful energy. Continuous high temperature working may cause deformation of metal parts or even bearing failure.

he improvement of the motor efficiency obtained by the proposed approach avoid such problems, especially the overheating of the winding insulation.

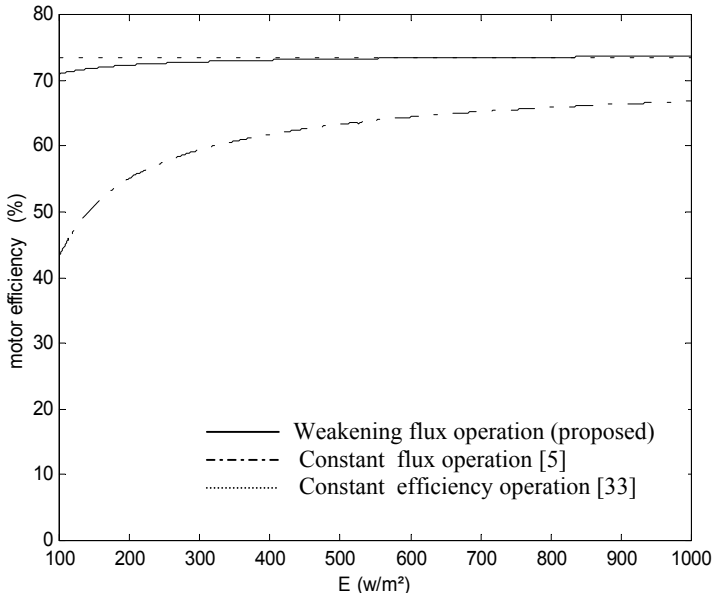

FIG 4.1 Motor efficiency curves

Figure 4.2 shows the pump flow-rate obtained by equalising equations (2.43) and (2.52). The pump succeeds in overcoming the geodetic head H_g and throws water to the delivery tank only when a certain speed is reached (ω = 200 rd/s in this case). The electric power threshold value corresponding to this limit is nearly 200 W; about 20 % of the rated motor power. This critical value is obtained at an insolation level E_{th1} = 327 W/m² for the system working with the proposed optimisation algorithm and that described in [33], whereas the system with constant flux does not contribute to water yield unless solar insolation exceeds the threshold value E_{th2} = 379 W/m².

This increase of the flow-rate is due to the proportionnality existing between it and the mechanical power on the shaft of a centrifugal pump [24]. The improvement of the mechanical power and hence of the flow-rate are obtained by the maximisation of the motor speed via the optimisation criterion. Consequently, this leads to a rise in the daily pumped quantity. By adopting the insolation model given by equation (2.53), and according to numerical integration of equation (3.26), the obtained daily water amount is :

- D = 28.84 m^3 for constant air-gap flux technic [5].
- D = 31.14 m^3 for the system described in [33].
- D = 31.00 m^3 for the proposed approach.

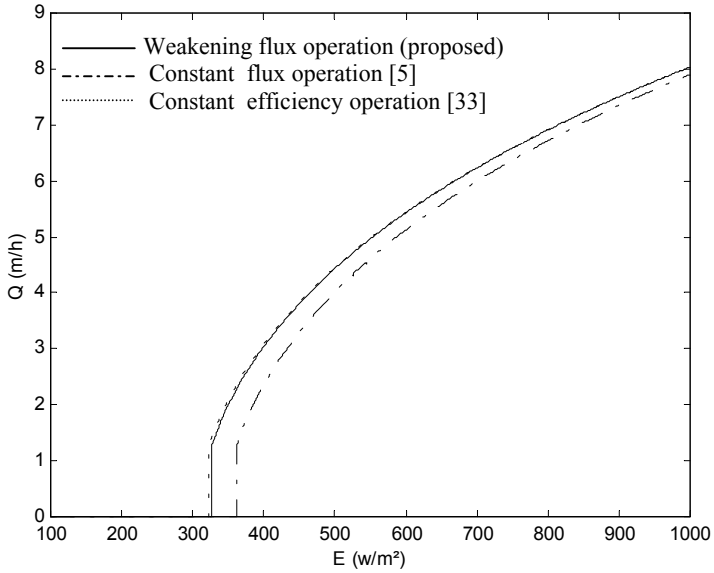

FIG 4.2 Pump Flow-rate characteristics

Figure 4.3 displays the improvement brought to the pump efficiency by the proposed technique, as well as that described in [33]. Compared with [5], this increase is more considerable for the weak values of insolation (E<650 W/m²); It inflicts the following two parameters:

- An increase of the total head H given by equation (2.43) as a result of the friction and shock losses reduction inside the pump.
- An increase of the flow-rate Q as a result of the leakage flow-rate decrease.

Consequently, the hydraulic power (ρ .g. H.Q) is enhanced.

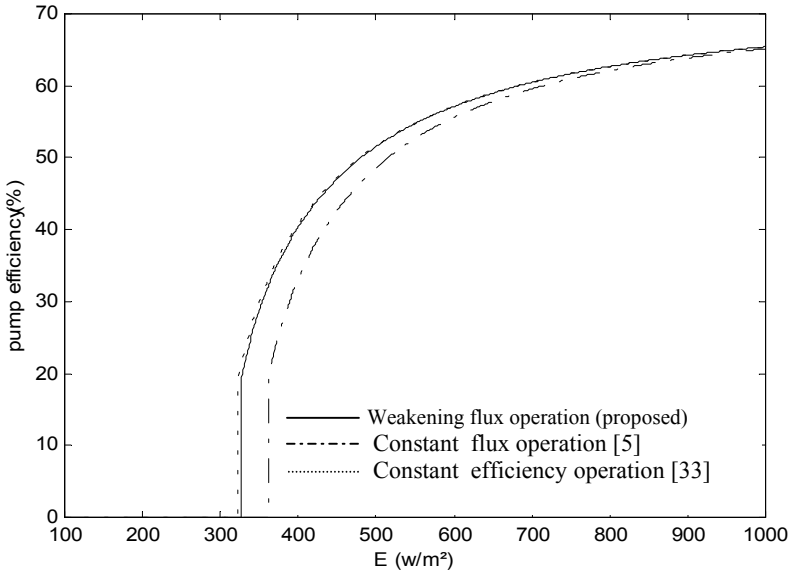

FIG 4.3 Pump Efficiency characteristics

Figure 4.4 illustrates motor air-gap flux represented by the (V_m/f) ratio. One can notice that the improvement of the motor efficiency is obtained by field weakening, especially for low insolation levels corresponding to low motor speed, and hence at weak load torques. This can be explained by the fact that at light loads, a sustenance of a nominal air-gap flux may be greater than necessary for the development of the required torque, and losses are high. The reduced flux yields essentially a motor iron losses decrease, since this kind of losses are flux-depending as described by the following equation:

$$P_{iron} = K_e . f . \phi^2 + K_h . f^2 . \phi^2 \qquad (4.1)$$

Where K_e and K_h are respectively eddy current and hysterisis coefficients.

Summarising, from Fig. 4.1 and Fig. 4.4, for a lightly loaded motor, a maximum efficiency is achieved with reduced air-gap flux. However, for the system described in [5], a nominal flux is permanently maintained (V_m / f ≅ 4.8) by the inverter control mode given by equation (3.6).

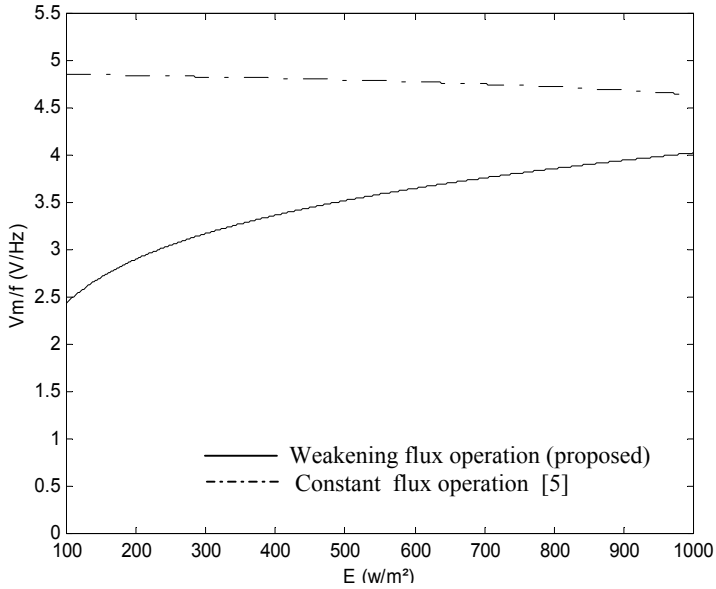

FIG 4.4 Air-gap flux curves

Figure 4.5 shows the generator Power-Voltage characteristics and maximum power locus showed together with the consumed power in the case of constant air-gap flux mode [5], and field weakening mode that is proposed in our study, while **Figure 4.6** illustrates the generator use efficiency characteristics. It is clear that for these two functionning modes, the power consumed by the system is strictly close to that maximal power absorbed by the system [33] for high insolation levels, and do not deviate significantly for lower values, bearing in mind that the MPPT block is omitted for these two cases. Consequently , the implemetation will be less complex , less expensive and more reliable. In addition, the use efficiency values are η_{use}>98 % for all insolation levels.

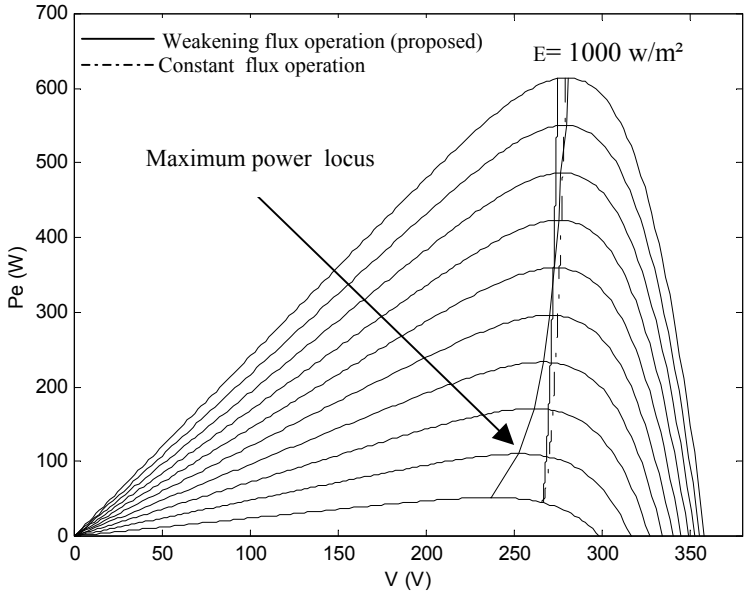

FIG 4.5 Operating point locus for different insolation levels

In **Figure 4.7a**, modulation index M is presented, while **Figure 4.7b** ilustrates the inverter output frequency. One notices that the modulation index is reduced once the frequency falls down, bringing therefore a decrease in motor voltage V_m since the generator voltage is approximately constant (see figure 4.5). It is also shown from the induction motor theory, that the inverter frequency and modulation index are varied to keep the ratio M/f at an

appropriate value leading to an air-gap flux reduction and to an optimum motor efficiency. If the ratio M/f is too high, then the magnetising current and core losses are excessive. If this ratio is too low, the rotor frequency rises unduly so that rotor currents and copper losses are excessive. Consequently, for every operating point, there is an optimum (M-f) pairing shown by figure 4.7, that gives the required steady-state torque with maximum efficiency [24].

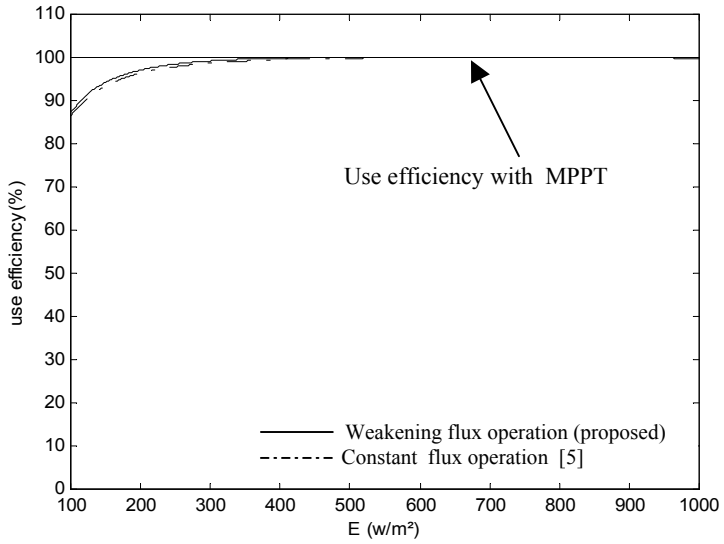

FIG 4.6 The Array Use efficiency characteistics

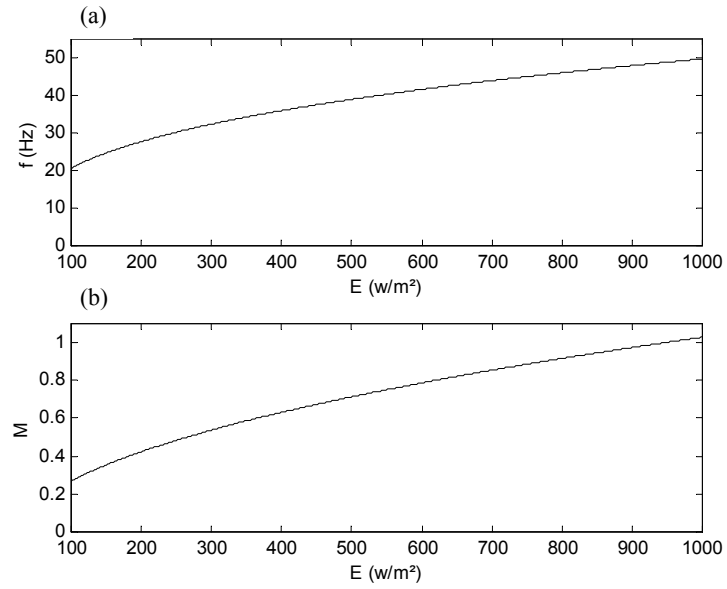

FIG 4.7 Modulation index and Frequency curves

Figure 4.8 illustrates motor slip versus insolation for the optimised system and that operating with constant air gap flux. One can remark that over the day, the two systems work with weak slip values that are lower than the breackdown motor slip given by the conventional relationship [39] :

$$s_b = r_2 \Big/ \left(l_2 . \omega_s\right) \tag{4.2}$$

In the present case S_b is equal to 0.5. Consequently, the induction motor works permanently in the stable area of the torque-speed characteristic, and no high speed oscillation will occur. Besides, from figure 4.8, one can notice that the optimum motor slip is always kept constant at nearly 0.043 . This optimised value is identified by the analytic expression given by [39] :

$$s_{op} = \frac{r_2}{(x_m + x_2)} \cdot \left\{ \frac{1 + x_m^2 / (r_1 . r_m)}{1 + r_2 / r_1} \right\}^{1/2} \tag{4.3}$$

The motor operation at this optimum slip implies that the equivalent circuit has no variable impedances, and hence the optimum efficiency value is independent from the motor voltage.
It is also important to underline that the system described in [33] provides similar results as the proposed approach.

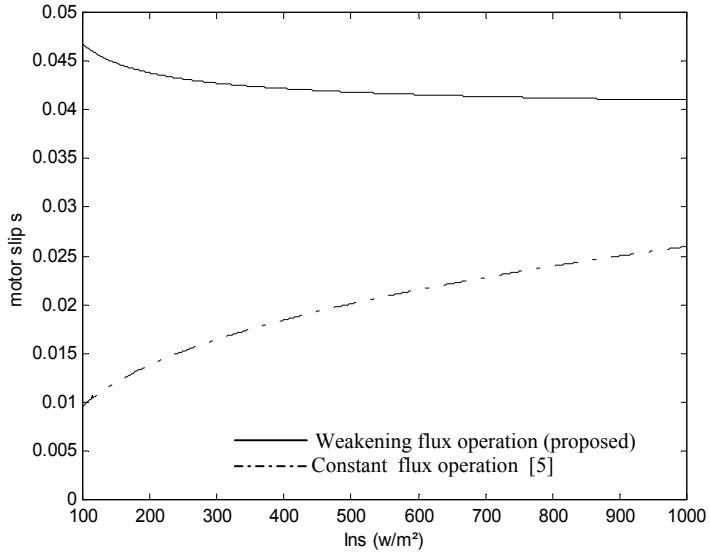

FIG 4.8 Motor slip curves

Figure 4.9 depicts the chopper ratio curve of the MPPT block incorporated in [33] versus insolation. It could be seen that the MPPT device is a buck-boost chopper since its ratio range varies from 0.5 to 2.8. This behavior is essentially caused by the fact that the driving induction motor and the monocellular centrifugal pump do not present the same nominal output and input power respectively. (the motor power is about 1kw, whereas the pump presents 521 w as nominal input power). Therefore, in the low insolation area (< 500 W/m²), the MPPT diminishes the array voltages obtained with the direct coupling system so to keep these voltages at the optimum ones. On the other hand, for the high insoltaion levels, the chopper tends to increase the array voltages. In addition, one can remark that at 500 W/m² the chopper ratio is equal to 1. At this point, an optimum coupling system without MPPT can be obtained.

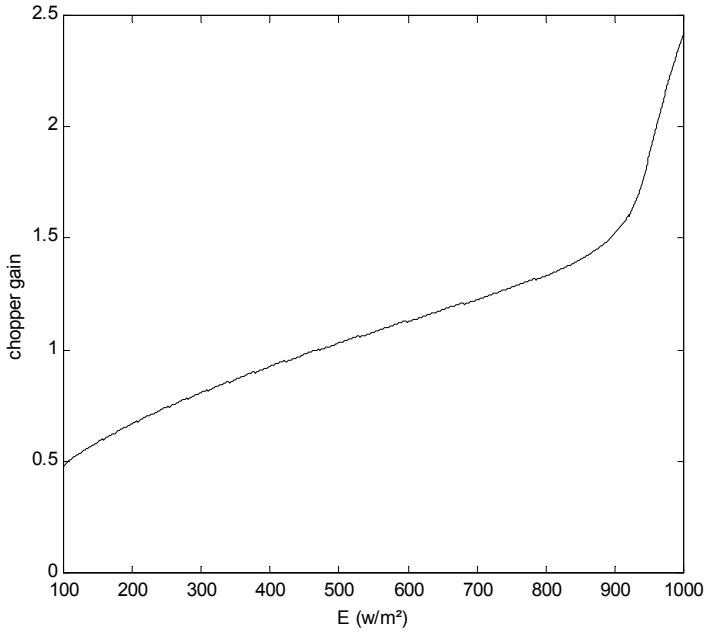

FIG 4.9 Chopper gain curve

As a conclusion, The simulation results show that an increase of plant performances is reached by the proposed approach. In addition, the generator voltage control law leads to a less expensive and a non complex implemetation. We manage therefore to combine the performances of the system with constant efficiency and the simplicity of implementation provided by the system with constant airgap flux.

B - Selective Harmonic Elimination and Pondered Minimisation PWM strategies :

The electronic control of the VS inverter is done by either the Selective Harmonic Elimination (SHE) or the Pondered Minimisation PWM strategies. These technics were explicitly exposed in the previous chapter.
In the present section, The simulation results using these technics are presented and discussed in a comparative way. **Figures 4.10– 4.15** show the system performance as function of insolation and for the reference temperature T_r=25°C.

In **Figure 4.10** the motor efficiency is presented. It could be seen that with the *'Harmonic Minimisation Method'* an optimum efficiency η_m=70 % is permanently maintained. This is obtained by a proper adjustment of the inverter frequency and the four switching angles so to establish an equilibrium between the stator copper and core losses. In fact, this represents an advantage as far as the system working with the *'Harmonic Elimination Method'* is concerned, especially for the weak and medium insolation values. In this latter technic, no feasible solution of the non-linear criterion was found to enhance the motor efficiency for the weak insolation range.

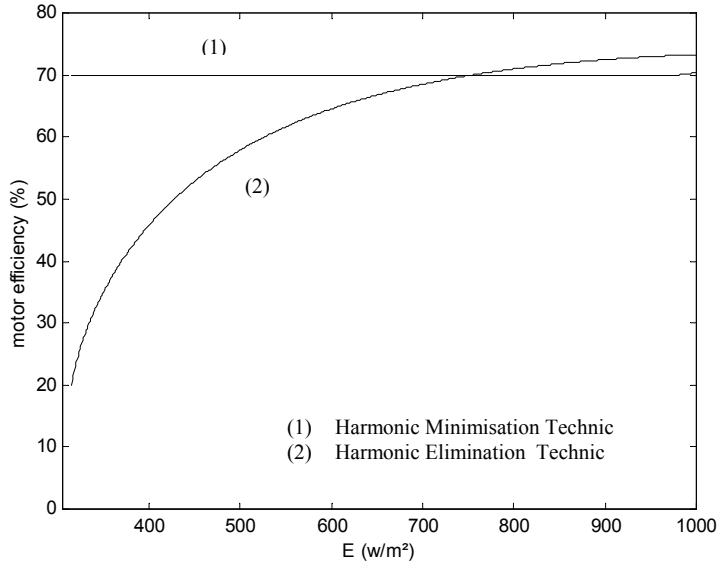

FIG 4.10 Motor efficiency curves

Figure 4.11 displays the pump flow rate obtained by equalising equations (2.43) and (2.52). The pump succeeds in overcoming the geodetic head H_g and throws water in the delivery tank only when a critical insolation level is reached. This threshold value is equal to E_{th1} = 340 W/m² for the system working with the *'Harmonic Minimisation Method'* and about 444 W/m² in the case of the *'Harmonic Elimination Method'*. Therfore, the solar radiation utilisability defined by equation (2.54) is improved as can be seen in **Table 1**.
In addition, due to the improvement of the pump flow-rate obtained with the *'Harmonic Minimisation Method'*, an increase of the daily pumped amount is then obtained. The obtained quantities are as follow:

- D = 26.10 m^3 for the *'Harmonic Elimination Method'*.
- D = 29.51 m^3 with the *'Harmonic Minimisation Strategy'*.

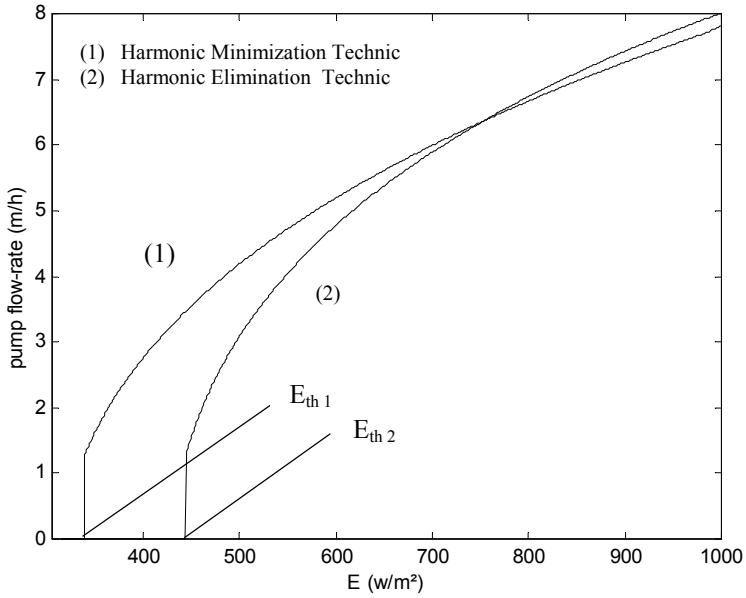

FIG 4.11 Pump flow-rate characteristics

Figure 4.12 shows the improvement brought to the pump efficiency by the '*Harmonic Minimisation Strategy'*. As can be seen, this figure reproduces the slope of the flow-rate curve, and where the obtained improvement is more notable at medium and weak insolation levels. This increase inflicts the following two parameters:

- An increase of the total head H given by equation (2.43) as a result of the friction and shock losses reduction inside the pump.
- An increase of the flow-rate Q as a result of the leakage flow-rate decrease [47].

Besides, In the middle of the day (E > 700 W/m²), the two curves coincids each other and the pump is at an average efficiency of 61 %, which is very close to its optimum value.

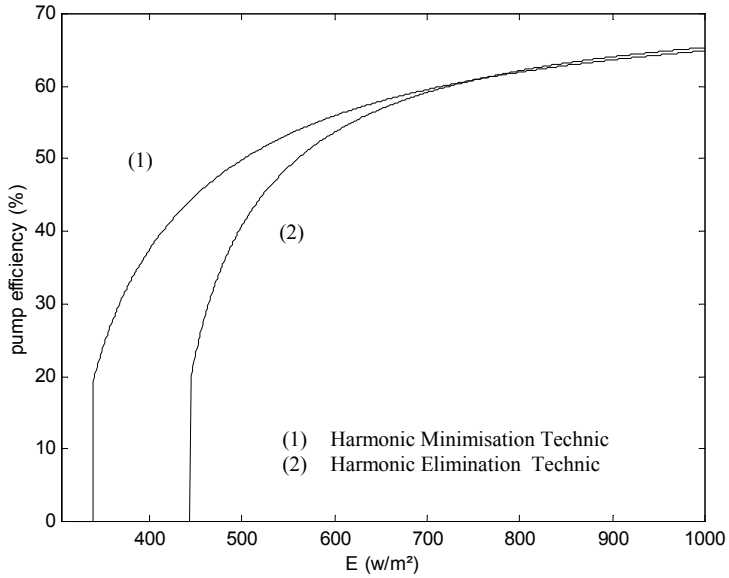

Fig 4.11 Pump efficiency curves

Figure 4.13 shows the fundamental component of motor power factor. As can be remarked, the displacement factor remains high regardless the insolation level (cos φ ≈ 0.88), which leads to a considerable reduction of the motor heating. The constant value of the power factor is caused by the fact that at an optimum motor efficiency, the machine works with a constant slip as shown in the first control technic. Therefore, the equivalent circuit presents constant input impedances [39].

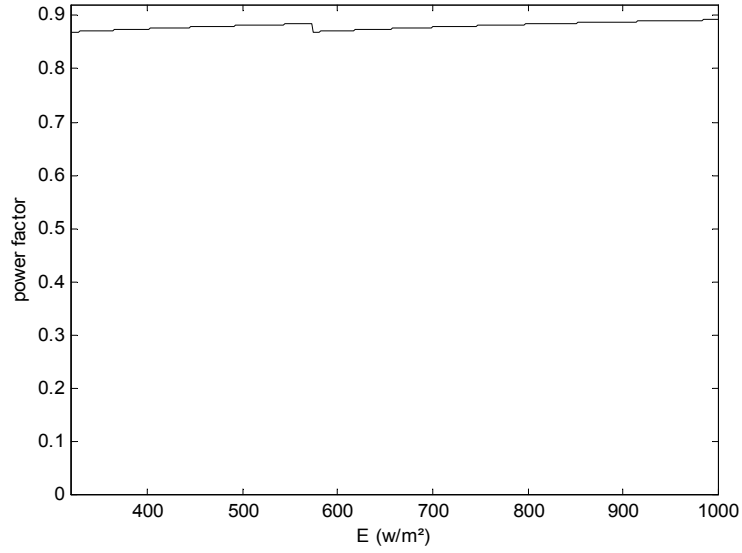

FIG 4.13 Motor power factor curve

In **Figure 4.14** the generator Power –Voltage characteristics and maximum power locus are showed together with the consumed power of the two described systems. It is clear that the extracted electric power for both system with *'Harmonic Minimisation Method'* and *'Harmonic Elimination Method'* is extremely close to the maximum one, leading to an optimum matching of the load; bearing in mind that the PV generator is connected directly to the VS inverter and without an MPPT block incorporated.

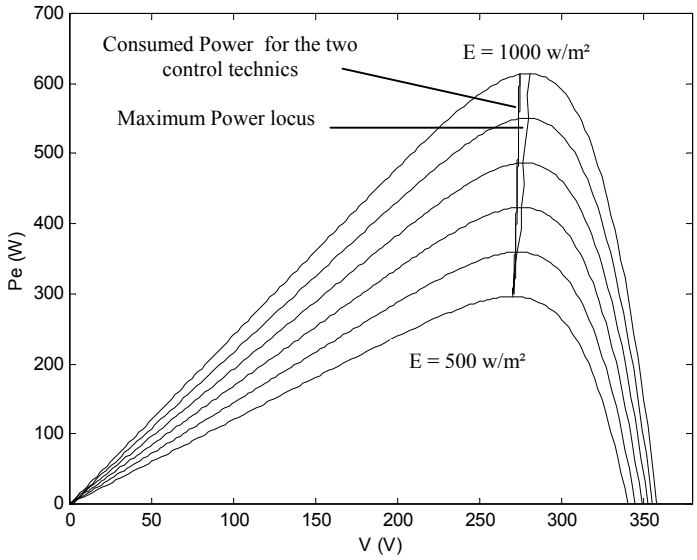

FIG 4.14 Consumed Electric power curves

Figure 4.15 displays the output inverter frequency. One notices that the frequency decreases once the insolation falls down causing the reduction of the motor losses that are frequency depending (iron losses). Also, in the low insolation range, the diminution of the air-gap flux in the case of the *'Harmonic Minimisation Method'* is more important than of the second technic, and therefore core losses considerably decrease. Contrary, for the high insolation levels, the sustenance of a high level air-gap flux leads to less motor efficiency value.

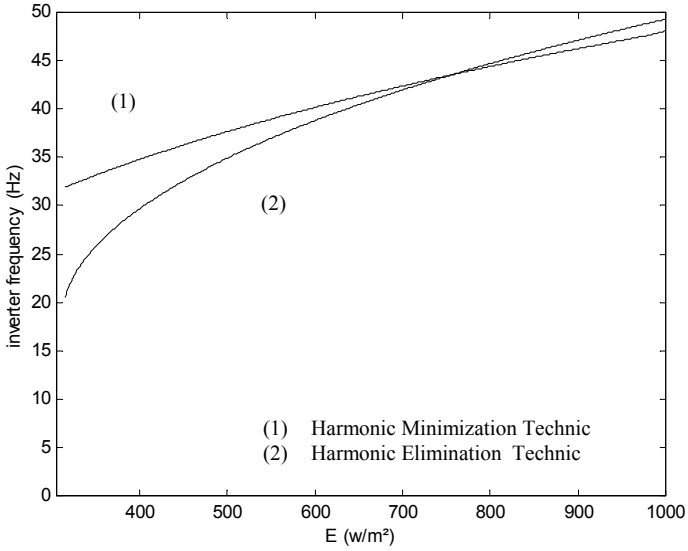

FIG 4.15 Inverter frequency locus

In **Figure 4.16**, the switching angles of the 'SHE' technic are illustrated as function of insolation. We can notice that constant values of these angles are obtained along the insolation curve (α_1 = 13 degs, α_2 = 20.5 degs, α_3 = 41 degs, α_4 = 45 degs). For an eventual implementation, these constants are stored and the corresponding pulse widths are generated in the time domain with the help of down-counters.

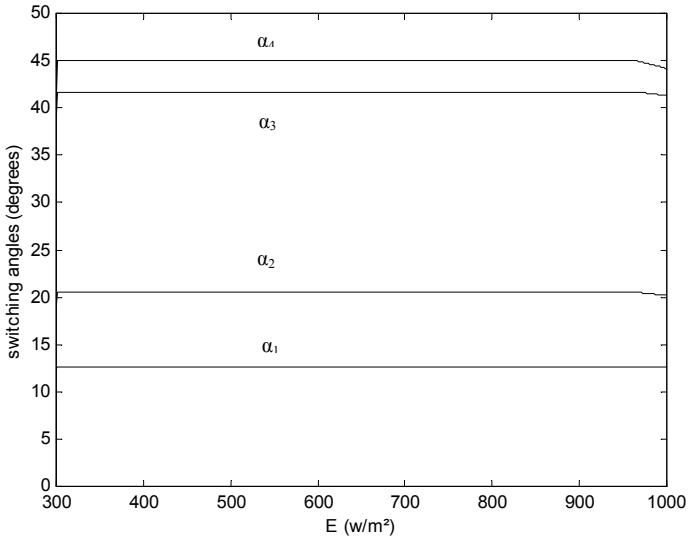

FIG 4.16 Switching angles curves

Fig. 4.17 shows the rms values of selected voltage harmonics, rapported to the square wave value and obtained for the peak insolation level E=1000 W/m² and where the inverter is controlled by the 'SHE' strategy . One notices that via the four switching angles, we arrive to control the fundamental magnitude, which represents 78 % of the square wave amplitude, and eliminate the undesirable low order harmonics (5, 7, and 11). In addition, the 13^{th} , 17^{th} and 19^{th} harmonics permanently represent respectively 23 %, 25 % and 10 % of the square wave rms value. These non-eliminated harmonics can be filtered by the motor itself or via an active-filter by the regeneration of the same harmonics with negative peak values [48].

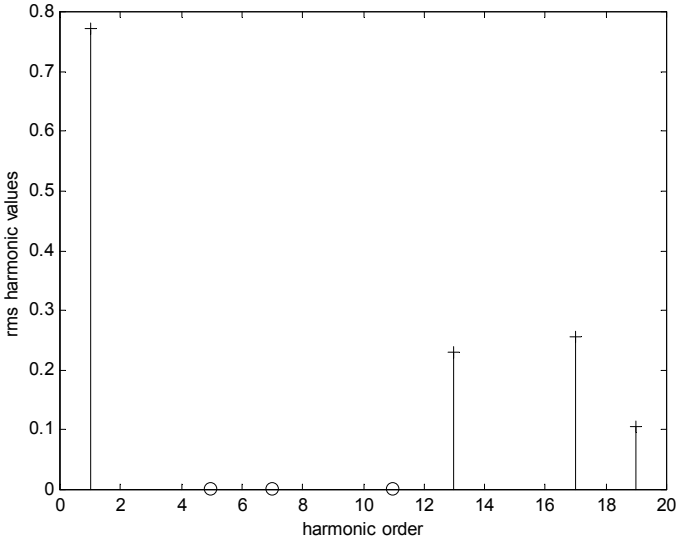

FIG 4.17 Harmonic rms values

In **Table 1**, some performances of the two considered systems obtained for a peak insolation level E =1000 W/m² and T_r = 25°C are summarised.

Table 1 System Performances

Control Technic	η_m *(%)*	*THD (%)*	μ *(%)*	α_1 *(rd)*	α_2 *(rd)*	α_3 *(rd)*	α_4 *(rd)*
H. E. T	73.0	48.5	89.2	0.22	0.34	0.71	0.76
H.M. T	70.0	21.0	97.3	0.06	0.10	0.63	0.63

From the above exposed results, we concluded that the *'Harmonic MinimiSation Technic'* presents a superiority as far as the *'Harmonic Elimination strategy'* is considered. It reproduces in fact the same performances improvement obtained with the sinusoiudal PWM control technic.

From **Table 1**, the THD factor is halphed when the *'Harmonic Minimisation Technic'* is applied, which leads to a better quality of the inverter output voltage.

It is also important to underline that in the case of the '*Harmonic Minimisation Method',* this factor increases relatively for low insolation levels ; whereas for the '*Harmonic Elimination Method'*, it remains permanently constant at 48.5%. To surmount this problem, a combinaison of sinusoidal PWM strategy and '*Harmonic Minimisation Method'* can be implemented, where the first technic acts at low insolation range (in the early morning and late afternoon) , whereas the inverter is controlled intermittently with the second strategy in the middle of the day.

4-2-2 INDUCTION MOTOR POWER FACTOR OPTIMISATION :

In the present section, the simulation results of the photovoltaic pumping system with the second optimisation criterion exposed in the previous chapter are presented and discussed. The inverter is controlled via the the '*Harmonic Minimisation Method'*. **Figure 4.18-4.21** display the system performance versus insolation and for the reference temperature T_r =25°C.

Figure 4.18 depicts the curve of the motor power factor. It could be seen that the input fundamental component power factor remains high (cos(φ)=0.88) regardless of the insolation level which leads to a considerable reduction of the stator current and then of the motor heating.

This constant value is caused by the fact that the motor presents constant input impedances.

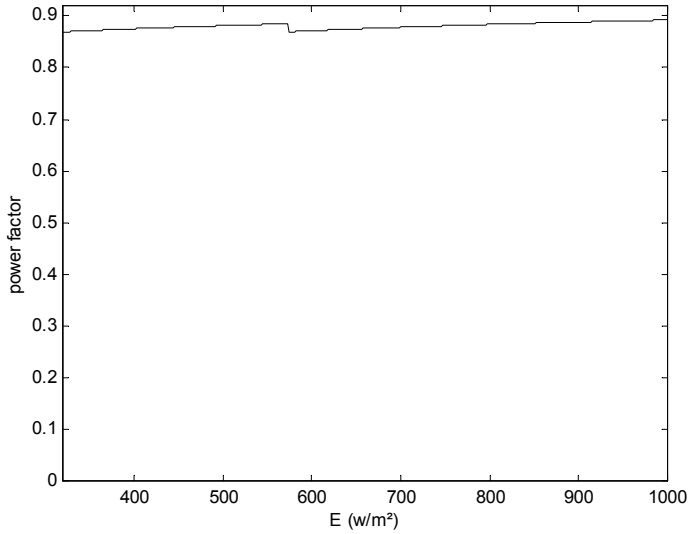

FIG 4.18 Motor power factor curve

Figure 4.19 shows the pump flow-rate obtained by equalising equations (2.43) and (2.52). The pump succeeds in overcoming the geodetic head H_g and throws water in the delivery tank only when a threshold insolation level is reached. This value is about E_{th}= 340 W/m². In addition, the obtained daily pumped amount is : D = 29.51 m^3.

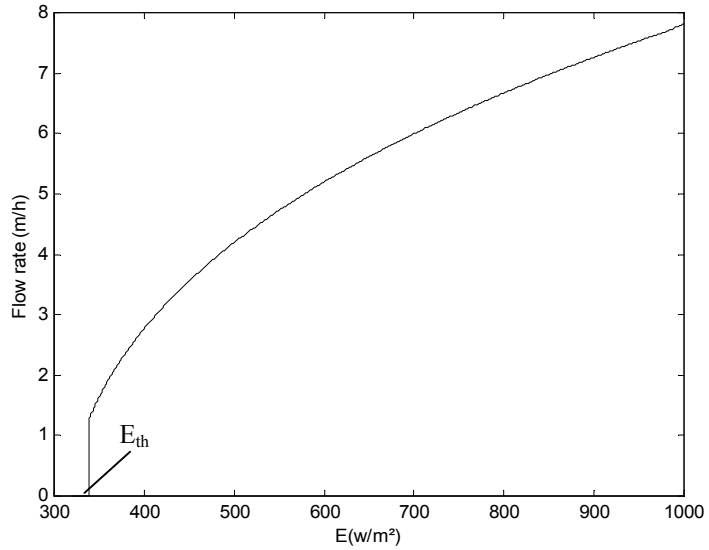

FIG 4.19 Pump fow-rate characteristic

Figure 4.20 illustrates the air-gap flux represented by the (V_m/f) ratio. One can notice that the improvement of the motor power factor is obtained by a field weakening, especially for low insolation values corresponding to weak load torques.

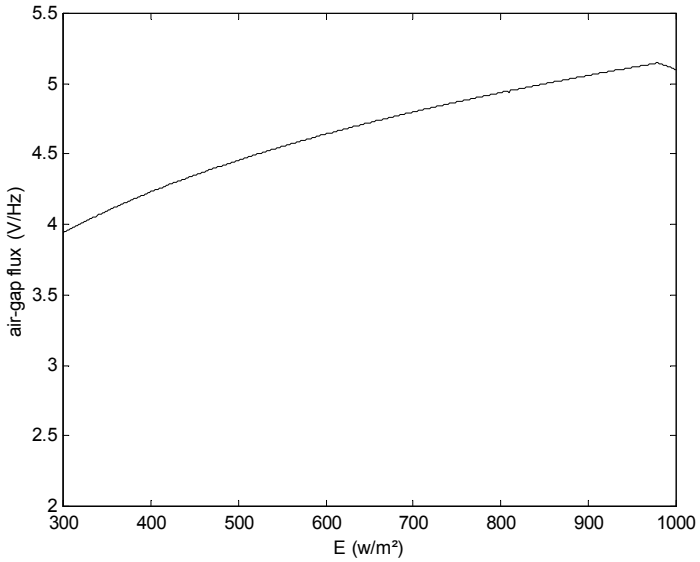

FIG 4. 20 Motor air-gap flux characteristic

Figure 4.21 displays the global efficiency of the plant, given by the hydraulic power to the insolate ratio:

$$\eta_G = \frac{\rho.g.H.Q}{A.E} \tag{4.3}$$

Here A is the effective array area.

We can see that the global efficiency values are low for all the insolation levels, which is essentially caused by the weak photovoltaic conversion. In addition, since the photovoltaic array is directly connected to the motor without battery, the plant efficiency reaches its optimal value only at the nominal insolation level (E=1000 W/m²) for which the system was sized.

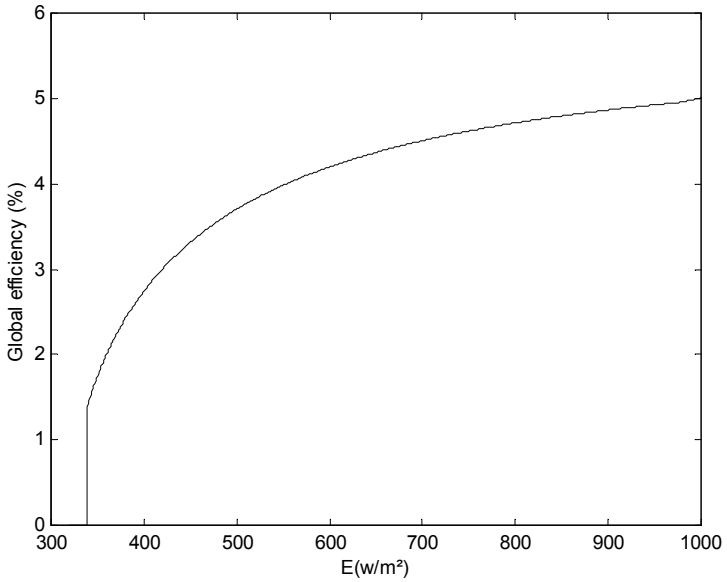

FIG 4.21 Global system efficiency curve

One can conclude that the second optimisation criterion (the power factor) reproduces the same performances improvement since the two objective functions are equivalent.

4.3 INFLUENCE OF HEAD CHANGING :

When water is discharged from a well, the inside watertable does not remain constant: It changes depending on the flowrate and the pumping time. It is, then, no longer justified to consider the geodetic head H_g as constant. Simulation runs using the proposed approach with motor efficiency optimisation, and where the geodetic head is changed by a step of 0.5 m. The temperature is kept constant at 25°C. In addition the inverter is conrolled by either *the Sinusoidal PWM strategy* or the *'Harmonic Minimisation Method'* since these two technics provide the best performances as showed in the previous sections.

4.3.1 *Sinusoidal PWM technic :*

The following simulation results show both the threshold insolation level E_{th} and the daily water volume D versus the geodetic head H_g, that are respectively presented in **Figure 4.22** and **Figure 4.23**. As can be seen, the threshold insolation and hence the electric power required to start pumping increases with head growth. Consequently, the daily water amount would decrease. These results confirm the behavior of a centrifugal pump which needs a relatively high speed to overcome the static head. The rotating displacement pumps present a viable solution of such situation, starting pumping water at nearly zero speed, and so a least threshold electric power is required as demonstrated in [47].

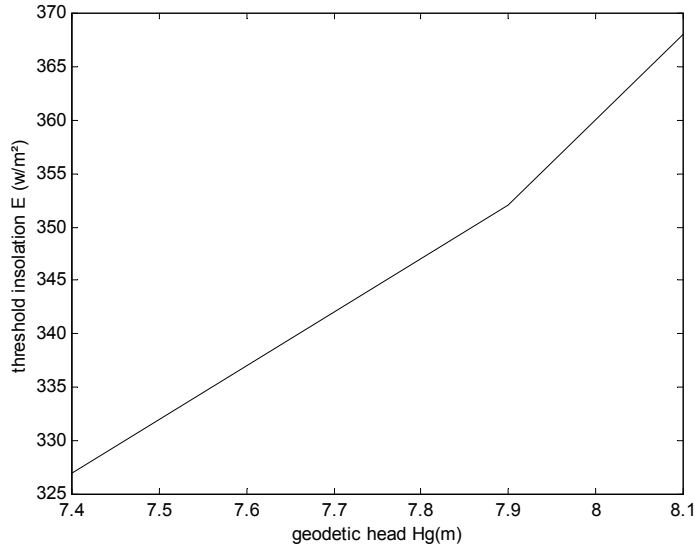

FIG 4.22 Threshold Insolation curve

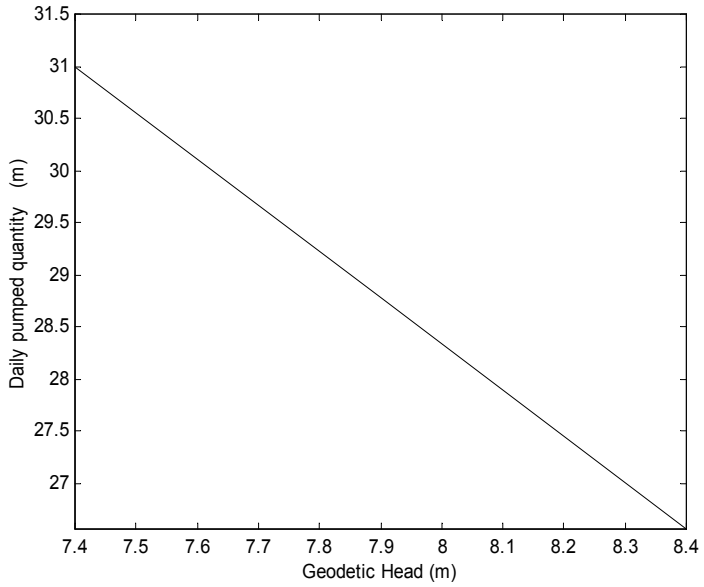

FIG 4.23 Daily Pumped Quantity for Head Changing

In **Table 2**, the system performances for the three considered geodetic head values and for a peak insolation level E =1000 W/m² are summarised. Since the load torque presented by equation (12) is assumed to be independent from the flow-rate, both the motor efficiency and the air-gap flux are unaffected by the head variations. In addition, the pump efficiency falls with the increase of head. This behavior is an effect of shock and friction losses increase inside the pump.

Table 2 Pumping System Performances

H_g (m)	η_m (%)	η_p (%)	D (m^3)	Flux (V/Hz)	E_{th} (W/m^2)	$P_{e\ th}$ (W)
7.4	73.6	65.4	31.00	4.02	327	186.0
7.9	73.6	64.4	28.77	4.02	352	202.3
8.4	73.6	62.7	26.57	4.02	394	283.5

4.3.2 *Harmonic Minimisation Technic :*

Figure 4.24 shows the daily water volume D versus the insolatioin geodetic head H_g, where the VS inverter is controlled by the '*Harmonic Minimisation Technic'*. In **Table 3**, the threshold insolation levels, the corresponding extracted electric power and the pump efficiency for the three considered geodetic head values are summed up.

The threshold insolation and hence the electric power required to start pumping increases with head increase. As a result, the daily water amount would decrease.
We arrive consequently to reproduce the simulation results obtained with the first control technic.

Table 3. System Performances for head changing

H_g (m)	η_p (%)	E_{th} (W/m²)	$P_{e\ th}$ (W)
7.4	64.95	339	135.97
7.9	63.84	371	150.10
8.4	62.64	470	163.80

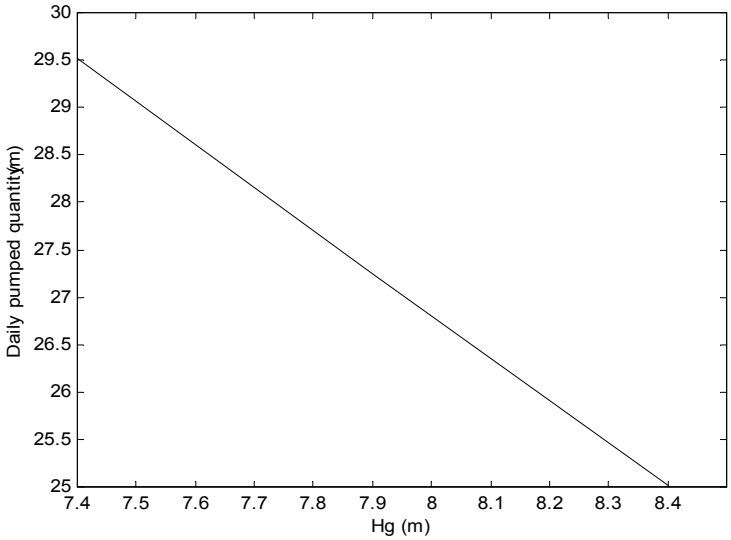

FIG 4.24 The daily pumped volume

4.4 INFLUENCE OF TEMPERATURE VARIATION:

As mentioned earlier in chapter 2, meteorological parameters, especially the array temperature, do not remain constant along a day, but change considerably. It is, then, worth investigating the influence of the daily average temperature variation on the predicted performances of the optimised system. In the present section, the inverter is controlled by the Sinusoidal PWM strategy since it provides the better performances, as well as the '*Harmonic Minimisation Technic'*.

In this case, the constant C_{10} showed by equation (3.7) is fitted in function of temperature by the following expression :

$$C_{10} = 259.17 - 0.8743.T \qquad (4.4)$$

Figures 4.25 to **4.28** display the simulation results versus insolation for three chosen cell temperatures : T = 0°C, T = 15 °C and T = 45 °C . The geodetic head is fixed at : Hg = 7.4 m.

As underlined in chapter 2, the decrease of temperature yields a significant increase of the electric power, and therefore the motor speed. We obtain then an improvement of the mechanical power at the pump shaft, which varies with the cube of the speed.

Figure 4.25 illusrates the flow-rate curve. This latter implies that :

- As a consequence of the speed increase, the threshold electric power (P_{eth} = 186 w) required to start pumping is obtained at a lower insolation level E_{th}, as shown in **Table 4**, allowing the pump to convey water earlier in the morning and ceases later at the afternoon. Doing so, we improve the solar radiation utilisability.
- The increase of the mechanical power as a consequence of temperature decrease leads to an improvement of the flow-rate and, then, to an elevation of the daily water amount, as shown in **Figure 4.26**.

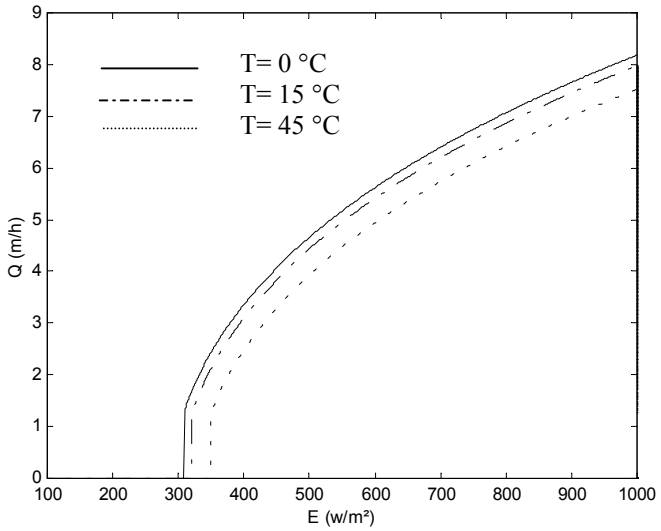

FIG 4.25 Flow-rate curves for variable temperature

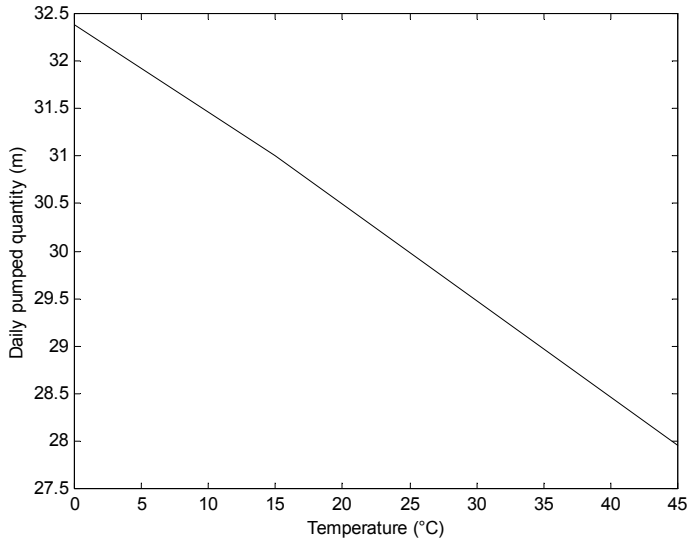

FIG 4.26 Daily pumped amount for variable temperature

Figure 4.27 depicts the pump torque curve , while in **Figure 4.28** the optimised air-gap flux is plotted. From these two curves, one can notice that for a given value of the incident insolation, the load torque decreases when the temperature goes up. The appropriate air-gap

flux to optimise the motor efficiency tends to decrease, which implies that in case of an induction motor driving light loads, an optimum value of the motor efficiency is obtained with a weak air-gap flux [39].

Table 4 System Performance for variable Temperature

T ***(°C)***	η_m ***(%)***	η_p ***(%)***	***D*** (m^3)	***Flux*** ***(V/Hz)***	E_{th} (W/m^2)	μ ***(%)***
0	73.65	65.69	32.38	4.03	308	91.34
15	73.63	65.29	31.00	3.81	320	90.67
45	73.59	64.28	27.96	3.36	349	88.71

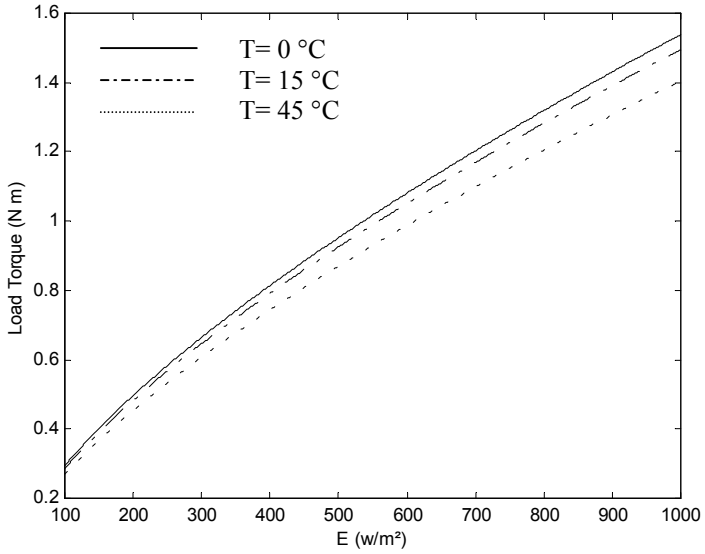

FIG 4.27 Load torque curves

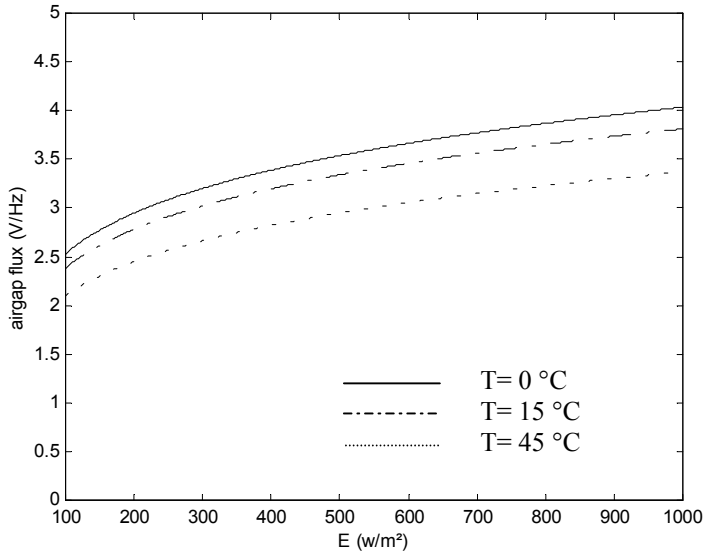

FIG 4.28 Optimised air-gap flux for variable temperature

4.5 THE ECONOMIC ASPECT:

To illustrate the economic performance brought by the proposed approach, the irrigated area by this solar pumping system is calculated under sahara climate conditions for two crops, namely potato and tomato. These are selected to meet food standards of the site. The chosen application site to test the developped algorithm is Tamanrasset station. Tamanrasset lies at a latitude of 22.76° north and a longitude of 05.52° east. The altitude of the site is about 1377.0 m, and is located in one of the most dry regions of Algeria. April to November is normally the dry season and the wet season is from December to May . The monthly average global irradiance collected for a Typical Meteorological Year varies between 5.17 kWh/m^2 /day and 7.61 kWh/m^2/day as depicted in **Figure 4.29**. The average temperature of the site is 28°c.

Water needs and Calculation of the irrigated surface :

The vegetative cycle of the crop generally includes: initial phase, development, flowering and maturity phases. Water needs of the crops during each phase are commonly estimated using the evapotranspiration concept, which results from soil evaporation and crop reference evapotranspiration (Et_r) as follows [49]:

$$E_t = K_c \, . \, E_{tr} \tag{4.5}$$

Where K_c is the crop coefficient.

Et_r is obtained by the daily corrected –model of Penman [49], and the calculated values for the site of Tamanrasset are illustrated in **Figure 4.29**.

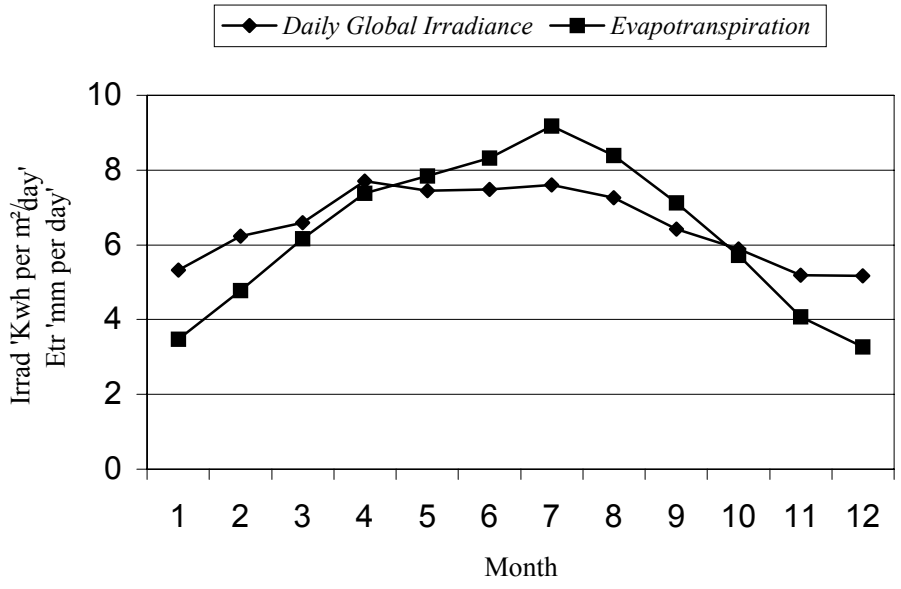

FIG 4.29 Monthly global irradiance and reference evapotranspiration at the site of Tamanrasset

Table 5 and **Table 6** shows respectively the sowing period and the crop coefficient for each vegetative phase for potato and tomato.

The total water needs over the vegetative cycle of the crop W_{tot} is the sum of water needs of the four vegetative phases of the crop.

The needed equation is :

$$W_{tot} = \sum_{k=1}^{4} W_{ph}(k) \tag{4.6}$$

Where $W_{ph}(k)$ is the water needs for the vegetative phase k.
The irrigated area S is the ratio between the volume of the pumped water during all the vegetative season D_{tot} and total water needs W_{tot}. The relationship is given by [49]:

$$S = \frac{D_{tot}}{W_{tot}} \tag{4.7}$$

Table 5 Water needs and crop coeff versus vegetative phase of potato

Vegetative phase	N_{ph} (day)	K_c	W_{ph} (mm)
Phase 1	25	K_{c11}= 0.40	61.70
Phase 2	30	K_{c21} = 0.52 K_{c22} = 0.89	152.31
Phase 3	30	K_{c31} = 1.15	267.58
Phase4	20	K_{c41} = 1.04 K_{c42} = 0.84	148.11

Where N_{ph} is the number of days per phase, K_c is the crop coefficient per phase and K_{cij} is the crop coefficient for j sections of phase i.

Table 6 Water needs and crop coeff versus vegetative phase of tomato

Vegetative phase	N_{ph} (day)	K_c	W_{ph} (mm)
Phase 1	30	K_{c11}= 0..36	79.70
Phase 2	40	K_{c21} = 0.46 K_{c22} = 0.77 K_{c23} = 1.01	232.58
Phase 3	45	K_{c31} = 1.2	474.30
Phase4	30	K_{c41} = 1.01 K_{c42} = 0.74	225.82

Figure 4.30 and 4.31 show respectively the pumped volume collected in the ten typical years and the irrigated area for the system working with the proposed approach. As can be seen,these results are well promising and present a reliable solution for other similar systems with greater dimensions.

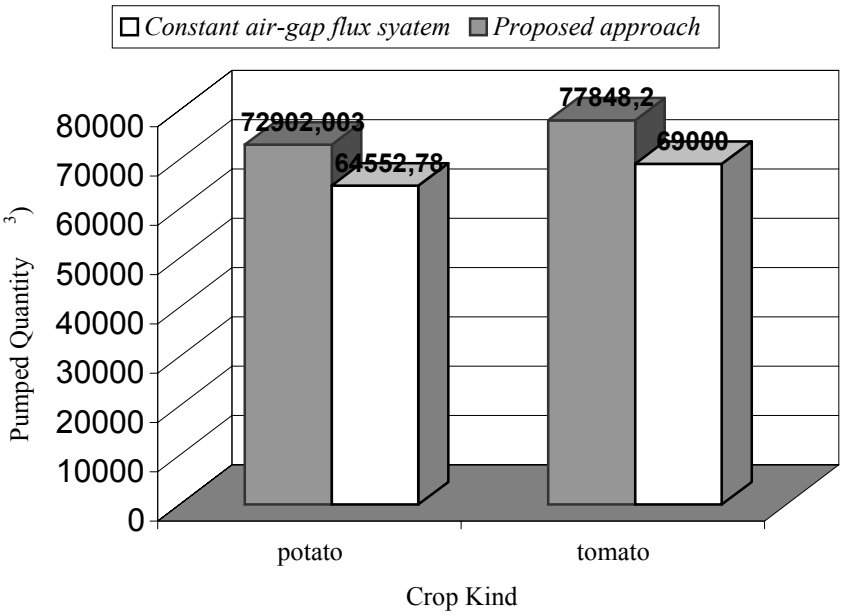

FIG 4.30 Water pumped volume (m^3) for ten typical years versus crop kind

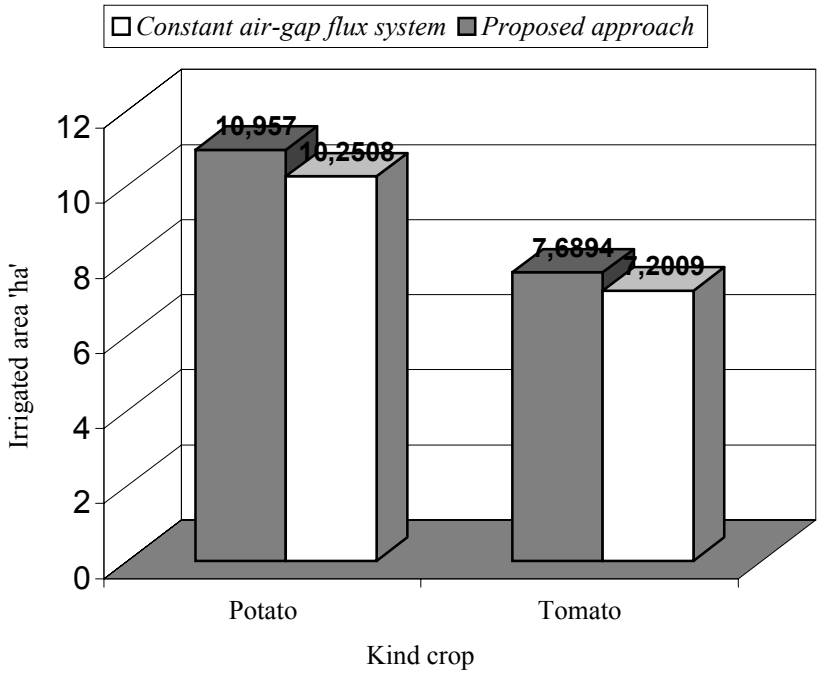

FIG 4.30 Comparison between irrigated fields for ten typical years

4. 6 INFLUENCE OF MOTOR SATURATION :

When using the linear model of an induction motor, the inductances values are those when the flux level takes its rated value.Of course these values are no more accurate when the machine is field weakened. In order to take into account more accurately the machine behavior, one has to consider the magnetic saturation.

To get simple equations, we propose to connect the core losses equivalent resistance in series with the mutual inductance.

Machine Parameters experimental determination:

The experimental tests used are the two classical ones: the no-load test and the locked rotor one. The tests were carried out for different currents and frequencies .

The machine used is **1 kw, 220/380 v, 50 Hz, 2880 r.p.m, 2.2 A, 3.3 N.m , closed rotor cage slots**. The machine was fed through a 100 Hz transistor inverter, and both active and reactive power were measured. Using the proposed induction motor, the machine paramters were obtained.

The core loss resistance is a function of frequency and flux level, but the change of R_{fs} value depends on the variation of frequency larger than that of rotor flux [50]. Therefore R_{fs} is approximately a function of frequency only.

The stator equivalent core loss resistance is determined from the classical experimental no-load test data as shown in fig.1 by :

$$R_{fs} = 0.1652.f + 0.0024.f^2 \tag{4.8}$$

At low speed, R_{fs} can be neglected compared to stator resistance but at high speed values, the slip frequency is nearly zero and the rotor core losses can be neglected.

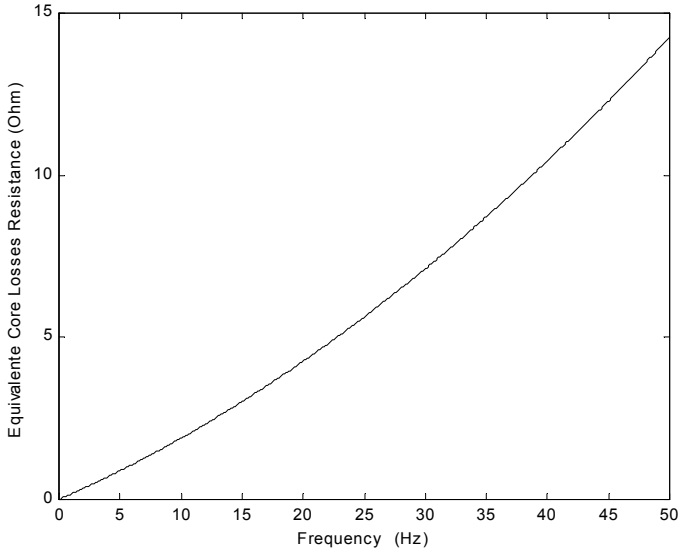

FIG 4.31 Stator core losses equivalent resistance curve

The synchronous speed test gives the stator total inductance L_{11} by measuring the reactive power.

Figure 4.32 gives the stator total inductance L_{11} as a function of stator current. The nominal magnetising stator current is 1.1A. Thus, the nominal flux level corresponds to a point where the stator inductance depends considerably on the magnetising current value. The experimental obtained inductance expression is:

$$\begin{aligned} |i_s| \le 0.65 \text{ A} \quad &\Rightarrow \quad L_{11} = 0.839 \text{ H} \\ |i_s| \ge 0.65 \text{ A} \quad &\Rightarrow \quad L_{11} = 0.7126 + 58.1387 . e^{\left(-9.4499 . |i_s|\right)} \text{ H} \end{aligned} \tag{4.9}$$

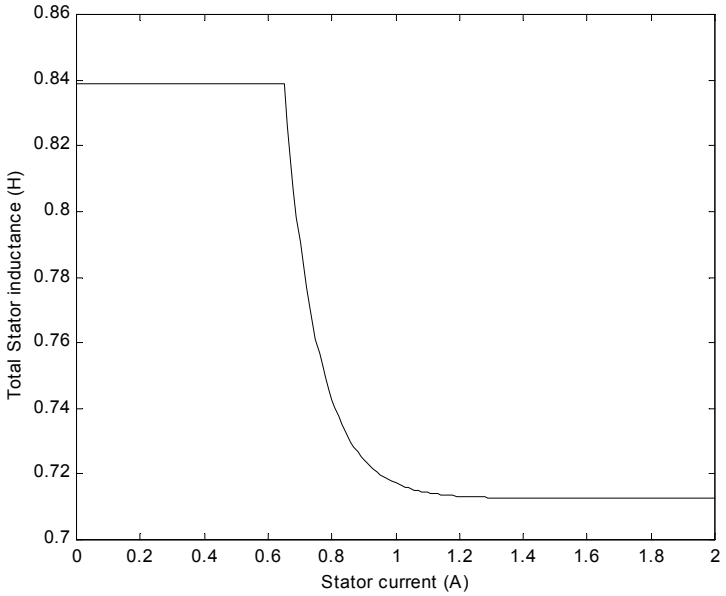

FIG 4.32 stator total inductance characterisic

An acceptable approximation is that, two inductances are defined: an unsaturated inductance L_{s0} which applies for insolation level lower than 300 W/m², and a saturated one for higher levels. L_{11} is than expressed by :

$$L_{11} = 0.7096 + 0.8635 \Big/ (-49.8815 + 0.629 . E) \quad (4.10)$$

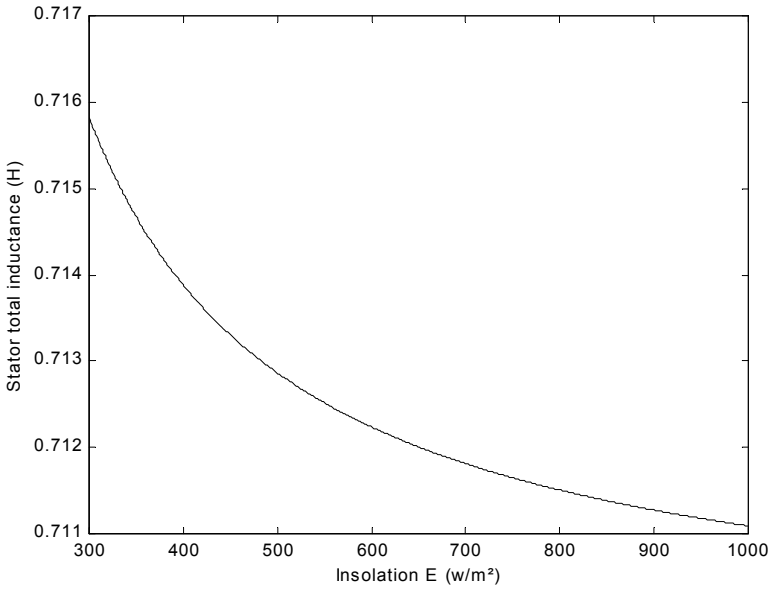

FIG 4.33 Cyclic stator inductance variation versus insolation level.

To investigate the effect of the magnetic armature saturation, a simulation of the system functionning under the proposed approach and with use of the Sinusoidal PWM strategy was carried out and the results were compared with those of the unsaturated motor.
Figure 4.34 displays the motor efficiency as function of insolation, while on **Figure 4.35** the air-gap flux is shown.
As can be seen, the saturated motor efficiency falls considerably while compared with the usual linear model for all the insolation range. This can be explained by the fact that when the

magnetic armature becomes gradually saturated, the iron losses increase causing the degradation of the motor efficiency. This situation is noteworthy for the high insolation values when the leakage flux considerably grows and the magnetic armature becomes more saturated.

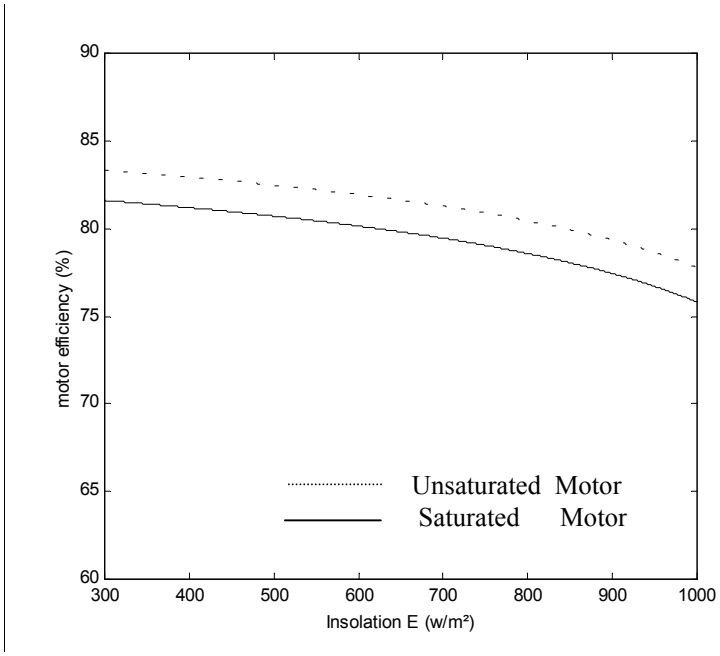

FIG 4.34 Saturation effect on the motor efficiency

One can remark from **figure 4.35** that the saturated armature was more defluxed especially for the high insolation values since at this region the hysterisis and eddy current losses are more notable.

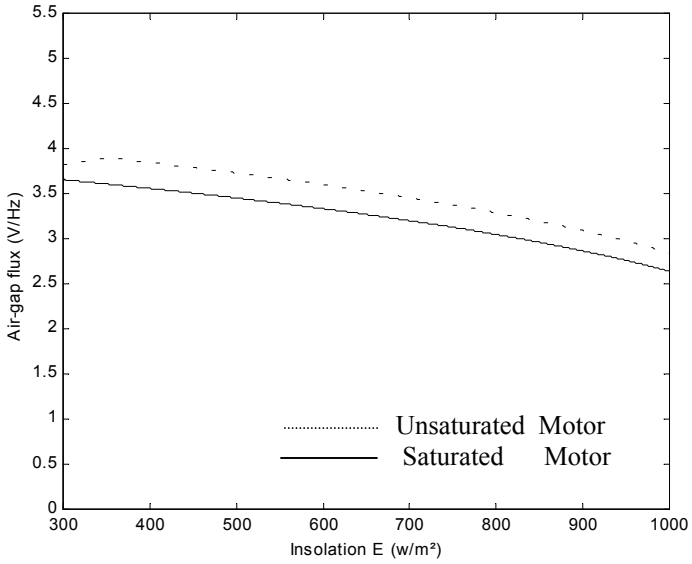

FIG 4. 35 Saturation effect on the motor air-gap flux

4.7 CONCLUSION:

In the frame of the present chapter, the operational behavior of the PVP system working under the optimisation approach was investigated in great detail on the basis of computer simulations. Simulations were created to extract the performances of the system. In addition, the influence of cell temperature, static head and motor saturation were also investigated in this chapter. Furthermore, To illustrate the economic aspect brought by the proposed approach, the irrigated area by this solar pumping system is calculated under sahara climate conditions for two crops. Concerning component efficiencies, the obtained results show that the proposed optimisation algorithm allows both a notable improvement of these efficiencies especially for low insolation levels and a less expensive implementation is obtained since the MPPT block is not incorporated. A reliable prediction of the long performances show that using the proposed approach we can significally improve the pumped amount and the irrigated area, which makes the system more promising.

CONCLUSION

The present work suggests how an optimal operation of a direct photovoltaic pumping system based on an induction motor can be achieved. The optimisation problem consists in maximising the daily pumped water quantity via the minimisation of a non-linear criterion for any operating point. This has led to an optimum ' v-f ' relationship useful in controlling the motor. The voltage source inverter feeding the motor was controlled via one of the following three PWM strategies called : the 'sinusoidal PWM strategy'; the *'Harmonic Elimination Technic'* or the '*Harmonic Minimisation Technic'*. The chosen optimisation criterion fixes the maximisation of the motor efficiency or the power factor, since these two objective functions provide similar results. The extracted electric power is controlled by the inverter frequency instead of MPPT, which leads to a less expensive and non complex implementation. Thus the advantages described in are acquired mean while overriding their inconvenient.

A comparative study was led on two systems described in [5] and [33]. The obtained simulation results show that an increase of all the system performances such as the daily pumped quantity, the motor power factor and the pump efficiency are reached by the proposed approach when either the 'sinusoidal PWM strategy' or the '*Harmonic Minimisation Technique'* is used. It is also important to underline that in the case of the '*Harmonic Minimisation Method',* the THD factor increases relatively for the low insolation levels . To surmount this problem, a combination of the sinusoidal PWM strategy and the '*Harmonic Minimisation Method'* can be implemented, where the first technic acts in the low insolation range (in the early morning and the late afternoon), whereas the inverter is controlled intermittently with the second strategy in the middle of the day. Concerning the motor operation, the system works with a variable air-gap flux and the slip values are lower than the breakdown motor slip . The functioning point remains then permanently in the stable area of the torque-speed characteristic.

When water is discharged from a well, the inside water-table does not remain constant : It changes depending on the flow-rate and the pumping time. It is, then, no longer justified to consider the geodetic head Hg as constant. Simulation runs using the proposed approach where the geodetic head is changed by a step of 0.5 m. The simulation results show that the threshold insolation and hence the electric power required to start pumping increases with head. Consequently, the daily water amount would decrease. These results confirm the behavior of a centrifugal pump which needs a relatively high speed to overcome system head. Rotating displacement (progressive cavity) pumps present a viable solution of such situation, starting pumping water at nearly zero speed, and so a least threshold electric power is required.

Furthermore, as known, meteorological parameters, especially the array temperature, do not remain constant all day long, but change considerably. The decrease of temperature yields a significant increase of the threshold electric power , and therefore of the motor speed. Consequently the pump convey water earlier in the morning and ceases later at the afternoon. Doing so, we improve the solar radiation utilisability.
Besides, the pump flow-rate, the pumped amount and subsystem efficiencies are degraded once the temperature increases and the appropriate air-gap flux to optimise the motor efficiency tends to decrease.
As a result of the temperature variation, the sizing of the system should be done in accordance with the average daily temperature of the site.

To illustrate the economic performance brought by the proposed approach, the irrigated area by this solar pumping system is calculated under sahara climate conditions for two crops, namely potato and tomato. These are selected to meet food standards of the site. The chosen application site to test the developed algorithm is Tamanrasset station.
The pumped volume collected in the ten typical years and the irrigated area for the system working with the proposed approach when compared with the system working under a constant air-gap flux [5] show well promising results; the benefits are respectively 6.88 % for potato and 6.78 % for tomato. The proposed algorithm presents a reliable solution for other similar systems with greater dimensions.

When using the linear model of the induction motor, the inductances values are those when the flux level takes its rated value. Of course these values are no more accurate when the machine is field weakened. In order to take into account more accurately the machine behavior, simulation runs with the optimisation criterion under the motor magnetic saturation and the results were compared with those of the unsaturated motor. From the figure displaying the total stator inductance, one can notice that the motor is not fully saturated over the insolation range since its value remains permanently in the knee of the stator inductance-phase current curve.

The saturated motor efficiency falls considerably while compared with the usual linear model for all the insolation range. This can be explained by the fact that when the magnetic armature becomes gradually saturated, the iron losses increase causing the degradation of the motor efficiency. This situation is noteworthy for the high insolation values when the leakage flux considerably grows and the magnetic armature becomes more saturated.
The saturated armature was more defluxed especially for the high insolation values since at this region the hysterisis and eddy current losses are more notable.

The new algorithm developed in this project provides many advantages, such as quick determination of all operating points of a given system, great flexibility in changing the system topology and a simple interface with standard pumping system components. This can be very useful in the interest efficient analysis and developing an effective PVPS.
The proposed optimisation algorithm can be eventually implemented via a microcontroller-card in the arid areas at the south of Algeria.

RECOMMENDATION

1- Accurate PVP-system design can benefit from a digital simulation based on appropriate system component models and characteristics that can be obtained from components manufacturers. However, one of the prerequisites for the accuracy is that the simulation tools have to be derived on the basis of the knowledge acquired from the evaluation of real experiences with such systems.
2- The design of PVP requires very accurate data from site location, especially about the demand and uses of water and the well dynamic characteristics. Appropriate testing should be improved and performed carefully before the system can be designed and reliable meteorological data must be available.
3- As a further research of the present work, a number of points not treated here can be undertaken with a detailed study :
    - In the present work, an approximate model of the hourly insolation was expressed for a standard clear day where the system was assumed to work in steady state for long periods; which is not accurate for cloudy days where the insolation varies considerably in short times. The system works then in

transient state the day long and the preferred optimisation method will be the dynamic programming of Bellman. A study on the system stability must be then added.

- The scalar control of the induction motor was adopted in this thesis. The vector control using different technics of artificial intelligency such as fuzzy logic, neural network or sliding mode can be a kindly addition to the effort given here. The dynamics for the control design are then seen to be highly non-linear.
- Instead of the VSI feeding the motor, one can use different inverter types, such as the NPC mode which can be a suitable solution due to the source division into many stages.
- Developments in the field of electronic, control and material technology have given impetus to new motor designs. Using high density PM motors based on rare-earth magnets (Samarium-Cobalt, Neodymium-Iron-Borron), high power/weight and torque/current ratios have been obtained. It is generally accepted that the high power density, high efficiency and fast dynamics of PM motors make them well suited for PV pumping in the rangr of few tens of kWs whereupon the cost advantages of the induction motor become significant.

4- The present thesis does not include an economic simulator testing a comparative study of the system cost for the three plants described here. Since the design of solar applications should consider the economic factors, the economic simulator is an important tool for analysing the effectiveness of system investment.

REFERENCES

[1] J.M. Koo, 'Development of a flat –plat solar collector design program', Master thesis, University of Wisconsin-Madison, 1999.

[2] 'Grid-Connected photovoltaic system design review and approval', Note, Florida solar energy center, 2001.

[3] R. Kyoungsoo, ' Two-loop controller for maximizing performance of a grid-connected photovoltaic-fuel cell hybrid power plant', PHD thesis, Virginia Polytechnic Institute, 1997.

[4] P.M.Williams, ' Development and analysis tool for photovoltaic-powered solar water heating systems', Master thesis, University of Wisconsin-Madison, 1996.

[5] R. Duzat, 'Analytic and Experimental investigation of a photovoltaic pumping system', PhD – work 2000, Oldenburg University Dissertation.

[6] Y.R.Hsiao and B.A.Blevins, ' Direct coupling of photovoltaic power source to water pumping system', Solar Energy, Vol 32, 1984.

[7] L. Merwe, G. Merwe, ' Maximum power point tracking-implementation strategies ', ISIE'98 Symposium Proc., Vol 1, N°1, pp 214-217, 1998.

[8] D.Langridge et al, ' Development of a photovoltaic pumping system using brushless DC motor and helical rotor pump', Solar Energy, Vol 56, N°2, pp 151-160, 1996.

[9] S. M. Alghuwainem, ' Steady State Operation Of DC Motors Supplied From Photovoltaic Generators With Step Up Converters', IEEE Trans. on Energ. Conv., Vol. 7, No. 2, pp 267-271, 1992

[10] M. Godoy, N. Franceshetti, ' Fuzzy optimisation based control of a solar array system', IEE proc. EPA, Vol. 146, N° 5, pp 552-558, 1999.

[11] I. H Atlas, A.M Sharaf, 'A novel on-line MPP search algorithm for PV arrays, IEEE Trans on Energ. Conv., Vol 11, N° 4, pp 748-754, 1996.

[12] T.F. Wu et al, 'Fuzzy-logic-controlled single-stage converter for PV-powered lighting system application', IEEE Trans. on Ind. App., Vol 47 , N° 2, pp 287-296, 2000.

[13] C. Hua, C. Shen, ' Study of maximum power tracking techniques and control of DC/DC converters for photovoltaic power system', 29th annual IEEE power electronics specialists conference, PESC 98 record, Vol 1, pp 86-93, 1998.

[14] S.J. Chiang, ' Residential photovoltaic energy storage system', IEEE Trans on IEM, Vol 45, N°3, pp 385-394, 1998.

[15] T. Hiama et al, 'Identification of optimal operating point of PV modules using neural network for real time maximum power tracking control ', IEEE Trans. on Energ. Conv., Vol 10 , N° 2, pp 360-667, 1995.

[16] T. Hiama et al, 'Evaluation of neural network based real time maximum power tracking control for PV system ', IEEE Trans. on Energ. Conv., Vol 10 , N° 3, pp 543-548, 1995.

[17] T. Hiama et al, 'Neural network based estimation of maximum power generation from PV modules using environmental information ', IEEE Trans. on Energ. Conv., Vol 12 , N° 3, pp 241-247, 1997.

[18] T. Senjyu, K. Uezato, ‘ Maximum power point tracker using fuzzy control for photovoltaic arrays’, proceedings of the IEEE International conference on Industrial Technology, pp 143-147, 1994.

[19] M. M. Saied, ‘Matching of DC Motor to Photovoltaic generator for Maximum Daily Gross Mechanical Energy ’, IEEE Trans. on Energ Conv, Vol. 3, No. 3, 1988, pp 465-471.

[20] M. Akbaba et al, ‘ Matching Of Separately Excited DC Motors To Photovoltaic Generators For Maximum Power Output’, Solar Energy, Vol. 63, N0. 6, 1998, pp:375-385.

[21] M. N. Eskandar, A. M. Zaki, ‘ A Maximum Efficiency Photovoltaic-Induction Motor Pump System’, Renewable Energy, Vol. 10, No. 1, 1997, pp 53-60.

[22] A. Moussi, A.Betka and B. Azoui, ‘Optimum design of a photovoltaic pumping system’, UPEC99, Leicester UK, 1999.

[23] A. Betka, A. Moussi, ‘Optimisation of photovoltaic water pump coupled with an optimal PWM inverter’, 47. Internationales wisssenschaftliches kolloquium, September 2002.

[24] A. Betka, A. Moussi, ‘Performance Optimization of a photovoltaic pumping system based on an induction motor drive’, Renewable Energy, Vol 29, N° 1,pp 2167-2181, 2004.

[25] J. Appelbaum, ‘ Starting and Steady State Characteristics of DC Motor Powered by Solar Cell Generator ’ , IEEE Trans. on Energ. Conv., Vol. 1, No. 1, 1986, pp17-25.

[26] J.R Potebaum, ‘Optimal characteristics of a variable frequency centrifugal pump motor drive’, IEEE Trans. on Ind. Appl., Vol IA-20 , N° 1, pp 23-31, Feb. 1984.

[27] B. Azoui et al, ‘ Photovoltaic pumping system with NdFeB brushless DC motor’, Electromotion, pp 19-27, 2001.

[28] W. R. Anis et al , ‘ Coupling of a volumetric pump to a photovoltaic array’, Solar Cells, Vol.14, pp 27-42, 1985.

[29] D.Weiner and A.Levinson, ‘Water pumping optimal operation’, Electrical machines and power systems, Electric machines and components, Vol 24, No. 3, pp 277-288, 1996.

[30] M. Veerachary, N. Yadaiah, ‘ ANN Based Peak Power Tracking For PV Supplied DC Motors’, Solar Energy, Vol. 69, N0. 4, 2000, pp: 343-350.

[31] C. L. P. Swamy and al, ‘ Dynamic Performance of a permanent Magnet Brushless DC Motor Powered by a PV Array for Water Pumping’, Solar Energy Materials and Solar Cells, Vol. 36, 1995, pp: 187-200.

[32] B.N.Singh, and al, ‘ Optimized Performance of Solar Powered Variable Speed Induction Motor Drive’, IEEE Trans. on Ind App, 1991.

[33] Y. Yao, P. Bustamente and R.S. Ramshaw, ‘ Improvement of induction motor drive systems supplied by photovoltaic arrays with frequency control’, IEEE Trans. on Energ. Conv., Vol 9, No. 2, 1994.

[34] O. Olorunfemi, ‘Analysis Of Current Source Induction Motor Drive Fed From Photovoltaic Energy Source’, IEEE Trans. on Energ. Conv., Vol. 6, No. 1, 1991, pp 99-106.

[35] M. Nayar et al, ‘A grid-interactive photovoltaic uninterruptible power supply using battery storage and backup diesel generator., IEEE Trans. on Energ. Conv., Vol 15, No. 3, 2000

[36] R. Smith et al, ‘ Analysis and Performance of Novel Two-Phase Drive for Fan and Water-Pumping Applications’, IEEE Trans on Ind. App., Vol 36, No 4, November 1989.

[37] F. Bryan, Master thesis, Solar Energy Laboratory, University of Wisconsin-Madison, 2000.

[38] S.Sirisukprasert, ‘ Optimized harmonic stepped-waveform for multilevel inverter’, Master thesis, Virginia university, 1999.

[39] J.M.D. Murphy and F.G. Turnbull, ‘power Electronics control of AC motors’, Pergamon Press 1985.

[40] B.K. Bose, ‘Power Electronics and AC drives’, New Jersey, 1987

[41] A. Betka, ‘ Optimisation d’un système de pompage au fil du soleil’, thèse de Magistère, université de Biskra, 1998.

[42] K.Khousem and L.Khousem , ‘ optimum matching of direct-coupled electromechanical loads to a photovoltaic generator’, IEEE Trans. on Energ. Conv. , Vol 8, No.3, 1993.

[43] K. Barra and all, ‘ Vector control of induction motor fed by photovoltaic generator’, CIMASI’2000, Casablanka, 2000.

[44] P. Famouri and J.J. Cathey, ‘ Loss Minimization Control Of An Induction Motor Drive’, IEEE Trans. on Ind. App., 1989, pp: 226-231.

[45] R. fletcher, ‘A new Approach to variable metric algorithms’, Computer Journal, Vol.13, 1970.

[46] Matlab Optimization toolbox manual.

[47] W. Bucher, ‘Improvements in Part Load Characteristics of Deep Well Pumps- Results of Comparative Field Tests’, 12th European Photovoltaic Solar Energy Conference, Amsterdam, April 1994.

[48] L. Cheng et al, ‘ Advanced photovoltaic inverter with additional active power line conditioning capability’, IEEE-PESC, pp 279-283, 1997.

[49] A. Hamidat et al , ‘ Small-scale irrigation with photovoltaic water pumping system in sahara regions’, Renewable Energy, Vol 28, pp 1081-1096, 2003.

[50] E. Mendes and A. Razek, ‘ A simple model for core losses and magnetic saturation in induction machines adapted for direct stator flux orientation control’, Power Electronics and variable drives, pp 192-179, 1994.

[51] S. R. Bhat et al, ‘ Performance Optimization of Induction Motor-Pump System Using Photovoltaic Energy Source’, IEEE Trans. on Ind. App., Vol. 23, No. 6, 1987, pp: 995-1000.

[52] G. B. shrertha, L. Goel, ‘A Study On Optimal Sizing Of Stand Alone Photovoltaic Stations’ IEEE Trans. on Energ. Conv., Vol. 13, No. 4, 1998, pp: 373-377.

[53] J. Samin et al. ‘Optimal sizing of Photovoltaic Systems in Varied Climates’ , Solar Energy Vol. 6, o. 2, 1997, pp: 97-107.

[54] R. Posorsky, ‘ Photovoltaic Water Pumps, An Attractive Tool For Rural Drinking Water Supply’, Solar Energy, Vol 58 No 4-6, pp 155-163, 1996.

[55] K. Kalaizakis, ‘ Optimal PV system dimensioning with obstructed solar radiation’, Renewable Energy, Vol 7, N° 1,pp 51-56.

[56] M.G Jabori, ‘ A contribution to the simulation and design optimisation of photovoltaic systems’, IEEE Trans. on Energ. Conv., Vol 6 , N° 3, pp 401-406,1991.

[57] T. J. Hammers et al, ‘Renewable energy for developing countries’, IEEE Trans. on Energ. Conv. , Vol 15 , N° 4, pp 481-493, 2000.

[58] W.Z.Fam and K. Balachander, 'Dynamic performances of a DC shunt motor connected to a photovoltaic array', IEEE Trans. on Energ. Conv. , Vol 3 , N° 3, pp 613-617, 1988.

[59] A. Azuoi et al, 'Sizing and Optimization models for photovoltaic pumping system using BLDCM Motor', AMSE, , pp 55-69, 2003.

[60] I. Glasner, J. Appelbaum, ' Advantage of boost Vs.buck topology for maximum power point tracker in photovoltaic systems, IEEE Trans on Energ. Conv., pp 335-358, 1996.

[61] J. Appelbaum, M.S. Sarme, ' The operation of permanent magnet DC motors powered by a common source solar cells ', IEEE Trans on Energ. Conv., Vol 4, N° 4, pp 635-642, 1989

[62] C. Hua, C. shen, ' Control of DC/DC converters for solar Energy system with maximum power tracking ', IECON' 97 Conf. Vol.2, pp 827-832, 1997.

[63] H.M . Mashaly et al, ' A photovoltaic maximum power tracking using neural network', Proc of the third IEEE conf. on Cont. Appl., Vol 1, pp 167-172, 1994.

[64] D.C Martins et al , ' Water pumping system from photovoltaic cells using a current fed parallel resonant push-pull inverter', 29th annual IEEE power electronics specialists conference, PESC 98 record, Vol 2, pp 1892-1898, 1998.

[65] H.D. Maheshappa et al, ' An improved maximum power point tracker using step-up converter with current locked loop', Renewable Energy, Vol 13, N° 22, pp- 195-201, 1998.

[66] M.A Choudhury, M.A. Rahman, ' Determination of operating conditions of submersible induction motors', IEEE Trans. on Ind. Appl., Vol 28, N° 3, 1992.

[67] J. Rodriguez et al, ' Optimal vector control of pumping and ventilation induction motor drives', IEEE Trans. on Ind. Electronics., Vol 49, N° 4, 2002.

[68] D.S.Kirschen, D.W. Novotny and T.A. Lipo, 'On-line efficiency optimization of variable frequency induction motor drive ', IEEE trans. on Ind. Appl., Vol IA-21, pp 610-616, 1985.

[69] C. Hua, C. Sher , ' Control of DC/DC converter for solar Energy system with maximum power tracking', National university of science & technology, taiwan, pp 827-832.

[70] M.H. Salama, ' A simplified approach for determining the minimum input power conditions for induction motors fed from variable frequency sources', Electric Machines and Power systems, Vol 11, N°1, pp 41-51, 1986.

[71] R.E . Kattan et al, ' Performance Analysis of a solar water pumping system', School of Electrical and Computer Engineering, Curtin university, Western Australia, pp 61-87.

[72] G.B. Shrestha, L. Coel ' A study on optimal sizing of stand alone photovoltaic stations', IEEE Trans on Energ.Conv., Vol 13, N°4, pp 373-378, 1998.

[73] J. Samimi et al, 'Optimal sizing of photovoltaic systems in varied climates', Solar Energy, Vol 60, N°2, pp 97-107, 1997.

[74] K. Kalaitzakis, ' Opimal PV system dimensioning with obstructed solar radiation', Renewable Energy, Vol 7, N° 1, pp 51-56, 1996.

[75] B.K.Bose, 'Microcomputer control of residentiql photovoltaic power conditioning system' IEEE trans on Ind. Appl., Vol 21, N°5, pp 1182-1191, 1998.

[76] A. Al-Amoudi, L. Zhang, ‘ Optimal control of a grid-connected PV system for power point tracking and unity power factor’, Power Electronics and variable speed drives, IEE proceedings, N°456, pp 80-85, 1998.

[77] L. Cheng and all, ‘ Advanced photovoltaic inverter with additional power line condioning capability’, IEEE Trans on power systems, pp 279-283, 1997.

[78] R. Liebenberg et al, ‘High efficiency long life actuator for PV water pumping applications’, 5th Europeqn Conf on PEA, pp 495-500m 1993.

[79] A.F. Boehringer, ‘ Self adapting DC- converter for solar spacecraft power supply’, IEEE Trans on AES., Vol 4, N°1, pp 102-111, 1968.

[80] M. A Green and K. Emery, ‘Solar Cell Efficiency Tables, Progress in Photovoltaics’ , Research and Application, Vol. 1, pp. 25-29, 1993.

[81] M.Daian, ‘High performance in low-flow solar domestic hot water systems’, Master thesis, University of Wisconsin-Madison, 1997.

[82] K.E. Kragan, ‘ Impact on a utility of an ensemble of solar hot water systems’, Master thesis, University of Wisconsin-Madison, 1994.

[83] B.J.Newton, ‘ Modelling of solar storage tanks’, Master thesis, University of Wisconsin-Madison, 1995.

[84] B. Lindgren, ‘ Power generation, Power electronics and power-systems issues of power converters for photovoltaic applications’, PHD thesis, Chalmers university of technology, Sweden, 2002

[85] J.N.Wolete, ‘An interactive menu-driven design tool for stand –alone photovoltaic systems’, Master thesis, Virginia university, 1998.

Abstract : The present work suggests how an optimal operation of a direct photovoltaic pumping system based on an induction motor can be achieved. The optimization problem consists in maximising the daily pumped water quantity via the minimisation of a non-linear criterion for any operating point. This has led to an optimum ' v-f ' relationship useful in controlling the motor. The voltage source inverter feeding the motor was controlled via one of the following three PWM strategies called : the 'sinusoidal PWM strategy'; the *'Harmonic Elimination Technic'* or the '*Harmonic Minimisation Technic'*. The chosen optimisation criterion fixes the maximization of the motor efficiency or the power factor, since these two objective functions provides similar results. The extracted electric power is controlled by the inverter frequency instead of MPPT, which leads to a less expensive and non complex implementation. Thus the advantages described in are acquired mean while overriding their inconvenient.

The obtained simulation results show that an increase of all the system performances such as the daily pumped quantity, the motor power factor and the pump efficiency are reached by the proposed approach when either the 'sinusoidal PWM strategy' or the '*Harmonic Minimisation Technic'* is used.

To illustrate the economic performance brought by the proposed approach, the irrigated area by this solar pumping system is calculated under sahara climate conditions for two crops. The pumped volume collected in the ten typical years and the irrigated area show well promising results.

The Author's biography :

March, 1969 : Mr Achour Betka is born in Biskra , Algeria.
June , 1991 : He obtained his diploma of Applied University Studies (DEUA) from Biskra University Option : Electrical Network in Electrical Engineering.
June, 1994 : He got his Engineer diploma,Option : Electrical Machines.
January, 1998 : The author is a holder of a Master degree in Electrical engineering.Option :Electrical Control from Biskra University.
From 1998 to 2004 : He worked as a Maitre Assistant at the institute of Electronics in Oum Elbouaghi University. He gave lectures on electrical machines, he also taught Master candidates on scalar control of the electrical machines.
2005 : He's a lecturer in the Electrotechnic Institute at Biskra University . He gives lectures on electrical machines reliability..His intrest fields are : The application of photovoltaic technologies in water pumping systems in remote arid areas. He's a member in a research project agreed on by the M.E.S.R.S at Oum Elbouaghi University. He's also a L.A.R.H.Y.S.S member (a research laboratory on surface and underground hydraulics at Biskra University).